Water gas-shift conversion in microchannel reactors using noble metal catalysts

Kubefu Maduna

Submitted in partial fulfilment of the requirements
of the degree of Master of Science in Chemical Engineering

February 2014

Centre for Catalysis Research
Department of Chemical Engineering
University of Cape Town
Cape Town
South Africa

Declaration

I know the meaning of plagiarism and declare that all the work in the document, save for that which is properly acknowledged, is my own

……………………………….   Date   …………………………….

Kubefu Maduna

Synopsis

Fuel cell technology will play a crucial role in future sustainable energy generation. Different types of fuel cells had been developed, of which Polymer Electrolyte Membrane Fuel Cells (PEMFCs) are the fuel cells of choice for small scale stationary and mobile applications that operate under transient conditions.

The feed for PEMFCs is hydrogen. For small scale stationary and mobile applications, the hydrogen, typically, has to be produced on-site from other energy sources, such as fossil fuels or fuel from renewable sources. At present, the most favourable approach appears to be a production train that starts with a steam reformer stage, which converts most of the primary fuel to syngas. In the subsequent water-gas-shift stage, most of the carbon monoxide in the syngas is converted to additional hydrogen and carbon dioxide. In a last stage, the small amount of carbon monoxide that remains in the stream is reduced to acceptable levels for use in the fuel cell.

In large scale industrial hydrogen production, the above concept (steam reforming – water gas-shift – hydrogen purification) is the state of the art, with the units operating under steady conditions for years once started. In contrast, the said small scale units will typically operate under transient conditions and in on/off mode. This requires catalysts that are stable with respect to occasional contact with air and condensation of the steam co-fed with the primary fuel and which do not require any activation or other conditioning prior to restart. Only noble metal based catalysts meet these requirements at present.

This study was aimed at the water-gas-shift (WGS) stage within this train. The basis of the study was the comparison of three commercial supported noble metal WGS catalysts and a state-of-the-art industrial iron/chromium high temperature WGS catalyst. All the catalysts were applied washcoated onto stainless steel microchannel reactor, either coated in-house or by the catalyst manufacturer, as well as defining an operational window for the noble metal catalysts. Three different feeds were

converted in these microreactors, which mimicked close to thermodynamic equilibrium composition effluents from a steam reforming stage that was fed with steam/ methane mixtures of different ratios. Reaction temperatures and space velocities were varied.

Mimicked WGS reactor feeds were derived from steam reformer feeds with steam/ methane molar ratios of 2.35, 3 and 5 and with almost complete conversion of the methane. WGS reaction conditions ranged from 275 to 450 ^{o}C and space velocities (dry) ranged from 23 000 to 230 000 ml/(h.g), with reaction pressure set at 1 barg. The target was a WGS reactor effluent (wet) with a carbon monoxide content of 1 mol% or less than 1 mol%.

It appeared that, for stoichiometric reasons, steam reformer feed steam/ methane molar ratios of around 5 and higher are required in order to achieve sufficient humidity of the stream that finally goes into the fuel cell, i.e., a stream that is saturated with water at the operation temperature of up to 100 ^{o}C for a conventional low temperature PEM fuel cell. From the experiments performed that these high steam/ methane ratios it is also required to shift the thermodynamic limit temperature for the ≤ 1 mol% (wet) carbon monoxide target to a temperature range in which the WGS catalyst is sufficiently active to allow high space velocities. The above also holds if the downstream fuel cell is a high temperature PEM fuel cell, which does not require high water vapour concentrations in the feed.

Two of the noble metal catalysts tested were found to be very active and also stable over prolonged time on stream, while the third catalyst was less active and also unstable under the reaction conditions applied. In comparison with the noble metal catalysts, the activity of the conventional iron/chromium high temperature WGS catalyst as applied in the first stage in large scale industrial hydrogen manufacture, was low.

Over the two most active noble metal catalysts and with the most humid one of the aforementioned feeds (as derived from a steam reformer feed with a steam/ methane molar ratio of 5), the target of

≤ 1 mol% carbon monoxide (wet) could be achieved at a pressure of 1 barg, a temperature of 350 ^{o}C and a space velocity of 230 000 ml/(h.g) dry or 400 000 ml/(h.g) wet, respectively. With the thermodynamic limit for achieving a 1 mol% carbon monoxide product still being significantly higher (at 395 ^{o}C) and the space velocities being rather high as well, either significantly higher space velocities or much lower carbon monoxide levels in the WGS effluent stream will be achievable for such high water content feeds at higher or lower reaction temperatures, respectively.

Acknowledgements

Great thanks to my supervisor, Prof. Jack Fletcher. Thank you for the wonderful opportunity that you gave me to be part of the fuel processing research team. I cannot thank you enough for the support, advice and the ever understanding patience you had for me.

Very warm thanks to Walter Böhringer without whom I would not have became the better man I am today. Thank you for the guidance, encouragement, patience and support. I appreciate your ever hard working character you inspired me with and the open door policy you had. Thank you for teaching me good research practices and hope that I will not be the last one to experience such.

Stephen Roberts, Niels Lüchters, Marc Wüst, Jacobus van der Merwe and Waldo Koortz, I cannot thank each and everyone of you for your everlasting support and guidance you cherished me with, thank you gentlemen. To both Yi Zhou and David Tsui, I am truly greatful for working with you and the knowledge I gained through you, I couldn't ask for any other fuel processing team. To the Centre for Catalysis Research and the Chemical Engineering Department, you will forever remain my home, the love and support I received from that friends and family will forever be treasured.

Thanks go also to Miranda Waldron from UCT Department of Physics for taking scanning electron microscope (SEM) images of the microreactor plates with washcoated catalyst.

To my ancestors, uGubevu waka Nokhala, wena waka malobola nge ngade, Ujiyane, thank you all for protecting me throughout these years. To my parents and siblings, I can not thank you enough for the love, patience, sacrifices, guidance and support. Without you all, I would not know the true meaning of life. A great thanks to Disebo, Chester and the community of friends that kept me calm and sane when I had doubts of reaching great heights.

Lastly, I would like to thank HySA/Catalysis for the financial assistance, I truly appreciate it.

CONTENTS

LIST OF TABLES

LIST OF FIGURES

Glossary

Binder	Additive with small particle size (organic or inorganic)
Drop test	Specific coating adherence test for the test plates
Fuel cell	Energy generating device
Metal sleeves	Used for insulation of microchannel reactor
Microchannel reactor	Coated microchannel reactor plates welded together face to face to conduct a chemical reaction
Microchannel plate	Microchannel plate with inlet and outlet portals
Microchannel test plate	Microchannel plate without inlet and outlet ports
Microchannel sealing/bonding	Joining of microchannel reactor plates to form microchannel reactor
Microsplitter	Reagent flow splitter to obtain lower flow rates
Microstructuring	Formation of microchannels in plate
Monolith	Substrate which is coated with catalytic material
Washcoating	Pre-synthesised catalyst and other additives are combined followed by coating onto the substrate

Nomenclature and symbols

Symbol	Description	Unit
A	Component A	
C_A	Addend (intersection of the calibration line)	
CH_4	Methane	
CO	Carbon monoxide	
CO_2	Carbon dioxide	
F_A	Fraction of A	
H_2	Hydrogen	
H_2O	Water	
HT-PEMFC	High Temperature PEMFC	
ΔH	Heat of reaction	kJ/mol
LT-PEMFC	Low Temperature PEMFC	
MCFC	Molten Carbonate Fuel Cell	
MFC	Mass Flow Controller	
P	Pressure	bar
PACFC	Phosphoric Acid Fuel Cell	
PEM	Proton Exchange or Polymer Electrolyte Membrane	
PEMFC	Polymer Electrolyte Membrane Fuel Cell	
PROX	PReferential OXidation	
PVA	PolyVinyl Alcohol	
$R_{f,A}$	Response factor (slope of the calibration line)	
S	Steam	
S/CH_4	Steam/Methane	
S/CO	Steam/Carbon monoxide	
SELMETH	SELective METHanation	

SEM	Scanning Electron Microscopy	
SOFC	Solid Oxide Fuel Cell	
SR	Steam Reforming	
SV	Space Velocity	$ml/(h.g_{cat})$
Syngas	Synthesis gas (mixture of H_2 and CO)	
T	Temperature	°C or K
WGS	Water-Gas Shift	
Xco	Conversion of carbon monoxide	

1. INTRODUCTION

Movement towards the implementation of hydrogen as an alternative fuel has been an active goal among energy scientists for many years since the International Energy Agency agreement on the Production and Utilisation of Hydrogen was established in 1974. Within this scenario, hydrogen fuel cell technology is attracting attention nowadays, since the efficiency of hydrogen fuel cells will be superior to those of conventional small scale power generation units, once hydrogen production techniques are efficient (Kolb, 2008).

Fuel cells require hydrogen for their operation and, consequently, numerous technologies are under investigation worldwide aimed at the production, storage, distribution and application of hydrogen in mobile and portable devices. The lack of a hydrogen infrastructure, in the short term, along with the highly attractive high energy density of liquid fossil and regenerative fuels, has created widespread research efforts in the field of distribution and on-site and on-board hydrogen production from various such fuels (Katikaneni & Song, 2002).

Fuel cell technology has a crucial role to play in the future of sustainable energy generation. The need of reliable hydrogen supply makes processing of fossil and renewable fuels a viable option. When fuel cell technology is applied, mobile and portable power generation systems require a compact hydrogen source, especially in small scale stationery level applications. Processing of liquid fossil and renewable fuels is a feasible option to meet the limited space demands of such power units due to the high density of liquid fuels (O'Connell et al., 2012).

The use of microchannel reactors in fuel processing for the above mentioned application seems to be a promising reactor technology with advantage over conventional fixed bed reactors (Ladebeck & Wagner, 2003).

The product from the first stage in the fuel processing train, the steam reformer, has high levels of carbon monoxide, which can be converted to carbon dioxide and additional hydrogen by the water-gas shift reaction in the second stage. With the research conducted thus far, no efficient, stable and non-pyrophoric supported catalyst for water-gas shift has been found for a small scale fuel processor that can produce enough hydrogen for powering a low kW fuel cell, such as a 1 kW PEM fuel cell, while reducing carbon monoxide content in the reformate to ≤ 1 vol% (Ladebeck & Wagner, 2003).

This study investigated one of the steps in developing fuel processing technology, which is water-gas shift conversion of the initially produced syngas (H_2/CO) towards hydrogen and CO_2. The study focused on screening commercial, supported noble and base metal catalysts applied in microchannel reactors, and identification of the best possible operating conditions.

The objectives of this research were:

- To increase H_2 concentration in syngas obtained from steam reforming for powering a PEM fuel cell, while reducing CO content in the reformate to ≤ 1 vol% (wet).

- To screen different commercial noble metal based catalysts coated onto microchannel reactor walls for WGS reaction at 1 bar gauge and in temperature range of 275-375 °C; and identify which commercially available noble metal based catalyst gives best performance (activity and stability).

- To compare commercially available noble metal catalysts with base metal catalysts coated on microchannels.

- To identify feasible operating conditions (range of space velocity and temperature) for a fuel processing device to power a PEM fuel cell.

2. LITERATURE REVIEW

2.1 Hydrogen Economy

Hydrogen is naturally present on the earth's surface only in combination with other elements. The production of hydrogen from these compounds requires energy. Hydrogen can be produced from any primary energy or fuel, such as coal, oil, natural gas, renewables such as biomass and by hydrolysis of water using electricity whose source can be sustainable (wind, solar etc.) (Winter, 2009). There are different hydrogen production techniques used in the industry depending on the energy source and the final application. The two most common techniques for small scale application are hydrocarbon reforming and ammonia cracking. Less common is pyrolysis of hydrocarbons into hydrogen and carbon in a water-free and air-free environment (Holladay et al., 2004).

2.1.1 Fuel cells

There are different types of fuel cells, developed and optimized for different purposes and environments, and each type has its particular fuel requirements. A very brief overview over the different requirements is given in Table 2-1.

Table 2-1: The different types of fuel cells currently in use, the role of the different fuel constituents and the specific requirements on fuel and fuel purity (Dicks, 2003)

Fuel constituent	Polymer Electrolyte Membrane Fuel Cells (PEMFCs)	Alkaline Fuel Cells (AFCs)	Phosphoric Acid Fuel Cells (PAFCs)	Molten Carbonate Fuel Cells (MCFCs)	Solid Oxide Fuel Cells (SOFCs)
H_2	Fuel	Fuel	Fuel	Fuel	Fuel
CO	Poison (limit = 10 ppm)	Poison	Poison (limit = 0.5 vol%)	Fuel[1]	Fuel[1]
CH_4	Inert	Inert	Inert	Diluent[2]	Diluent[2]
CO_2 and H_2O	Diluent	Poison[3]	Diluent	Diluent	Diluent
S-compounds	Few studies to date[4]	Unknown	Poison (limit = 50 ppm S)	Poison (limit = 0.5 ppm S)	Poison (limit = 1 ppm S)

[1] In reality CO reacts with H_2O initially producing H_2 and CO_2 via WGS

[2] A fuel in the internal reforming MCFC and SOFC. CH_4 reforms with H_2O to H_2 and CO faster than reacting as a fuel at the electrode.

[3] That CO_2 is a poison for the alkaline fuel cell, more or less rules out the use of this type of fuel cell with reformed fuels.

[4] Must be below detection limit.

Basically, the lower the operating temperature of the fuel cell, the more severe are the requirements in respect of catalyst poisoning, feed constituents and impurities and, consequently, the greater are the requirements on fuel processing and purification. For example, fuels fed to Phosphoric Acid Fuel Cells (PAFCs) need to be hydrogen-rich and contain only about 0.5 % CO or less. The fuel fed to Polymer Electrolyte Membrane Fuel Cells (PEMFCs) need to be essentially CO free while, in contrast, both the Molten Carbonate Fuel Cells (MCFCs) and the Solid Oxide Fuel Cells (SOFCs) are capable of utilizing CO through the WGS shift reaction that occurs within the cell. Sulphur is even a stronger poison for catalysts in most types of fuel cells. Purity requirements with respect to sulphur are, therefore, more stringent than with respect to CO. SOFCs and internal reforming MCFCs can also utilize methane as the fuel, whereas the other fuel cells cannot. It is still unknown whether or not PEMFCs can directly utilize some hydrocarbons, such as propane, even if that will result in poor performance (Dicks, 2003).

2.1.1.1 Polymer Electrolyte Membrane Fuel Cells (PEMFCs)

For the purpose of this review, only Polymer Electrolyte Membrane Fuel Cells (PEMFCs) are considered with more detail. These fuel cells are composed of a proton exchange membrane (most common material used is Nafion) acting as a conducting material. The surfaces on either sides of the membrane serve as the electrodes and typically a platinum catalyst is used on both sides of the membrane (Kolb, 2008).

PEM fuel cells typically operate at low pressure, just slightly higher than atmospheric pressure. There are two types of PEMFCs, namely, Low Temperature PEMFC (LT-PEMFC) and High Temperature PEMFC (HT-PEMFC). These cells differ with respect to the operating temperature and CO tolerance. LT-PEMFCs operate at temperatures between 80-100 °C, need a hydrogen rich feed and can only tolerate less than 10 ppm of CO, whereas HT-PEMFCs operate at temperatures between 100-120 °C, also need a hydrogen rich feed but can tolerate up to 1 vol% of CO. The low tolerance of CO in PEMFCs is due to the strong adsorption of the CO on the active sites of the platinum catalyst at the low temperatures applied that drastically reduces the number of active sites available for hydrogen adsorption. Depending on the type of PEMFC, the purity of the feed stream needs to be tailored to a low CO concentration (< 1%), if not, an effectively CO-free hydrogen stream (< 10 ppm) (Dicks, 2003).

PEM fuel cells must be supplied with humid feed streams. Yuan and Wang (2008) emphasize that "water balance and management are an important concern in PEM fuel cell systems control" and that "maintaining a perfect water balance during dynamic operation processes is crucial to fuel cell performance and lifetime". Full hydration of the membrane of the PEM fuel cell must be maintained at all times, since this strongly impacts on the performance of the cell and its lifetime. In contrast, a

non-optimal water balance, i.e., the presence of too little or too much water negatively affects the performance of a PEM fuel cell and its lifetime.

While state of the art PEM fuel cells require water vapour-saturated or almost saturated feed streams (Yuan & Wang, 2008), some of the more recent research in the field not only aims at developing fuel cells that are less sensitive towards varying or non-optimal water vapour levels in the feed streams but also at developing fuel cells for constant operation using significantly less humidity than water vapour-saturated feed streams (Conrad, 2010; Pintauro & Wycisk, 2008).

2.1.2 Fuel processing for fuel cells

Fuel processing may be defined as the conversion of the raw primary fuel into the fuel required by the fuel cell system. For LT-PEMFCs, this fuel needs to be hydrogen that is very pure with respect to CO, but may contain CO_2 and CH_4 and has to contain H_2O. A typical fuel processor for this application and the use of hydrocarbon as the primary fuel entails three major stages prior to the actual fuel cell. These are Steam Reforming (SR) which converts most of the primary fuel (hydrocarbons) to hydrogen-rich syngas, followed by a Water-Gas Shift (WGS) stage that converts most of the CO to CO_2 and H_2 using H_2O and that way produces more of the final H_2 fuel. In order to achieve high purity H_2 for LT-PEMFCs, the remaining CO is converted to either CH_4 by Selective Methanation (SELMETH), or to CO_2 by Preferential Oxidation (PROX). CH_4 and CO_2 are non-catalyst poisoning compounds with respect to PEMFCS. Schematic diagrams of fuel processors for the production of H_2 suitable for either high temperature or low temperature PEM fuel cells (< 1 vol% CO and < 10 ppm CO, respectively) are shown in Figures 2-1 (A) and (B). In an integrated systems, typical for small, mobile devices, the tail-gas from the fuel cell is used to feed the burner of the SR, since it still contains a significant percentage of H_2 (Dicks, 2003).

Steam reforming of hydrocarbons, preferentially methane (natural gas) is used in industry for hydrogen production. The basic reforming reactions of methane (CH_4) and other hydrocarbons (C_nH_m) are as follows:

$$CH_4 + H_2O \rightleftharpoons CO + 3H_2 \qquad \Delta H_{rxn,\ 25\ °C} = 206\ kJ\ mol^{-1} \qquad \textbf{rxn 2-1}$$

(Dicks, 2003)

$$C_nH_m + nH_2O \rightarrow nCO + \left(\frac{m}{2} + n\right)H_2 \qquad 206 > \Delta H_{rxn,\ 25\ °C} > 0\ kJ\ mol^{-1} \qquad \textbf{rxn 2-2}$$

(Ghenciu, 2002)

$$CO + H_2O \rightleftharpoons CO_2 + H_2 \qquad \Delta H_{rxn,\ 25\ °C} = -41.1\ kJ\ mol^{-1} \qquad \textbf{rxn 2-3}$$

(Dicks, 2003)

(A) Fuel processing for high temperature PEMFC

H_2O
CH_4 → SR → H_2-rich syngas → WGS → H_2-rich fuel gas → HT-PEM Fuel Cell

(B) Fuel processing for low temperature PEMFC

H_2O
CH_4 → SR → H_2-rich syngas → WGS → H_2-rich fuel gas → SELMETH → CO-free fuel gas → LT-PEM Fuel Cell

O_2 → PROX
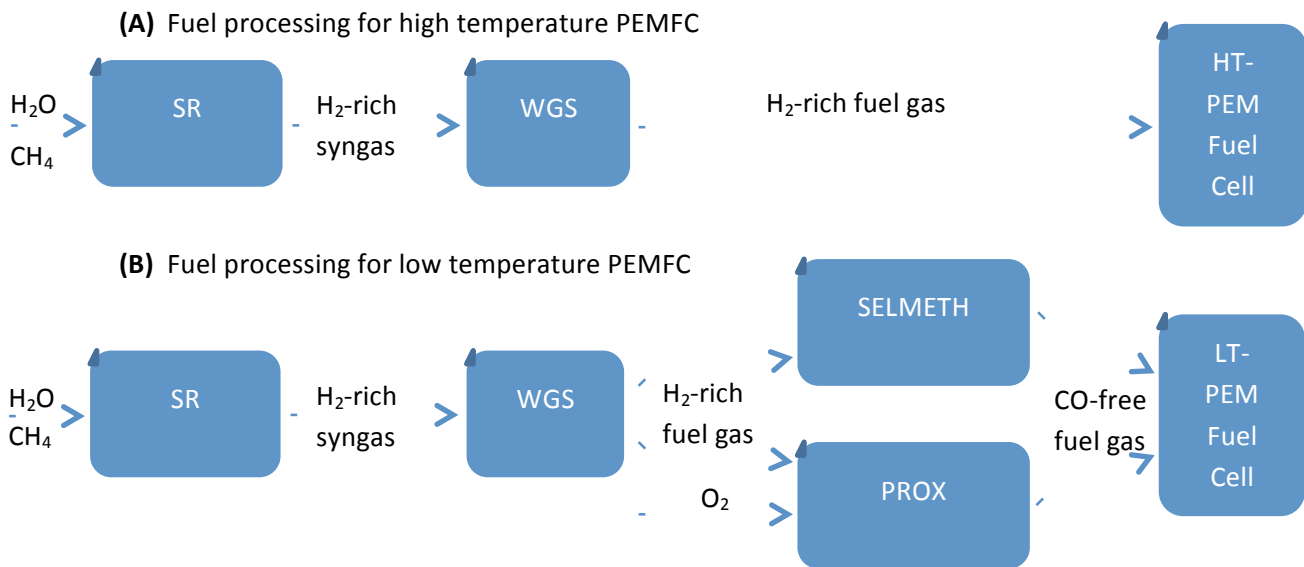
Figure 2-1: **Schematic diagrams of fuel processors for the production of H_2 from primary fuel CH_4 suitable for high temperature (A) and, with additional purification, low temperature PEM fuel cells (B).**

For large scale industrial hydrogen manufacture, the above conversions are carried over supported nickel catalysts at elevated temperatures and pressures, typically about 800 °C and 35 bar, respectively (Lloyd, 1996). Reactions 2-1 and 2-3 are reversible and equilibrium limited. Over a catalyst that is active for reactions 2-1 and 2-2, reaction 2-3 almost always occurs as well. This means that, if all of these reactions occur at the same time, an overall product gas mixture of CO, CO_2 and H_2, together with unconverted CH_4 and steam, will make up the SR reactor effluent stream (Dicks, 2003). Typically, the composition of the reformate produced is at or close to thermodynamic equilibrium distribution. The actual composition of the product is governed by the temperature of the reactor (actually the catalyst bed outlet temperature), the operating pressure, the composition of the dry feed gas, and the proportion of steam fed to the reactor. Thermodynamic data to determine the composition of the equilibrium product gas for different operating conditions is available (Lloyd, 1996). Figure 2-2 is an example, showing the effect of temperature on equilibrium composition of a steam reformer product.

With Reaction 2-1, there are three molecules of H_2 and one molecule of CO produced for every pair of CH_4 and H_2O molecules reacted. Le Chatelier's principle states that the equilibrium conversion will shift to the right (i.e. in favour of making H_2) if the pressure in the reactor is kept low. Therefore, high pressure will limit conversion of CH_4, since the number of molecules on the left side of the reaction equation is lower. In contrast, there is no effect of pressure on the equilibrium distribution in the WGS reaction (reaction 2-3), since it is equimolar.
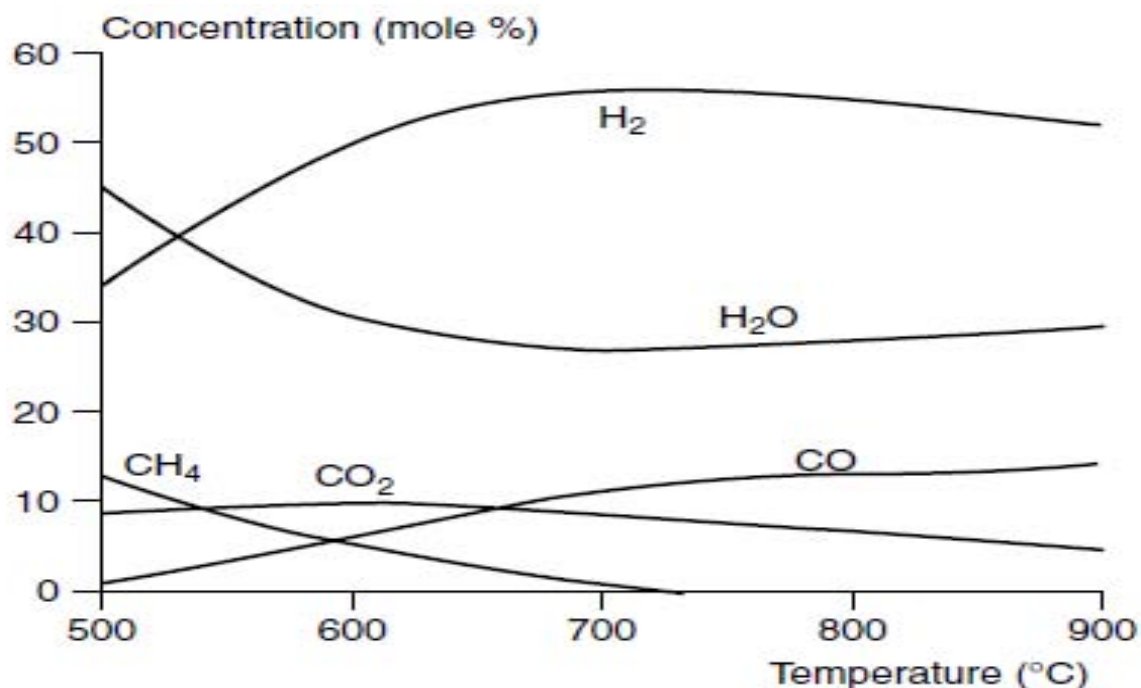
Figure 2-2: **Equilibrium concentrations of methane steam reforming product constituents as a function of temperature at 1 bar and 5:1 molar $H_2O:CH_4$ feed ratio (Lloyd, 1996)**

Another feature of reactions 2-1 and 2-2 is that they are endothermic, while the simultaneous WGS reaction is moderately exothermic. Consequently, CH_4 conversion and H_2 formation are thermodynamically more favoured at elevated temperatures and low pressures. Figure 2-2 shows that at low pressures as typically applied in a PEM fuel processing train, temperatures above 700 °C are required to achieve high or almost total CH_4 conversion. Steam also affects the equilibrium for all of reactions 2-1, 2-2 and 2-3. According to Le Chatelier's principle, the forward reaction will be favoured if the percentage of steam is increased. Therefore, producing more H_2 requires more steam. In practice steam/carbon (e.g. H_2O/CH_4) ratios of more than 2 are applied (Lloyd, 1996).

Elevated temperatures in the SR stage are counter-productive for producing maximum H_2 yields, since the equilibrium for the simultaneous WGS reaction (reaction 2-3) is far to the left of the equation at these temperatures, but needed for the 'complete' conversion of CH_4. The main purpose of the proceeding WGS stage is, therefore, to produce more H_2 as it converts the remaining CO to CO_2 and H_2O to H_2. This is achieved over a catalyst that promotes WGS but not methanation and is operating at lower temperature so that the WGS equilibrium is shifted to the right. After the WGS stage, the concentration of the remaining CO in the wet gas is usually < 1 mol% (Kolb, 2008).

The water-gas shift stage and reaction was the subject of this thesis. A detailed review of the respective literature is given in Section 2.2: Water-Gas Shift Reaction.

For low temperature PEM fuel cells, removal of the carbon monoxide remaining after the WGS reactors is essential, since the Pt catalyst in these cells can only tolerate CO contents < 10 ppm (Kolb, 2008). This is usually done in one of two ways, namely Preferential Oxidation (PROX) or Selective Methanation (SELMETH).

In the PROX reactor O_2 is added to the WGS stage outlet stream that reacts with the CO over a noble metal catalyst at a temperature of about 100 °C according to the following reaction,

$$CO + 0.5O_2 \rightarrow CO_2 \qquad\qquad \Delta H_{rxn, 25\,°C} = \text{-284 kJ mol}^{-1} \qquad \textbf{rxn 2-4}$$
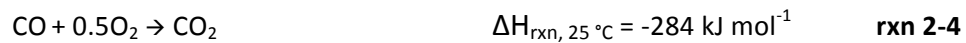
which removes the CO as desired. Catalysts are available, over which the level of CO can be reduced to less than 10 ppm (Kolb, 2008). CO_2 neither poisons the fuel cell catalyst nor are the WGS and the PROX reaction reversible in the fuel cell.

A major disadvantage of the PROX reaction is that the catalysts are not only selective to adsorbing and oxidizing CO, but also H_2. This undesired reaction takes place according to reaction 2-5:

$$H_2 + 0.5O_2 \rightarrow H_2O \qquad\qquad \Delta H_{rxn, 25\,°C} = \text{-244 kJ mol}^{-1} \qquad \textbf{rxn 2-5}$$
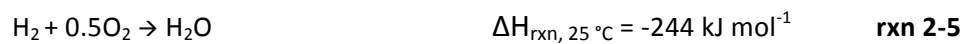
This undesired side reaction not only consumes target product H_2 but can also lead to water content management issues (Zalc & Löffler 2002). The biggest problem of employing PROX is, however, the potentially explosive nature of this stage due to the mixture of H_2, CO and O_2, at elevated temperature, whose properties can be above ignition limits, and the presence of a noble metal oxidation catalyst. Measures must be taken to ensure that an explosive mixture is not produced. This is particularly a problem in cases where the flow rates of the gases in the system are frequently (or constantly) changing, such as with PEM fuel cells on portable devices (Dicks, 2003).

Selective Methanation (SELMETH) of CO is an approach that eliminates the risk of producing explosive gas mixtures. The SELMETH reaction is the reverse of the steam reforming reaction (i.e. equation 2-1) according to equation 2-6,

$$CO + 3H_2 \rightarrow CH_4 + H_2O \qquad\qquad \Delta H_{rxn, 25\,°C} = \text{-206 kJ mol}^{-1} \qquad \textbf{rxn 2-6}$$

The obvious disadvantage of the method is that 3 molecules of H_2 are consumed per molecule of CO removed. As a result, the efficiency of the fuel processor is reduced. However, the quantities involved are small and SELMETH can reduce CO content to the level that is acceptable for low temperature PEM fuel cells. The methane that is produced does not poison the fuel cell. In addition, in an integrated system (Dicks, 2003), it can still serve as a fuel for the burner of the reformer (depending on the technology used). Catalysts are available, which promote this reaction to proceed

at about 200 °C without reacting the CO_2 present, so that the carbon monoxide levels eventually are lower than 10 ppm (Dicks, 2003).

2.2 Water-Gas Shift Reaction

WGS reaction is an equilibrium limited reaction that catalytically converts CO and H_2O to CO_2 and H_2. The reaction proceeds according to the following equation

$$CO + H_2O \rightleftharpoons CO_2 + H_2 \qquad \Delta H_{rxn,\ 25°C} = -41.1\ kJ/mol$$

(Lloyd, 1996)

The reaction is equimolar and also mildly exothermic. Therefore, the equilibrium constant decreases as temperature increases but the position of equilibrium is not affected by pressure. The reaction is carried out industrially for the production of H_2 mostly for ammonia synthesis (Lloyd, 1996). Since the equilibrium of the reaction favours the desired product (H_2) at low temperature, while high temperatures increase the reaction rate, a trade-off between reaction rate and conversion is the ideal solution. Hence, two reactors in series, operating at different temperatures, are normally employed for this reaction in industry. The first stage operates at high temperature of about 400 °C in order to achieve high rates and to convert water and most of the CO present to H_2 and CO_2. This stage is referred to as the High Temperature Shift (HTS) stage. The second stage operates at low temperature of about 200 °C, in order to achieve high conversions of the remaining CO and maximise H_2 yields. This stage is referred to as Low Temperature Shift (LTS) stage. Excess H_2O is applied to push CO conversion further (Wheeler et al., 2004).

Industrial HTS operates in a temperature range of 310-450 °C over an iron oxide/chromium oxide catalyst. This catalyst is typically made up of 90 wt% iron oxide and 10 wt% chromium oxide, but this ratio can vary from one manufacture to another. In industry, the HTS stage typically operates at a pressure of around 30 bar, with a steam/dry gas molar ratio of between 1 and 2, at a dry gas space velocity of around 10,000 per hour (Lloyd, 1996) and for 2-5 years until the relatively slow thermal sintering that occurs has caused a decrease in activity that is no longer acceptable (Rhodes et al., 1995). Since WGS is equilibrium limited and exothermic, the CO concentration can only be reduced to about 3 % at the high operating temperatures required for the HTS catalyst to be sufficiently active (Rhodes & Hutchings, 2003).

Industrial LTS operates at milder conditions and the operational temperature ranges between 200 and 230 °C. LTS uses a copper/zinc oxide/alumina catalyst with the industrial constituents present in approximately 1:1:1 molar ratio. In industrial operation, the LT WGS stage typically operates at a pressure not exceeding 40 bar (Ladebeck & Wagner, 2003) and a dry gas space velocity

of around 10,000 m^3/(h.t$_{cat}$) for 2-4 years. The catalyst suffers from rapid deactivation by sintering at temperatures above 240°C and is highly sensitive to sulphur poisoning. Therefore, it can only be used with a sulphur-free feed (Rhodes et al., 1995). Since CO conversion is more thermodynamically favoured at the low temperatures applied in the LTS stage, CO concentration can be further reduced to about 0.1-0.3 % (Lloyd, 1996).

2.2.1 Thermodynamics of WGS

As outlined above, reaction temperature is the important variable in WGS conversion. WGS is mildly exothermic with ΔH$_{rxn}$ of -41.1 kJ/mol (Rhodes et al., 1995). The value of the equilibrium constant,

$$K_p = \left(p_{H_2} \cdot p_{CO_2}\right) / \left(p_{H_2O} \cdot p_{CO}\right)$$

decreases with increasing temperature and conversion is thus equilibrium limited at higher temperature (Rhodes et al., 1995), see Figure 2-3. While, the reaction proceeds faster at high temperatures, Le Chatelier's principle suggests, see Figure 2-3, that in order to maximize conversion (i.e., H$_2$ formation), low operating temperatures are required.
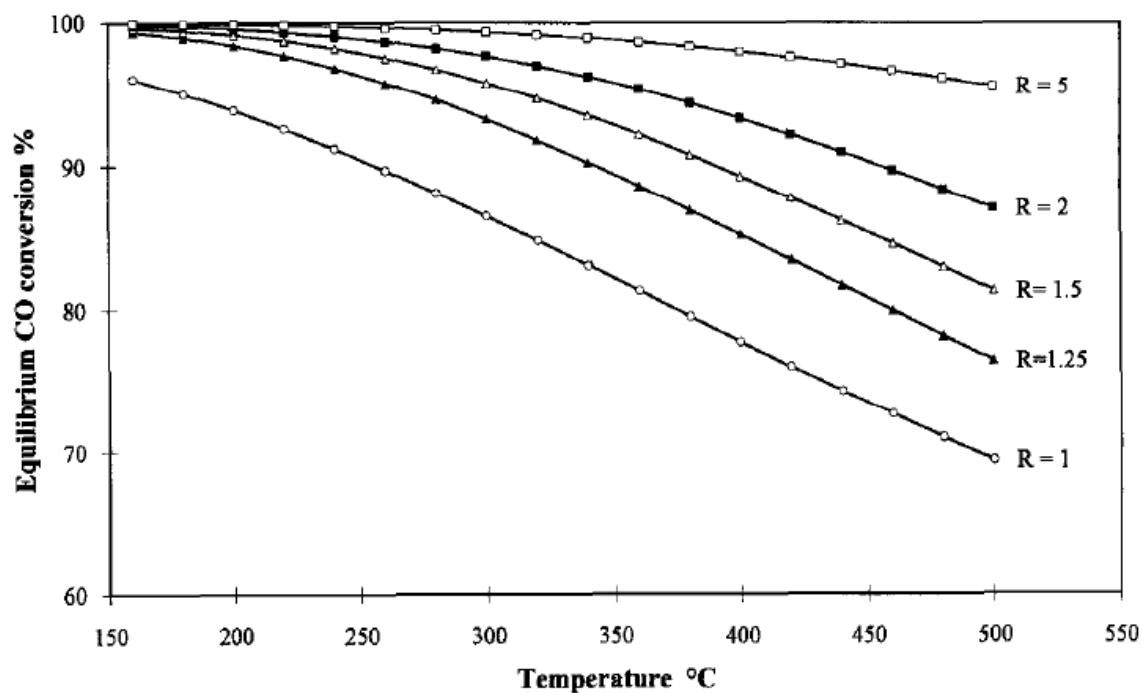
Figure 2-3: **WGS equilibrium conversion of CO at different temperatures and steam to carbon monoxide (S/CO) molar ratios R (Xue et al., 1996)**

Feed composition affects the equilibrium conversion of CO as well. This is due to the feed's steam to carbon monoxide (S/CO) ratio that drastically affects equilibrium conversion. An increase in the S/CO ratio results in an increase in the equilibrium conversion of CO (Xue et al.,, 1996) as shown by the

effect of 'R' in Figure 2-3. Industrially, the HTS stage is operated at a S/CO molar ratio range of 2-14 in order to achieve high equilibrium conversion of CO (Lloyd, 1996).

2.2.2   Proposed mechanism

Over the years, different reaction mechanisms for the WGS reaction have been proposed.

2.2.2.1 Mechanism over base metal supported catalysts

Two mechanistic pathways have been proposed based on either (a) an associative mechanism or (b) a regenerative mechanism. Both mechanisms were first proposed by Armstrong and Hilditch in 1920 (Rhodes et al., 1995).

The associative mechanism was developed based on data gathered from a copper chromite catalyst (Rhodes et al., 1995). The mechanism involves the adsorption of CO and H_2O onto the catalyst surface. Once adsorbed, an intermediate of unspecified structure forms and subsequently decomposes into both CO_2 and H_2 as products (Reaction 2-7).

$$CO + H_2O \rightarrow (intermediate) \rightarrow CO_2 + H_2 \qquad \textbf{rxn 2-7}$$

The regenerative mechanism involves a cyclic change in the oxidation state of the catalytic material that is affected by the reactants (Rhodes et al., 1995). In its simplest form, it can be understood as the lysis of water on the reduced catalyst surface to produce H_2, leaving the catalyst surface oxidised. CO then reduces the catalyst surface to form carbon dioxide so that the catalyst surface returns to its original reduced 'pre-reaction' state (Reactions 2-8 and 2-9).

$$H_2O + Red \rightarrow H_2 \; + \; Ox \qquad \textbf{rxn 2-8}$$

$$CO \; + \; Ox \; \rightarrow CO_2 + Red \qquad \textbf{rxn 2-9}$$

2.2.2.2 Mechanism over noble metal supported catalysts

A typical WGS reaction mechanism on noble metal supported catalysts can simply be described as follows (Sun et al., 2005): CO adsorbs on the surface of the noble metal. H_2O adsorbs dissociatively on the surface of the support and upon forming H_2 as a product that desorbs, the surface of the support is left oxidized. The adsorbed oxygen atoms migrate to the noble metal site and react with the adsorbed CO to form CO_2 which desorbs. The entire process can be seen as a surface reaction of two species, H_2 and CO, adsorbed on two separate sites, namely the support and the metal site.

An analogous mechanism, as expressed by reaction equations 2-10, 2-11 and 2-12 was suggested by Bunluesin et al., (1998) when the oxygen-storage properties of ceria-supported Pt, Pd, and Rh catalysts were studied (Θ = vacant surface site):

$$CO \quad + \quad \Theta \quad = CO_{ad} \qquad\qquad\qquad \textbf{rxn 2-10}$$

$$H_2O \ + Ce_2O_3 = 2CeO_2 + H_2 \qquad\qquad\qquad \textbf{rxn 2-11}$$

$$CO_{ad} + 2CeO_2 = Ce_2O_3 + CO_2 + \Theta \qquad\qquad \textbf{rxn 2.12}$$

Germani & Schuurman (2006) proposed a mechanism that comprises the formation of a carboxyl complex by the reaction of CO (adsorbed on the surface of platinum) with a surface hydroxyl group on the surface of ceria. Once a neighboring platinum site becomes free, the carboxyl complex reacts with a second hydroxyl group on the surface of ceria to form adsorbed hydrogen and carbon dioxide which desorb as both H_2 and CO_2.

2.3 Reactor Development

Different reactor types for WGS have been studied and used in industry depending on the application. For the fuel processor of portable fuel cell power generation devices, utilization of microchannel reactors has been identified as a means for process miniaturization (Atkinson & McDaniel, 2010; Holladay et al., 2004;Kolb et al., 2005a; Kolb & Hessel, 2004; Kolb, 2008; Parak, 2011).

2.3.1   Microchannel reactors

Microchannel reactors are compact reactors that have channels with diameters in the sub-millimetre to millimetre range. On the walls of these channels the catalyst is deposited in the form of a thin layer. These small channels and thin layers enable more rapid mass transfer between the fluid phase and the catalyst layer, inside the catalyst layer itself, and heat is dissipated more quickly than in conventional reactors, which happen to have larger diameters. The use of microchannel processing makes it possible to greatly intensify chemical reactions enabling them to occur at rates 10 to 1000 times faster than in conventional reaction systems (Atkinson & McDaniel, 2010). The major techniques applied and relevant steps are described in this section.

2.3.1.1 Advantages and disadvantages of microchannel reactors

Microchannel reactors have several advantages specific to either laboratory or industrial application. In laboratory applications, microchannel reactors provide flexible reactor designs due to size reduction and, as a kind of high throughput design for catalyst testing, by possible parallel arrangement of multiple reactors that allows to obtain a large quantity of data faster and at lower operational costs than with standard laboratory methods (Kolb & Hessel, 2004). In industrial applications, the reduction in size helps to reduce the amount of time required when scaling up from laboratory to industrial scale, since microchannel reactor scaling up is just done by stacking (numbering up) of many laboratory scale microchannel reactors. This helps to avoid or reduce costs for redesign and pilot plant operation (Bayer et al., 2005).

Other advantages of microchannel reactors compared to conventional reactors arise from their unique process intensification capabilities. One of the focal aspects giving microchannel reactors superior performance is an increased surface-to-volume ratio for the catalyst of between 500 and 50 000 m^2/m^3. The advantages that arise from these high surface-to-volume ratios include superior mass and heat transfer properties and improved hydrodynamic transport flow patterns. The exceptional properties allow safe operation also if reactions are highly exothermic, whilst securing less deviation from optimal temperatures (Parak, 2011). Higher conversions at higher space velocities than with conventional reactors are also achievable for various reactions, due to the high mass transfer rates possible in microchannel reactors (Atkinson & McDaniel, 2010).

The biggest disadvantage of using microchannel reactors is fouling, since that can easily lead to reactor clogging due to the small channel dimensions. This fouling in microchannel reactors occurs mostly with reactions that are prone to coking. Carbon forming can block the microchannels and effectively cause a loss of activity. Increased blocking of channels also causes an increase in pressure drop across the reactor and possible clogging of equipment, which eventually leads to a rundown of the process (Holladay et al., 2004).

2.3.1.2 Micro-structuring

When manufacturing microchannel reactors, selection of the material of construction must take into account temperature and pressure range of the intended application, corrosion, thermal properties and to a lesser extend the electrical properties (Brandner, 2012). Reactors can be made from many materials such as stainless steel, aluminium alloys, copper, silver or titanium. Stainless steel has been used for some time to fabricate microchannel reactor plates due to the mechanical stability and robustness of the material at high temperatures (Kolb & Hessel, 2004). Iron-chromium alloys that completes stainless steel are particularly advantageous due to the formation of an oxide layer on the surface upon a thermal pre-treatment process, in which the layer acts as an anchor for the coated catalyst (Zapf et al., 2003)

There are numerous techniques applied to form the microchannels on the plates. Techniques such as micro-milling, electro-discharge machining, wet chemical etching, punching, embossing, laser micro-machining and sintering are the preferred methods for the micro-structuring of the plates. Hessel et al. (2005) give detailed information for each method applied for mass production.

For the purpose of this review, only wet chemical etching is explained in some detail, since this was the method applied for the micro-structuring of the stainless steel plates utilised. In wet chemical etching, a photo-resist is applied for masking and an aqueous iron (III) chloride solution is applied for etching. Wet etching is the technique of choice, because it is possible to produce a relatively wide

range (100 μm - 600 μm) of channel depths (Kolb & Hessel, 2004). However, the chloride in the etching solution has been found to migrate onto and into the stainless steel of the plates, eventually leading to catalyst deactivation. It is because of the high chloride residues that a thorough pre-treatment of the wet-etched microchannel plates must be done prior to catalyst application in order to reduce the chlorine content.

2.3.1.3 Pre-treatment of microchannel plates

Various microchannel plate pre-treatment methods have been studied (Zapf et al., 2003). It revealed that plate calcination in air at 800 ˚C greatly reduced the chlorine content in the stainless steel microchannel plates. Another favourable outcome of the calcination process is the formation of an oxide layer on the channels walls that greatly helps to improve the adherence of the catalyst coating on these walls.

2.3.1.4 Catalyst coating

Unlike conventional fixed-bed reactors where the catalyst is packed into the reactor as a bed, microchannel reactors require the catalyst to be incorporated by deposition onto the walls of the microchannels.

Several coating techniques like suspension coating (wash-coating), sol-gel deposition, electrophoretic deposition, impregnation, electrochemical deposition and electroplating, vapour deposition etc. have been studied and applied (Meille, 2006). One of the preferred coating techniques is wash-coating, i.e. the application of an aqueous suspension, with additives, of fine catalyst particles. This technique allows both, coating of a catalyst carrier and coating of a ready-made catalyst. Wash-coating can be applied on ceramic or metallic monoliths as well as on stainless steel or aluminium plates (Kolb, 2008).

The wash-coating suspension consists of the catalyst in powder form and deionised water. The inclusion of additives in the suspension optimises the properties with respect to the quality of the washcoat with regard to uniformity and adhesion. A detailed description of the procedure suggested by Zapf et al. (2003) is given in Section 4.2.2: Wash-coating method. Wash-coating, optimised, was found to give high quality catalyst coatings with a good coating adhesion and a uniform catalyst distribution between various channels (Zapf et al., 2006).

2.3.1.5 Uniformity of the coating

The thickness of the coating must not differ between the walls and the bottom of the microchannels. This requires (i) a stable wash-coating suspension and (ii) optimized suspension viscosity. In order to get a stable suspension, the pH must be adjusted, so that it differs from that of the isoelectric point of the solid particles (which otherwise would not be charged and precipitate).

The typical additives applied for the purpose are organic acids and bases (such as acetic acid) that decompose upon calcination (Zapf et al., 2003).

Suspension viscosity determines whether or not the suspension sticks to the channel walls upon drying (resulting in a thicker catalyst layer on the walls), flows down to the bottom of the channels (resulting in a thicker catalyst layer at the bottom) or, if optimized, resulting in a rather uniform thickness of the layer. Suspension viscosity can be adjusted by a number of means such as concentration and particle size or size distribution (if variable), as well as additives such as dissolved polymers (e.g. polyvinyl alcohol, PVA). The latter also acts as a temporary binder during drying (Zapf et al., 2003). SEM images of cross-cut, coated microchannel plates can reveal the uniformity/ non-uniformity of the coating.

2.3.1.6 Adhesion of the coating

Adhesion is based on particle-wall and intraparticle attraction, that is, the higher the mutual contact area, the higher the binding forces. The major contribution to good adhesion is said to come from the thermal pre-treatment of the microchannels plates, which generates a thin oxide layer that matches the chemical nature of the wash-coat (Zapf et al., 2006). Particle size also plays a role, since with small particles the mutual contact area is higher (Truter, 2011).

Adhesion can be probed by a 'drop' test (developed by Zapf et al. 2006) for which the coated microchannel plates were mounted on a metal body which is allowed to fall onto a steel plate several times. A detailed description of the method and the equipment used is given in section 4.2.6.1 (Catalyst adhesion). Quality of adhesion is evaluated based on the two criteria. The first criterion is based on SEM images of the coated catalyst after the 'drop' test and whether they show fully coated channels and crack-free coating. The second criterion is the weight loss by the 'drop' test that must be less than 1 % of the coating (Zapf et al., 2006).

2.4 WGS Catalysts

Until recently, the shift reactors in fuel cell systems of the kilowatt scale have been using industrial Fe/Cr and Cu/Zn/Al catalysts, but the typical inconstant operation of these systems, namely transient and on/off operation, presents some operational difficulties, (Ladebeck & Wagner, 2003) and this is also a safety hazard as the catalysts in their reduced state are pyrophoric and may ignite when exposed to air (Dicks, 2003). The ideal properties of WGS catalysts used to produce hydrogen for small scale fuel cell operations differ from those for the traditional industrial applications. Also, for small scale fuel cells and fuel processing applications, simplicity of design and operation is a key factor (Ladebeck & Wagner, 2003). Table 2-2 outlines the requirements for WGS catalysts as part of the fuel processing chain for small scale transient operation fuel cell units.

Table 2-2: **WGS catalyst requirements for fuel processing application for small scale, transient operation fuel cells (Ladebeck & Wagner, 2003)**

Requirement	Remark
Volume reduction	Critical for mobile but not for stationery application
Weight reduction	Critical for mobile but not for stationery application
Low cost	Critical
No catalyst reduction required	Critical
Air tolerant	Critical
Water tolerant	Critical
Poison tolerant	Desirable

The focus of research in this field is on novel catalysts that are able to operate at high space velocities and low temperatures. Several materials have been studied and are being studied including base metal and precious metal catalysts (Hilaire at el., 2001; Farrauto et al., 2003; Ladebeck and Wagner, 2003). Base metal based catalysts are cheap and have higher activity than noble metal based catalysts per unit mass of catalyst but tend to have lower sulphur tolerance, are less stable in air (some are pyrophoric) (Dicks, 2003).

Compared to the industrial use of WGS catalyst, the requirements for WGS catalysts in small scale and typically transient fuel processing for fuel cells are different. Industrially, Fe/Cr and Cu/Zn/Al catalysts are applied whose oxidic precursors are reduced before operation by a slow and controlled reduction process followed by long period of uninterrupted operations. Upon interruption or shutdown, the reactor must be purged with inert gas to remove the wet feed and product gas from the catalyst bed to prevent condensation of the steam carried with upon cooling down and catalyst reoxidation. In contrast, in small scale and transient fuel processing changes of operational conditions and frequent shutdown and cooling/ condensation, even occasional exposure to air are common and must not lead to reoxidation, ignition or other damage to the catalyst (Ladebeck & Wagner, 2003).

Similar to conventional base metal catalysts, supported noble metal catalysts have been known to be active for the WGS reaction for many years (Ladebeck & Wagner, 2003). Noble metals are known to be resistant to corrosion and oxidation in moist air, unlike most base metals. Noble metal based catalysts, therefore, meet the requirements for WGS catalysts to be applied in small, transient

operation fuel processing chains, namely insensitive to /stability against air, moist, condensation and being non-pyrophoric. Noble metals are considered to be (in order of increasing atomic number) ruthenium (Ru), rhodium (Rh), palladium (Pd), silver (Ag), osmium (Os), iridium (Ir), platinum (Pt) and gold (Au). Noble metals tend to be precious, due to their scarcity in the Earth's crust.

2.4.1 Activity of base metal and noble metal based WGS catalysts

Radhakrishnan et al. (2006) studied the activity of various noble metals (Pt, Pd, Ru, Rh, Ir and Au) on ceria-zirconia oxide supports in WGS reaction under both high temperature and low temperature shift conditions that simulated the steam reformate stream of both shifts. The supported Pt catalyst gave the highest activity on a per noble metal basis, with overall activity ranking found to be as follows:

$$Pt > Rh > Ru = Pd > Ir > Au$$

However, both rhodium and ruthenium supported catalysts were found to be prone to methanation.

Ghenciu (2002) compared the performance of a Johnson Matthey Pt-containing WGS catalyst to a Pt/CeO$_2$ catalyst with the same noble metal content and to a conventional Cu/ZnO-Al$_2$O$_3$ low temperature WGS catalyst converting a synthetic reformate containing 11.4 mol% CO (dry) at identical space velocities (per total mass of catalyst) as shown in Figure 2-4. At the lowest temperatures (below 270 °C) the base metal catalyst, per unit mass of catalyst, was most active. This was no surprise as the commercial Cu/ZnO-Al$_2$O$_3$ catalysts are known and designed for to be very active at low temperatures. Johnson Matthey Pt-containing WGS catalyst was found to be more active than the two other catalysts from 270 °C onwards. Pt/CeO$_2$ was also found to be more active than the commercial Cu/ZnO-Al$_2$O$_3$ catalyst, but only so at temperatures above 350°C.

Other PGM based, non-pyrophoric catalysts have been developed for even lower temperature operation. One of the novel Johnson Matthey WGS catalysts has been tested in their fuel processor and has been found to also be active under 'transient' system conditions, with no decrease in activity for more than 1500 h at 250–260 °C (Ghenciu, 2002). With this performance and durability, WGS can be conducted in one single stage by Johnson Matthey's fuel processor, which translates into a large reduction in reactor volume compared to using a commercial Cu/ZnO-Al$_2$O$_3$ catalyst (Ghenciu, 2002).

Brooks et al. (2002) compared the activity of microchannel reactor coated base metal and noble metal catalysts using a low shift reformate stream feed with 4.6 mol% CO and steam to dry gas molar ratio of 0.5 (see Figure 2-5). The two catalysts compared were the Süd-Chemie Cu-Zn low temperature WGS catalyst labelled T2650 and the Süd-Chemie precious metal/CeO$_2$ catalyst labelled PMS5.
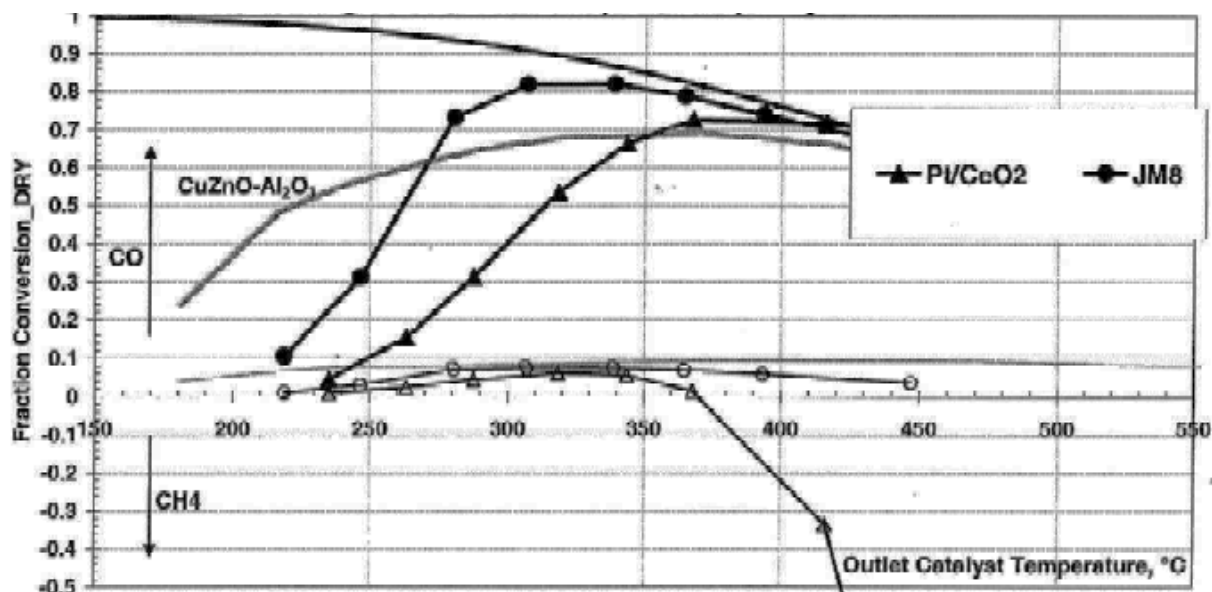
Figure 2-4: **Performance of a Johnson Matthey Pt-containing WGS catalyst compared to a Pt/CeO$_2$ catalyst with the same metal content and a conventional Cu/ZnO-Al$_2$O$_3$ low temperature WGS catalyst converting synthetic reformate containing 11.4 mol% CO at space velocity of 67,500 cc/g$_{cat}$/hr (dry). Values < 0 on the graph indicate formation of CH$_4$ and values > 0 indicate CO conversion (Ghenciu, 2002)**

PMS5 was found to give significantly higher CO conversion than T2650 at even higher gas hourly space velocity. T2650 is industrially operated only at low temperatures between 200 and 240 °C (Rhodes et al., 1995), since it starts sintering if being exposed to higher temperatures.

Germani et al. (2005) also confirmed that Pt/CeO$_2$ coated catalysts are active for WGS reaction from temperatures as low as 250 °C onwards.

The effect of the support on the activity of platinum catalysts was investigated by Rosa et al. (2006). Activities of alumina, ceria, titania and mixed ceria/titania supported catalysts (all containing 0.5 wt-% of platinum) were compared (see Figure 2-6). The activity ranking was found to be as follows (Rosa et al., 2006):

<center>ceria/titania > titania > ceria > alumina</center>

The ceria/titania based catalyst was also claimed to be more stable than the others after having operated for about 100 hours at 375 °C (648 K). However at this temperature, CO conversion could have been too close to or at equilibrium conversion (as shown in Figure 2-6) to clearly show the stability of the catalyst, especially since the experiment was ran for a rather short time.
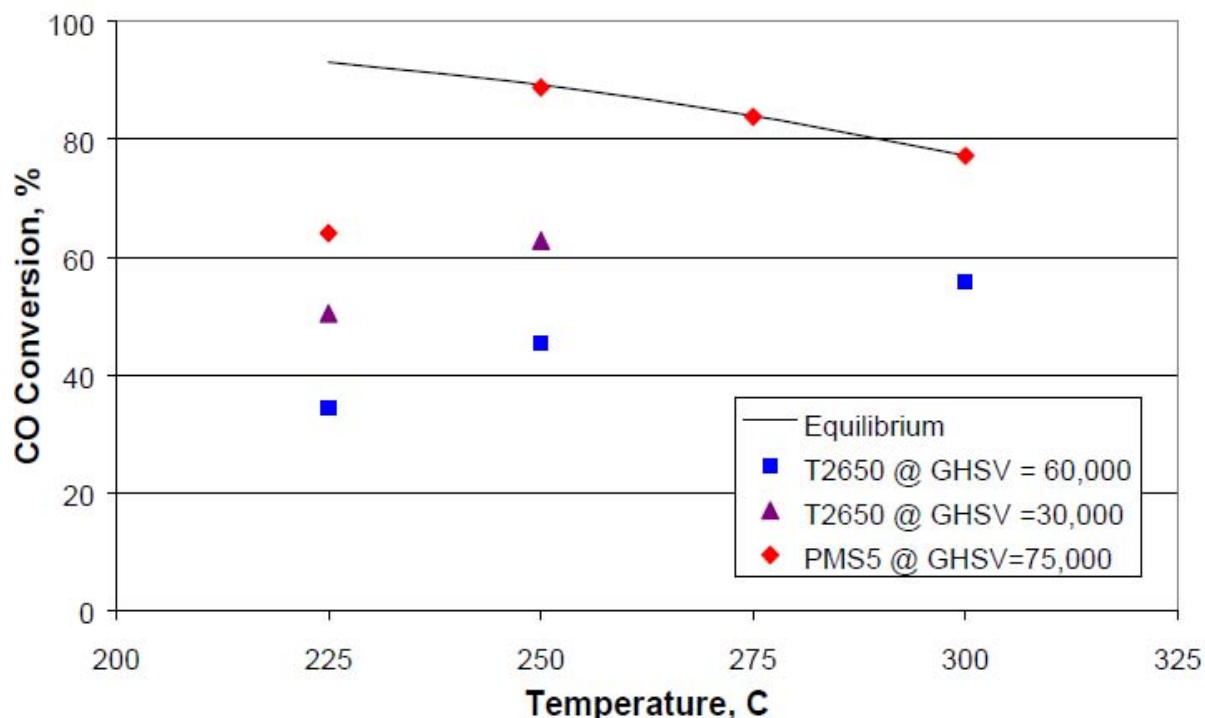
Figure 2-5: Performances of Süd-Chemie Cu-Zn catalyst T2650 and Süd-Chemie precious metal/CeO₂ catalyst PMS5 using low shift reformate stream feed with 4.6 mol% CO and steam to dry gas molar ratio of 0.5 (Brooks et al., 2002)

The activity of a Pt/CeO₂ catalyst for the WGS reaction was also found by Farrauto et al. (2003) to be approximately 15 times higher than the activity of a Pt/Al₂O₃ catalyst at identical Pt loadings. Germani et al. (2005) tested Pt/CeO₂/Al₂O₃ WGS catalysts in microchannel reactors, containing between 0.8 and 1.4 wt.% platinum and between 8 and 20 wt.% ceria, with the balance being alumina. The catalyst containing 1.4 wt.% platinum and 8.3 wt.% ceria showed the highest activity.

Kolb et al. (2005b) varied the platinum content of their Pt/CeO₂/Al₂O₃ wash-coated catalysts between 1 and 5 wt.%, while the ceria content ranged between 6 and 40 wt.%. The optimum platinum content was found to be between 3 and 5 wt.%, while the optimum ceria content was between 12 and 13 wt.%.

2.4.2   Stability of base metal and noble metal based WGS catalysts

Zalc et al. (2002) stated that the stability of Pt/CeO₂ catalysts is insufficient for fuel processing applications due to rapid catalyst deactivation. However, Zalc et al's conclusion is based on 70 hours on stream experiments that may just have covered the often observed initial settling in period but not shown whether or not activity stabilizes after longer time on stream. Johnson Matthey Pt/CeO₂ catalyst, despite showing high initial activity in the temperature range between 325 and 400 °C with real reformate, deactivates over an extended time on stream (Ghenciu, 2002).
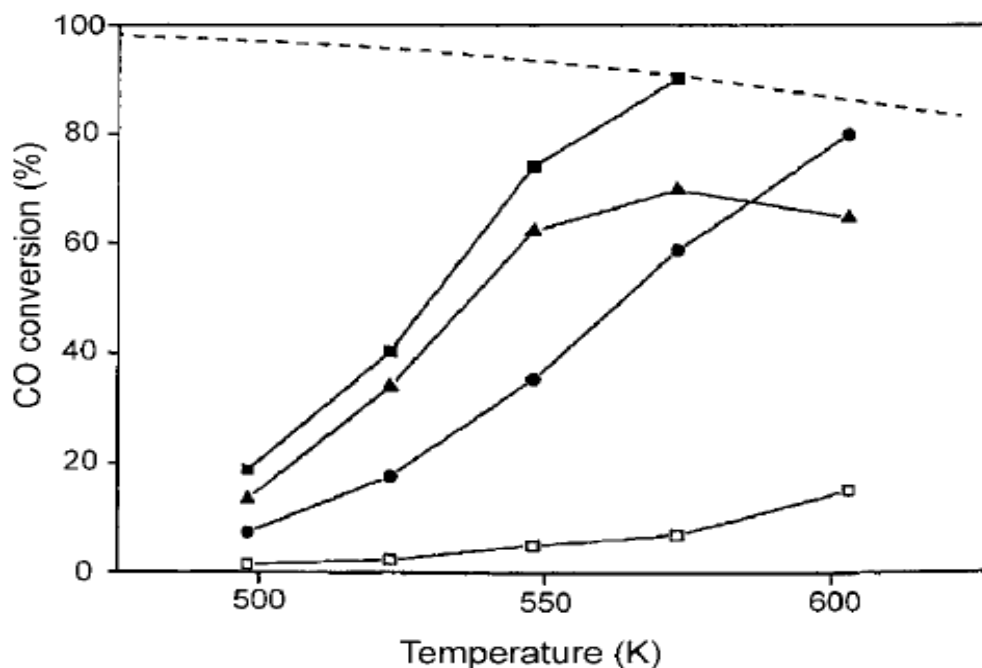
Figure 2-6: WGS conversion of model syngas over supported platinum catalyst (0.5 wt% Pt). Supports (□) alumina;(●) ceria;(▲) titania and (■) ceria/ titania with feed: 28 vol.% H_2, 0.1 vol.% CH_4, 4.4 vol.% CO, 8.7 vol.% CO_2, 29.2 vol.% N_2, 29.6 vol.% H_2O; SV = 21,200 ml/(h. g_{cat}) (Rosa et al., 2005)

Choung et al. (2005) reported activity and stability gains of $Pt/CeO_2/ZrO_2$ catalysts when adding rhenium. However, the stability of this catalyst was only tested for 60 hours. Kolb et al. (2007) reported stable performance of Pt/CeO_2 catalyst coatings in microchannel reactors on HT WGS duty of about 1000 hours on stream.

Work done at Nextech on different Pt/CeO_2 catalyst formulations showed that certain promoter or dopants helped with stability issues (Swartz et al., 2003). Three different Pt/CeO_2 catalysts of the same metal content were tested under identical conditions. It was found that promoted catalysts were not only more active, but also more stable compared to the non-promoted samples. Figure 2-7 shows the activity of these non-promoted catalysts , sample (B), constantly and rather rapidly deactivating over time-on-stream right from the beginning of the experimental run while promoted samples (C) and (D) hardly do so. However, the paper does not disclose the nature of the promoters added.

Deactivation of Pt/CeO_2 WGS catalysts was found to be related, amongst others, to the growth of the ceria crystallites over extended time on stream, which decreases the total BET surface area of the catalyst and also impairs the Pt dispersion in that this may have blocked-off some of the platinum particles (Ghenciu, 2002).
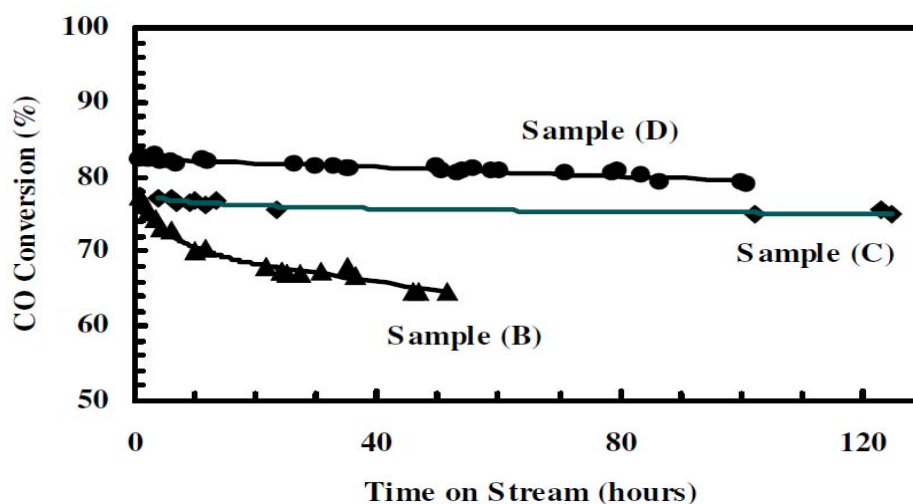
Figure 2-7: WGS activity versus time-on-stream for three Pt/ceria (1 wt% Pt) catalysts, non-promoted sample (B) and promoted samples (C and D), compared under identical testing conditions (feed composition: 8 mol% CO, 12 mol% CO_2, 32 mol% H_2, 31 mol% He, and 17 mol% H_2O, T = 280 °C, SV ~ 144,000 cc/g-hr) (Swartz et al., 2003)

Liu et al. (2005) and Ghenciu (2002) suggested the formation of carbonate-like species over both Pt and ceria as the possible cause for deactivation and showed that no sintering of the Pt particles occurred. Liu et al. (2005) also investigated the performance of Pt/CeO_2 catalysts after having been exposed to a typical reformate simulating start, shutdown (cool down) and re-start of a fuel processor system (for details of the procedure applied, see figure caption of Figure 2-8). Significant aging of the catalyst had occurred after just 5 minutes of exposure to the low temperature of 60°C under wet reformate, as shown in Figure 2-8. This was attributed to the rapid formation of carbonates over both Pt and ceria under these low temperature conditions.

2.4.3   Methane formation and selectivity

One of the major but undesired side reactions during WGS is methanation. This is a reaction that is thermodynamically possible under the working conditions of a WGS reactor. Different catalysts have been shown to be more or less prone to promote methanation.

Wheeler et al. (2004) investigated methanation selectivity during WGS reaction of Ru, Rh, Ni, Pt and Pd monolith coated catalysts for short contact times in the temperature range between 300 and 800°C. The order in which the metals promoted methanation was found to be

Ru > Rh > Ni > Pt > Pd

Methane formation over Pt and Pd was less than 1 % under the reaction conditions applied, while over the other metals it was higher and exceeded 10 % for Ru.
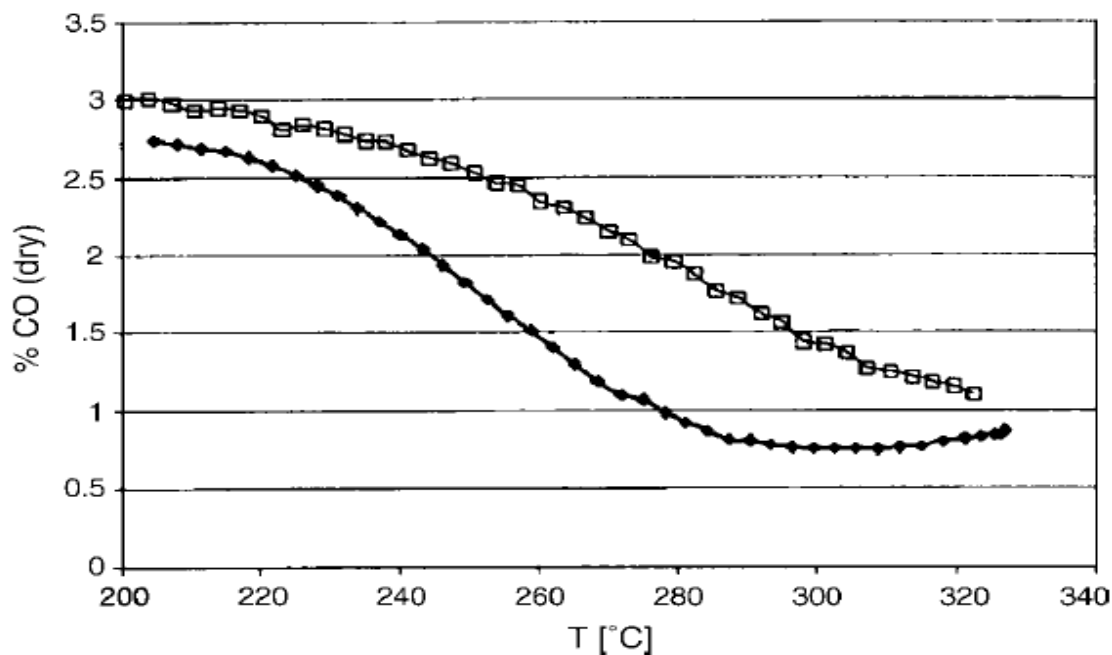
Figure 2-8: **Percentage CO left unconverted, showing the effect of aging on the performance of a 2% Pt/CeO$_2$ catalyst by exposure to reformate at low temperature. Experiments were carried out by way of temperature programmed reaction.**

Experiment I was carried out over the fresh catalyst (♦). After the final temperature was reached, the catalyst was rapidly cooled to 60 °C under wet feed gas flow and held for 5 minutes. Thereafter the temperature programmed heating up was repeated (experiment II, □). Reformate composition: 3 vol.% CO, 15 vol.% CO$_2$, 48 vol.% H$_2$, 34 vol.% N$_2$; 26% vol.% steam, WHSV$_{DRY}$ = 20,000 (h^{-1}) (Liu et al., 2005)

Kolb et al. (2005a) investigated the performance of a commercial HTS catalyst and a number of supported noble metal catalysts for WGS reaction in microchannel reactors. Catalysts were tested under typical HT-WGS conditions (temperature between 350-400 °C) and typical LT-WGS conditions (temperature between 300-350 °C) and typical feeds, both at the same wet gas space velocities. Table 2-3 gives a summary of the conversions obtained over all the catalysts tested.

Table 2-3: CO conversions achieved over different catalysts under typical HT-WGS (9 mol% CO, 8 mol% CO_2, 49 mol% H_2 and 34 mol% H_2O) LT-WGS (3 mol% CO, 14 mol% CO_2, 55 mol% H_2 and 28 mol% H_2O), $WHSV_{wet}$ = 93 $Ndm^3/h.g_{cat}$ (Kolb et al., 2005a)

Catalyst	Conversion (%) under LT-WGS conditions (300 °C)	Conversion (%) under HT-WGS conditions (400 °C)
Fe_2O_3/Cr_2O_3 (commercial HTS catalyst)	0	6
$Pt/CeO_2/Al_2O_3$	20	57
$Pt/CeO_2/ZrO_2/Al_2O_3$	22	51
$Pt/Pd/CeO_2/Al_2O_3$	6	17
$Pt/Rh/CeO_2/Al_2O_3$	23	95
$Pt/Ru/CeO_2/Al_2O_3$	67	83
IMM catalyst (composition not disclosed)	60	- -
WGS CO equilibrium conversion	60	72

It was found that the introduction of the second noble metal to the $Pt/CeO_2/Al_2O_3$ catalyst did not improve the Pt based catalyst's performance. In fact, $Pt/Rh/CeO_2/Al_2O_3$ and $Pt/Ru/CeO_2/Al_2O_3$ proved to be most active and selective for methanation, which resulted in CO conversion over $Pt/Ru/CeO_2/Al_2O_3$ even exceeding CO WGS equilibrium conversion under applied conditions. This corresponds to the results Wheeler et al. (2004) reported, where samples, which contained only platinum, palladium and ceria, showed no tendency towards methane formation in contrast to rhodium or ruthenium containing samples.

2.5 WGS Catalyst Performance Requirements

WGS reaction is an important stage to reduce CO content to less than 1 mol% in the fuel processor for fuel cell applications. Finding the right formulation for the catalyst and correct size of the reactor is of great importance. The development of WGS catalysts for fuel processors for transiently operating PEMFCs must address the setbacks of the currently available industrial WGS catalysts in that regard.

With respect to the intended application, the requirements for the WGS catalysts for processing of fuel for fuel cells that are operating under transient conditions, are as follows (Ghenciu, 2002):

- High activity at relatively low temperature (300 °C, if not less)
- High selectivity for WGS over a range of H_2O/CO ratios with no side reactions, particularly no methanation occurring, that consume valuable hydrogen
- Large range of space velocities
- Guarantee of steady CO outlet concentration
- Stability under typical reformate feed supplied
- Stability against condensation
- Resistant to poisons such as hydrogen sulphide and chlorine
- Non-pyrophoricity in order to eliminate pre-conditioning steps and secure durability under steady state and transient conditions
- Mechanical stability during use
- Small catalyst volume

This study is hoped to help achieve some of the above mentioned requirements transient operation.

Supported noble metal catalysts, typically containing 1 % or more of the noble metal, were found in the medium temperature range to be comparable in activity per unit mass of catalyst to the state of the art industrial Cu/Zn based low temperature WGS catalysts. However, low reaction temperature is more unfavourable for the noble metal catalyst in this regard than for Cu/Zn based catalysts.

Noble metal catalysts meet the aforementioned requirements of non-pyrophoricity, durability under transient conditions and higher stability against condensation and they appear still sufficiently active at temperatures as low as 225 °C and at the typical S/C ratios in the WGS to bring down the CO content of the WGS reactor product to 1 vol% (wet) or less at dry gas space velocities around 50 000 ml/ (g_{cat}.h) or higher. The activities of the various noble metals for WGS rank as follows:

$$Pt > Rh > Ru = Pd > Ir > Au$$

The activity of noble metal catalysts is much dependent on the support, with ceria and titania supported catalysts being much more active for the WGS reaction than alumina supported catalysts. On the other hand, it appears that ceria supported noble metal catalysts deactivates rather rapidly, which process can only moderately be slowed down by addition of promoters. Lifetimes of these catalysts are insufficient for the purpose intended. Under transient conditions, once temperature is low enough for the steam in the reaction mixture to condense, ceria supported catalysts appear to deactivate very rapidly.

Some of the noble metals, rhodium and ruthenium in particular, are unsuitable for WGS catalysis, since they are also active for CO methanation, i.e. the undesired reverse steam reforming reaction. In contrast, platinum and palladium are little active for methanation under WGS conditions (see Table 2-3, higher than WGS equilibrium conversions.

Reportedly (Ghenciu, 2002, see Figure 2-3), Johnson-Matthey's noble metal catalyst JM-8 is both very active and selective for the WGS reaction, comparable to Cu/Zn catalysts, but also very stable with activity remaining constant for more than 1000 hours on stream. However, the composition of this catalyst has not been disclosed.

3. OBJECTIVES OF THE STUDY

3.1 Aim

To screen commercial supported noble and base metal catalysts coated on the walls of microchannel reactors for water-gas shift reaction and optimize it to produce a fuel to power a PEM fuel cell with maximum H_2 yield and reduce CO level to ≤ 1 vol% (wet).

3.2 Objectives

The objectives of this research were the following:

- To produce H_2 from steam reforming derived syngas for powering a PEM fuel cell, while reducing CO content in the reformate to ≤ 1 vol% (wet).

- To screen different commercial noble metal based catalysts coated onto microchannel reactor walls for WGS reaction at 1 bar gauge and in temperature range of 275-375 °C; and to identify which catalyst gives best performance (activity and stability).

- To compare commercially available noble metal catalysts with base metal catalysts coated on microchannels.

- To identify feasible operating conditions (steam to CH_4 ratio in the upstream steam reforming stage, range of space velocity and temperature) for a fuel processing device to power a PEM fuel cell.

3.3 Hypothesis

Based on the literature review, the following hypothesis is proposed:

- Noble metal catalysts perform well when coated onto microchannel reactor walls.

- The target CO concentration of < 1 vol% (wet) can be reached.

3.4 Key Questions

- Which catalyst is best?

- How will the steam to CH_4 ratio in the upstream steam reforming stage affect the conversion of CO?

- What temperature and space velocity will be suitable to reduce CO content to ≤ 1 vol% (wet)?

- What is the operational window in terms of temperature and space velocity at 1 barg?

- How stable and durable is the chosen catalyst at the chosen conditions?

- How do PM catalysts compare to base metal catalysts in microreactors?

4. EXPERIMENTAL

4.1 Materials Used

4.1.1 Catalysts

Commercial catalysts were supplied by different manufacturers. Table 4-1 gives a list of the catalysts used, with the forms they were received and applied for testing.

Table 4-1: List of catalysts used.

It should be noted that all of the catalysts tested are commercial catalysts that have been provided by the manufacturers under no analysis agreement.

Catalyst code	Origin of catalyst	Active metal	Carrier	Form received	Shape as received	Applied as
X	Commercial (undisclosed)	Noble metal	Undisclosed	Pre-reduced	Powder	Coated[2]
WY-1	Commercial (undisclosed)	Noble metal	Undisclosed	Pre-reduced	Coated	Coated[3]
WY-2	Commercial (undisclosed)	Noble metal	Undisclosed	Pre-reduced	Coated	Coated[3]
HTS	Süd-Chemie (G-3C)	Fe-Cr	Alumina	Oxidic	Pellets[1]	Coated[2]
LTS	Süd-Chemie (C 18-7)	Cu-Zn	Alumina	Oxidic	Pellets[1]	Coated[4]

[1] Milled using a pestle and mortar and sieved to 200-250 µm

[2] Coated in-house using a method adopted from Zapf et al. (2003)

[3] Coated by the manufacturer

[4] Coated by IMM, Mainz, Germany using the method by Zapf et al. (2003)

4.1.2 Other materials used

Table 4-2 list all other materials used with the manufactures name, properties and the actual final use of the material.

4.2 The Microchannel Reactor

4.2.1 Microchannel plates

The microchannel washcoating test and the reactor plates were obtained from Ätztechnik Herz GmbH in Rottweil, Germany. The plates were made from stainless steel 1.4571 (corresponds to SS 316) with the elemental composition given in Table 4-3. The microchannels were formed by wet chemical etching (Section 2.3.1.2: Micro-structuring).

Table 4-2: **List of other materials used**

Material	Manufacturer	Properties	Use
Polyvinyl alcohol (PVA)	Fluka	Beads, 500 μm[1]	Organic binder for catalyst coating slurry
Deionized water	n/a	n/a	Feed and solvent for catalyst coating slurry
Argon (Ar)	Afrox	99.99 %[1]	Feed (internal standard) and GC carrier gas
Hydrogen (H$_2$)	Afrox	99.99 %[1]	Feed and GC carrier gas
Carbon monoxide (CO)	Afrox	99.99 %[1]	Feed
Carbon dioxide (CO$_2$)	Afrox	99.99 %[1]	Feed
Isopropanol	Merck	99.99 %[1]	Plate cleaning
Silicon Carbide (SiC)	Elcarbo	300 μm[1]	Vapouriser packing

[1]As reported by the manufacturer

Table 4-3: **Microchannel plate material composition (stainless steel 1.4571 standard) (Ätztechnik Herz GmbH, Rottweil, Germany)**

Element	Percentage (wt %)
C	≤0.08
Si	≤1.00
Mn	≤2.00
P	≤0.045
S	≤0.015
Cr	16.5 - 18.5
Mo	2.0 – 2.5
Ni	10.5 – 13.5
Ti	5 x C ≤ 0.70
Fe	Balance

A schematic view of the microchannel reactor plates used is shown in Figure 4-1A with dimensions provided in Table 4-4. In order for the microchannel reactor to be connected to the feed and products lines of the experimental setup, 1/8" holes were made at the inlet and outlet ports of the microchannel reactor, as shown in Figure 4-1A, to fit and weld in 1/8" stainless steel tubes. For this purpose two microchannel reactor plates were clamped together and holes were drilled into the centres of the inlet and outlet ports.

Test plates for washcoating and washcoat adherence tests differed from the microchannel plates in that they were designed for higher catalyst load. They were longer and carried more microchannels. The test plates are presented schematically in Figure 4-1B with characteristic dimensions also presented in Table 4.4. The material used for the test plates was the same as used for the reactor plates.
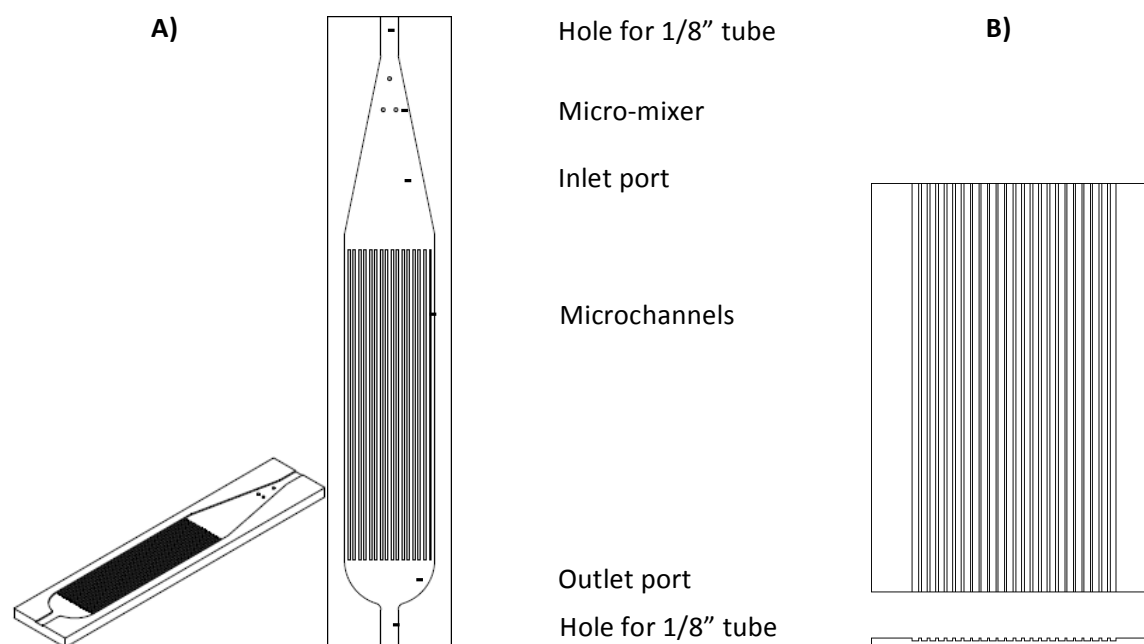
Figure 4-1:   Design of (A) microchannel reactor plate and (B) microchannel washcoating test plate (top and side views) (Truter, 2011)

Table 4-4:   Dimensions (mm) of microchannel reactor and microchannel washcoating test plates

	Microchannel reactor plate	Microchannel washcoating test plate
Channel width	0.4	0.4
Channel depth	0.25	0.25
Bridge width	0.3	0.3
Channel length	40	50
Plate width	11.6	24.9
Plate boundary wall width	2.2	5.05
Number of channels	17	36
Total plate length	81	50
Inlet port length	30	
Outlet port length	11	

4.2.2   Wash-coating method

The washcoating method used to coat catalysts in-house onto the microchannel plates was based on the method developed for γ-Al_2O_3 wash-coating by IMM (Zapf et al., 2003). Refer to Table 4.1

4.2.2.1 Pretreatment of steel plates

Prior to pre-treatment, an identification number was engraved on the back of each plate. The plates were chemically cleaned and subsequently thermally treated before coating in order to remove residues from the drilling process, chlorine residues left from the etching process and to form an oxide layer to improve the adhesion of the catalyst washcoat. The cleaning process comprised treating the plates with isopropanol at ambient temperature in an ultrasonic bath for 10 minutes followed by drying in a fume cupboard at ambient conditions (Zapf et al., 2003). The plates were subsequently calcined in air at 800 ˚C for 2 hours applying the temperature programme presented in Figure 4-2. During the calcination process a rough metal oxide layer of similar properties as the washcoat to be deposited formed on the channel walls, which improves adherence of the washcoating (Zapf et al., 2006). Upon thermal treatment the plates lost their metallic silver colour and turned to a darker colour due to the formation of the metal oxide layer. The calcined plates were weighed to the fourth decimal place. It should be noted that, once calcined, the plates were only handled wearing nitrile gloves to prevent contamination and mass changes resulting from contact with bare hands.
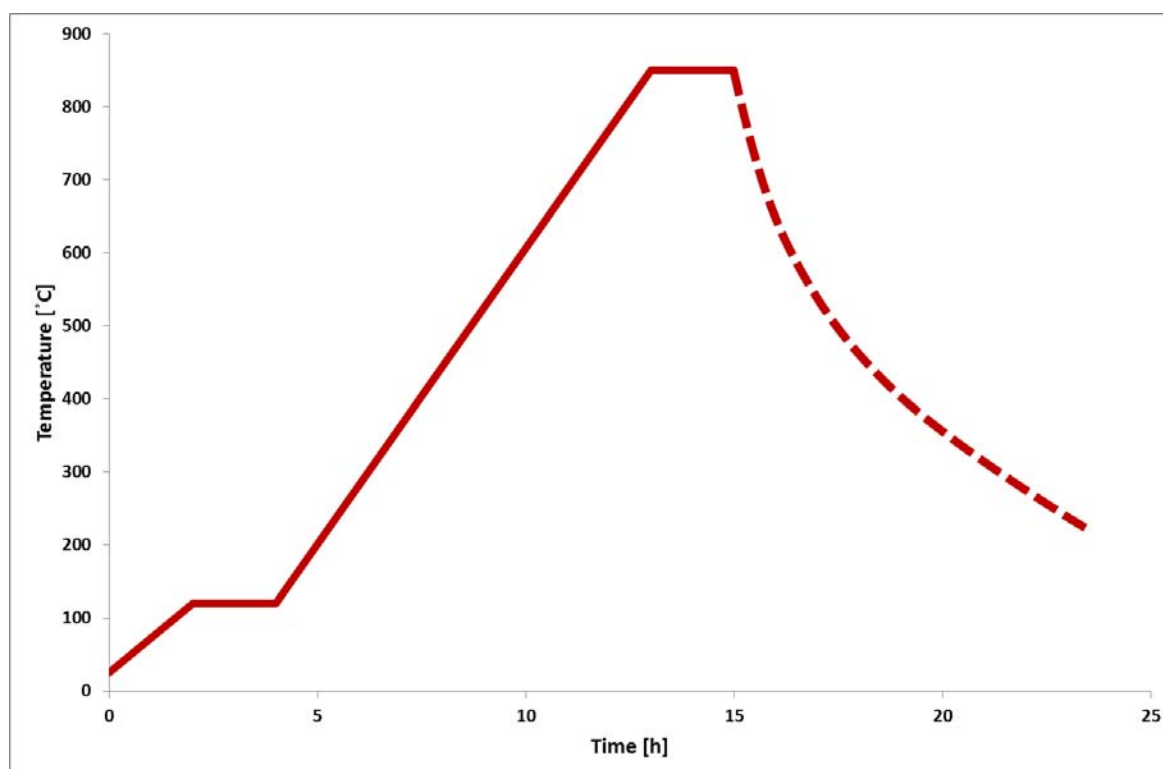
Figure 4-2: Temperature programme for the microchannel plate thermal pre-treatment in air (temperature ramping was 1 °C/min, at the end the furnace was switched off and cooling to ambient temperature was natural, as indicated by the dashed curve)

4.2.2.2 Preparation of washcoating suspension

The wash-coating suspension was synthesised using the general methodology described by Zapf et al. (2006). The γ-Al$_2$O$_3$ of Zapf et al. (2006) was substituted by the catalyst agglomerate powder. Table 4-5 shows the composition of the washcoating suspensions prepared.

Table 4-5: Composition of the washcoating suspensions prepared

Compound	Amount (g)
Catalyst agglomeration powder* (refer to Table 4.1)	10
Deionised water	37.5
Polyvinyl alcohol (PVA)	2.5

* It should be noted that the particles size may have decreased during stirring when using the device applied (Truter, 2011). However, the final size was not determined.

The washcoating suspensions were prepared in glass bottles with a screw cap that allowed the suspension container to remain tight at all times, therefore preventing water evaporation. In order for the suspension temperature to be monitored, the suspension container was placed in a water

bath on a magnetic stirrer plate and the temperature of the water bath was controlled by a heating plate and measured using a thermocouple. A magnetic stirrer bar was inserted in the suspension container and used to continuously stir the suspension. The full detailed apparatus schematic diagram is shown in Figure 4-3.

Thermocouple

Screw cap

Glass bottle

Water bath

Magnetic stirrer/ heater plate
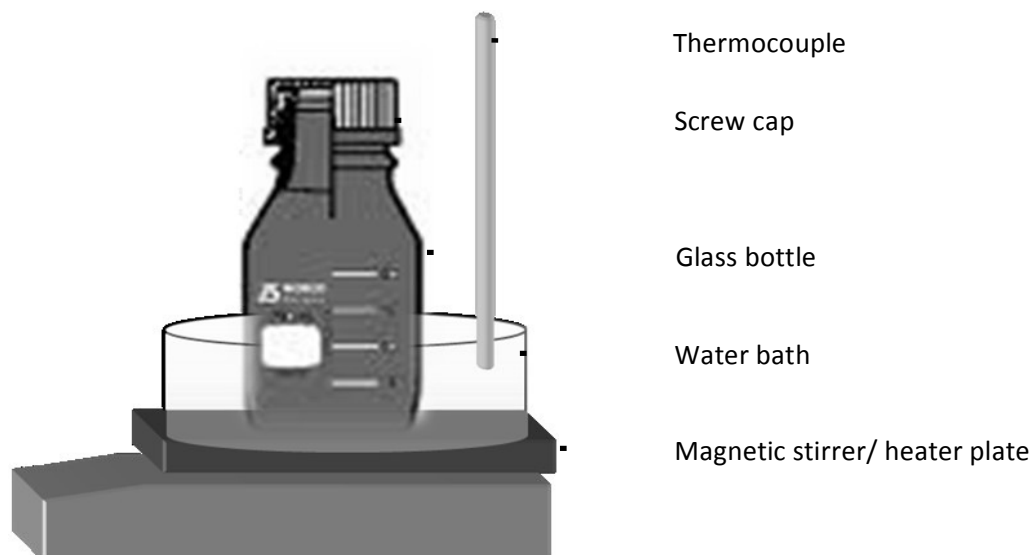
Figure 4-3:   Experimental setup for wash-coating suspension preparation (Truter, 2011)

4.2.2.3 Preparation of organic binder solution

The addition of an organic binder (PVA) to the suspension was important to ensure that the suspension became homogenous and to help the adhesion of the coated catalyst layer on the microchannel walls. To prepare the organic binder solution, the respective quantities of polyvinyl alcohol (PVA) beads and deionised water (Table 4-5) were charged to the suspension container. The charge was stirred at a speed of 160 rpm and kept at 65 ˚C. Once the PVA had dissolved (after about 3 hours), stirring was stopped and the solution was left over-night at ambient temperature.

4.2.2.4 Preparation of catalyst suspension

Once the binder solution was prepared, the respective quantity of catalyst powder (Table 4.5) was added. The temperature of the suspension container was once again set at 65 ˚C for 2 hours whilst stirring at 160 rpm. Thereafter, the suspension was stirred at ambient temperature for 3 days. A simple test was used to qualitatively determine whether or not the suspension was ready for coating. The test involved checking the sharpness of the suspension 'edges' by swirling the suspension container and observing the edges of the suspension on the container walls. If the edges were smooth, the suspension was considered homogenous and ready for coating. If the edges were not smooth the suspension required further homogenization, achieved by continuous stirring at room temperature. If smooth edges were not achieved with further stirring, the suspension was not of good quality and discarded.

4.2.3 Plate masking

To prevent coating on the inlet and outlet ports of the microchannel reactor plates, both ports were masked with polymer tape ('selo-tape') prior to coating the microchannel reactor plates, as shown in Figure 4-4.

Polymer tape
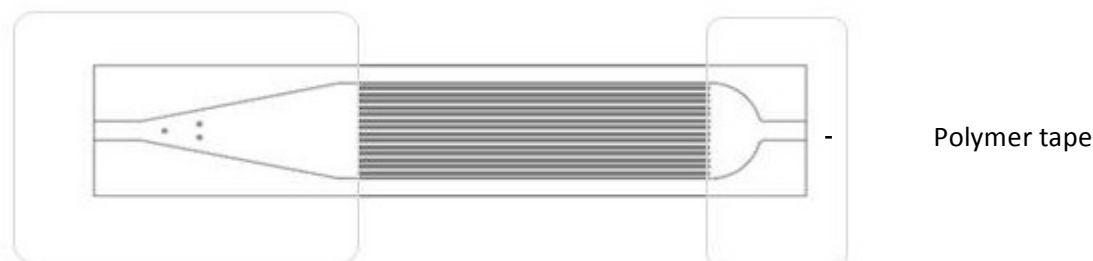
Figure 4-4: Masking of microchannel reactor plate ports (Truter, 2011)

The edges of the tape were placed as close to the ends of the microchannels as possible to prevent (minimise) any catalyst to be deposited on the inlet or outlet ports of the microchannel reactor plates. The sides of the tape were then pressed down with cotton buds, to ensure that the suspension would not trickle under the tape. The sides parallel to the length of the channels were not taped since this would make it difficult to remove excess catalyst suspension during the catalyst coating process. The taping was only done to reactor plates since test plates do not have such ports (Figure 4-1B).

4.2.4 Catalyst coating

For the coating, the plates were placed on a sheet of paper towel. The catalyst was subsequently coated onto the stainless steel plates by placing about 2 ml of suspension in the centre of the plate as shown in Figure 4-5.
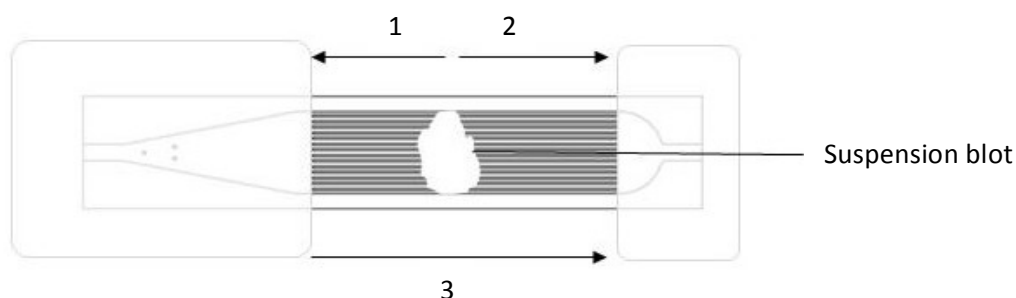
Suspension blot

Figure 4-5: Method used to coat the microchannel plates with suspension (1-3 indicates the order and direction in which the suspension was scraped) (Truter, 2011)

It is important to add a sufficient amount of catalyst suspension to the plate, since adding more suspension at a later stage would have resulted in layering and affected the quality of the washcoat (Zapf et al., 2003). A scraper which consisted of a sharp polymer blade was used to spread the

catalyst suspension. Once a blot of catalyst suspension had been placed in the middle of the microchannels, one half of the suspension was scraped from the centre of the blot to the one end of the microchannels (1), ensuring that the suspension had reached and completely filled the ends of all channels. Subsequently, this procedure was repeated on the other side (2). Finally, the suspension was scraped once over the whole length of the plate (3), such that the channels were left full of coating suspension and excess suspension was removed.

4.2.5 Post-treatment

Once coated, the plates were left to dry at ambient conditions for 3 hours. As the coating dried, its colour changed from clear to white. A homogeneously coated plate dried evenly from the outside edges to the centre. After drying, the tape was removed and the plates were placed in a furnace for calcination. Figure 4-6 shows the temperature program applied for the calcination of the washcoats. Calcining was done to remove water and the organic binder (PVA), thus leaving only the catalyst on the microchannels walls. The calcination temperature depended on the type of catalyst (active metal) used and was adjusted accordingly (Figure 4-6). The plates were then cleaned to remove excess catalyst present in any area other than in the channels. This cleaning was done using cotton buds to avoid removing any of the metal oxide layer since this would influence the plate weight.
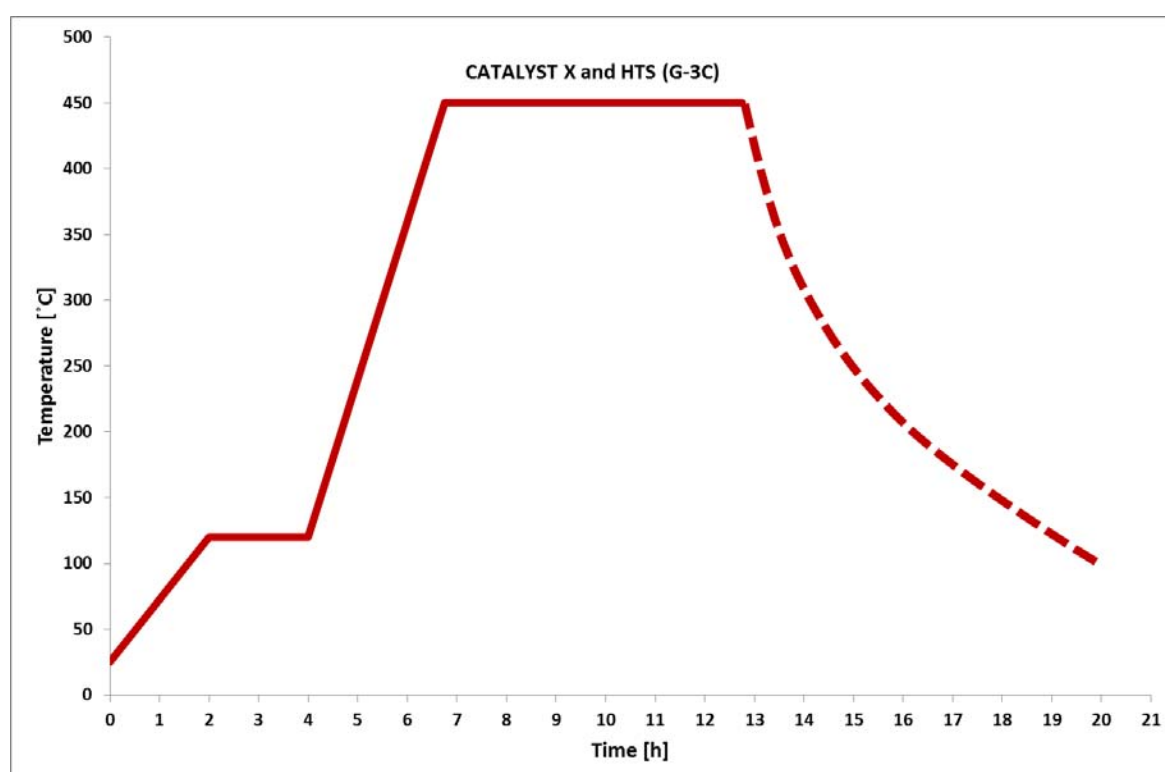
Figure 4-6: Temperature programs for the calcination of the coated microchannel plates in air (temperature ramping was 1 °C/min, at the end the furnace was switched off and cooling to ambient temperature was natural, as indicated by the dashed curve).

4.2.6   Characterization of catalyst washcoat

4.2.6.1 Catalyst adhesion

The adherence of the washcoat to the stainless steel microchannel test plates was evaluated by a 'drop test'. The microchannel plates were weighed to the 4th decimal place and the individual catalyst loadings were determined by comparing the weights of the loaded plates to the weights of the unloaded plates.

The 'drop test' has been developed by Zapf et al. (2006) to measure the mechanical stability of a catalyst coating (adherence of the coating to the channel walls). The instrument that was developed by Zapf et al. (2006) and used in this study to perform this measurement is schematically shown in Figure 4-7. The microchannel test plate, of a known mass, was attached to the stainless steel block, which was then allowed to a gravitational fall down a metal guide rod onto the stainless steel base.

Stainless steel block (720g)

Mounted coated test plate

55 cm

Stainless steel plate
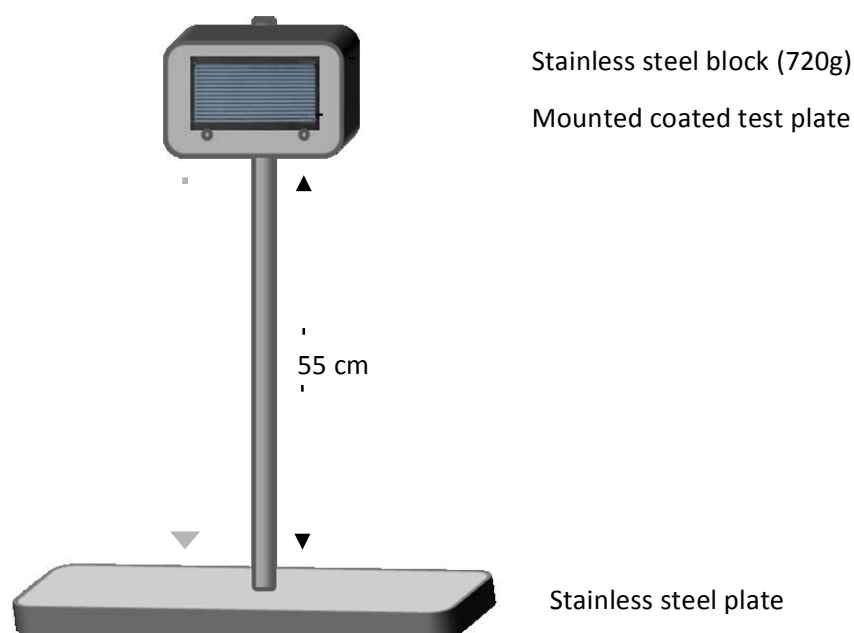
Figure 4-7:   Drop test experimental apparatus (Zapf et al., 2006)

For an adhesion test, the test plate was repeatedly dropped 10 times before weighing the test plate again. The percentage weight loss was calculated as follows:

$$\text{Weight loss } (\%) = \frac{(\text{weight of coated plate} - \text{weight after adhesion test}) \times 100}{(\text{weight of the coated plate} - \text{weight of uncoated plate})}$$ **eqn 4-1**

The percentage weight lost calculated from equation 4-1 was the criterion for the quality of adhesion. The drop test was only done during the optimisation of the procedure, that is, on coated test plates, since it was assumed that both test plates and reactor plates had the same material properties and channel dimensions, which would lead to the same adherence test outcomes.

4.2.6.2 Coated catalyst layer uniformity

The morphology of the catalyst coating was examined using a FEI Nova Nano SEM 230 with a Field Emission Gun (FEG) Scanning Electron Microscope (SEM). These studies were carried out at the Electron Microscopy Unit, Department of Physics, University of Cape Town. The SEM instrument was operated at 5 kV with various working distances and magnifications. The microchannel test plate was mounted on a sample holder in a vertical position and placed under the electron beam. The coated plate was examined by taking cross-sectional images of as shown in Figure 4-8. On these cross sectional images, the uniformity of thickness and distribution of the coated catalyst on the channel walls can clearly be seen.
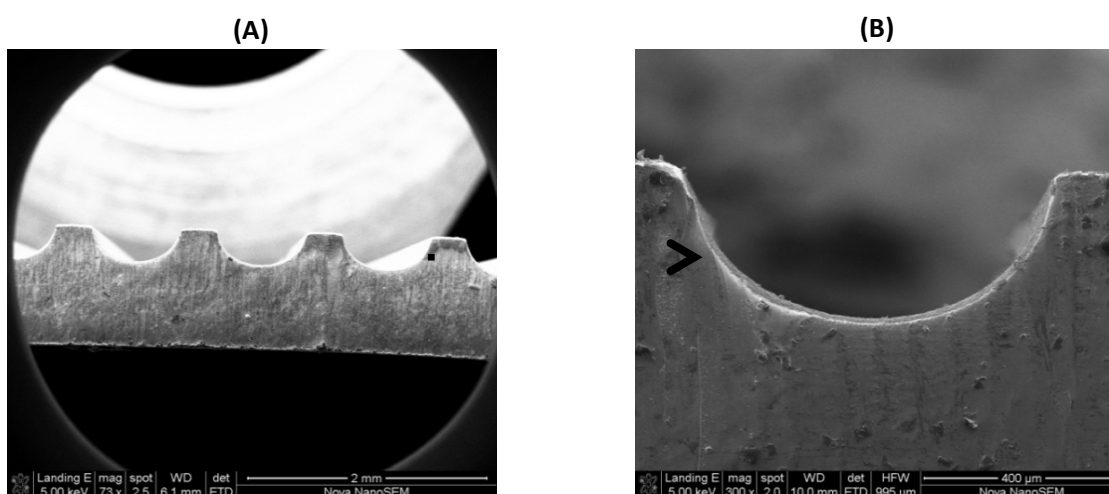
Figure 4-8: Cross-sectional image of a microchannel test plate showing a uniform thickness and distribution of the washcoat on the channel walls (Images taken at UCT Department of Physics)

4.2.7 Reactor plates welding

Microchannel reactors have a sandwich design with two micro-structured reactor plates being attached to each other face to face. The coated reactor plates together with the inlet and outlet 1/8" stainless steel tubes were sealed together by laser welding to form a complete microchannel reactor. Pulsed-laser welding was chosen due to its accuracy and ability to confine the high temperature of the welding process to a very small area on the boundary walls of the microchannel reactor, thus protecting the catalyst coating from thermal degradation. Laser welding was carried out by Polyoak Packaging (Pty) Ltd, 90 Waterford Rd., Deep River, 7801, Cape Town. Figure 4-9 shows the components of the reactor before and after welding.
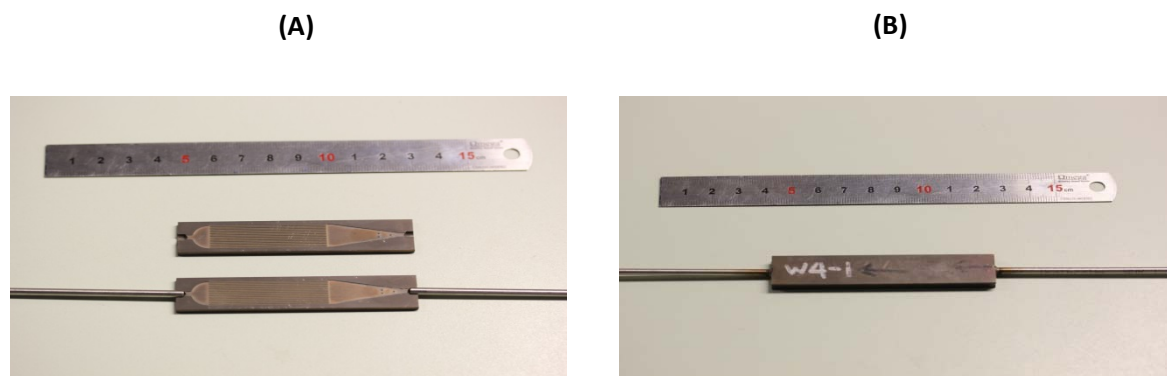
Figure 4-9: Microchannel reactor and components (A) before and (B) after welding

4.3 The Experimental Apparatus

A flow sheet of the steady state, continuous flow experimental apparatus constructed and used is shown in Figure 4-10. The apparatus consists of a down-flow microchannel reactor assembly preceded by feed supply devices and followed by analytical devices. The reactor assembly (Figure 4-12) resembled a rod of 3/4'' diameter and 50 cm length. However, the 'rod' consisted of several sections, namely a head that carried water and gas inlet ports, followed by an evaporator, brass sleeves that carried the microchannel reactor and the outlet tubing. The entire assembly was housed in a zoned heating block. The major components of the experimental system are described as follows:

4.3.1   Feed supply

4.3.1.1 Dry gas mixture

The gases were supplied from a pressurised cylinder for CO_2 and from the inhouse gas lines for the other gases. Gases were first passed through filters (F-1 to F-5) to remove any possible solids entrained in the line. Pressure regulators (PR-1 to PR-5) regulated the pressure of the gases being supplied to the mass flow controllers (MFC-1 to MFC-5, Brooks) and finally to the blend pot. A spring loaded back pressure regulator (BPR-1) was used to regulate the pressure of the blend pot.

Additional mass flow controllers (MFC-6 and MFC-7 of different ranges) helped control the flow of the gas inlet port of the mixed dry gas to the reactor, while most of the gas mixture was vented through the spring loaded back pressure regulator (BPR-1). Mass flow controllers had been calibrated against a bubble meter.

As a safety precaution, check valves (CV-1 to CV-6) were installed to protect the mass flow controllers against any backflow from the reactor. Pressure relief valves (1-3) were installed to vent out gas or liquid in the event of downstream line blockages.
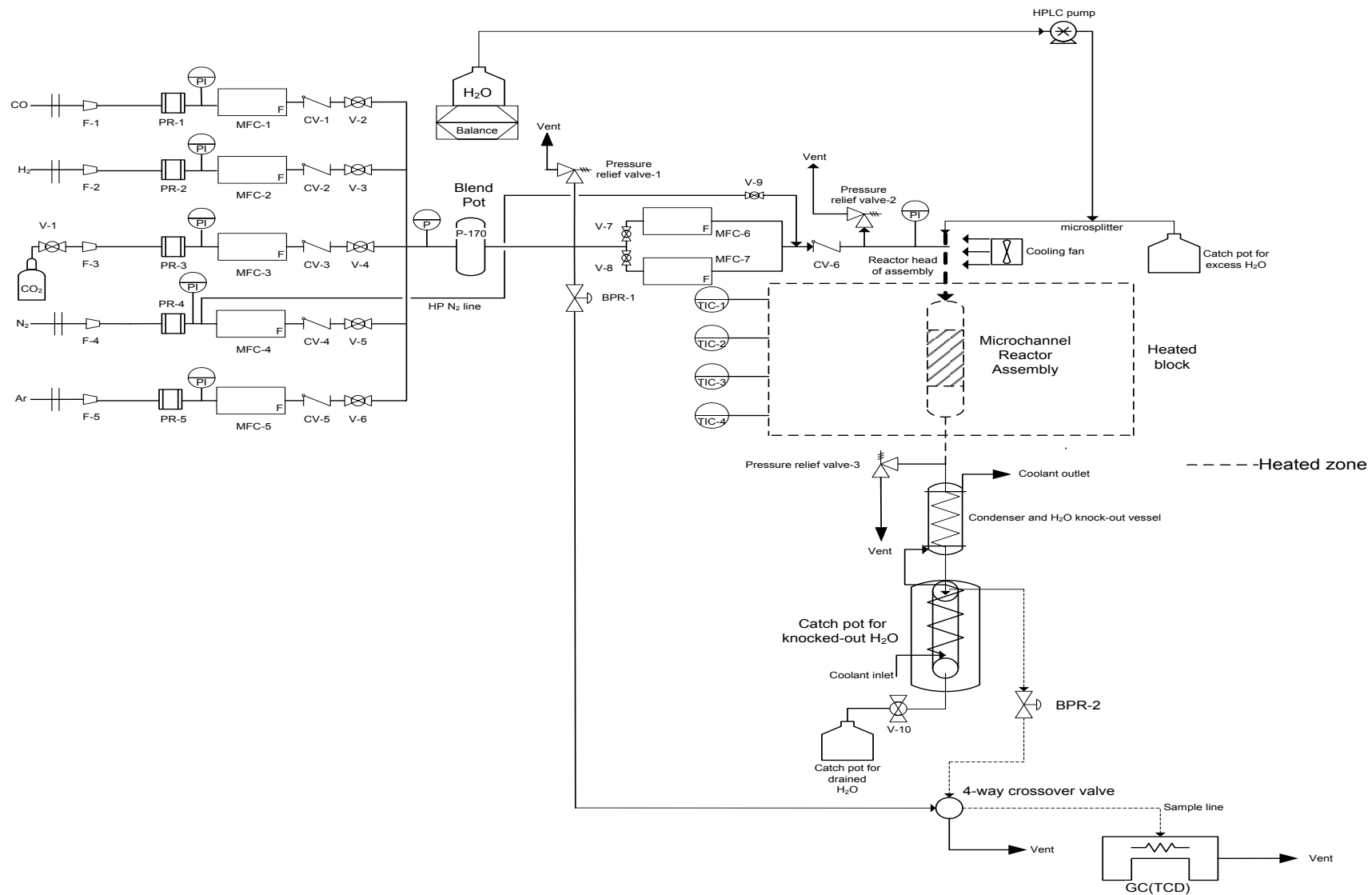
Figure 4-10:   Flowsheet of the experimental apparatus

4.3.1.2 Steam formation – the evaporator

Degassed deionized water was supplied from a glass bottle using a duel piston Model 1500 HPLC pump (Scientific Systems Inc. 0.001-10 ml/min, adjustable in 0.001 ml steps) and passed through a microsplitter. The partial stream divided by the microsplitter was led to an evaporator situated above of the microchannel reactor assembly. The evaporator was packed with inert silicon carbide particles of approximately 300 micron. The bottom end of the evaporator (outlet end) was located inside the reactor heating block while the top end extended above the block (see Figure 4-10). The temperature of the evaporator was adjusted so that the top end was kept below the boiling point of water at the working pressure of 1 barg (by aid of a cooling fan). The end of the water supply line, a fused silica capillary of 0.05 mm internal diameter, was fitted to the liquid inlet port on top of the head of the reactor assembly with a graphite ferrule. The end of the capillary extended into the top layers of the evaporator's SiC packing. Upon trickling through the SiC packing, water slowly evaporated and mixed with the dry gas fed. A temperature gradient along the evaporator, produced by the cooling fan at the top and the heating block at the bottom (see Figure 4-10), allowed water to steadily evaporate on its way to the hot end without boiling and constantly to forming steam. Exiting the evaporator, a homogeneously mixed and steadily flowing steam/gas feed of the desired composition was obtained and flowed to the microchannel reactor through a 1/8" stainless steel tube.

The pump/ microsplitter combination was calibrated against water collected in the knock-out pot (see Section 4.3.3: Condenser and knock-out pot) after ramping overnight at different pump rates and with an empty reactor installed. Pump calibrations are documented in Appendix III.

4.3.2 **Microchannel reactor assembly**

In order to incorporate the microchannel reactor into the experimental configuration shown in Figure 4-10, a specific reactor assembly had to be constructed. The assembly consisted of a series of tubes and round sleeves of 3/4'' outer diameter, which was fitted into a heating block such that the microreactor was located in the isothermal zone.

4.3.2.1 Isothermal zone

A standard fixed-bed reactor (3/4'' tube with a central thermowell 1/8" stainless steel tubing and a head identical with that of the microreactor assembly), packed with silicon carbide particles, was inserted into the reactor furnace. The tube was placed so that it extended above of the heating block by 5 cm. The reactor furnace comprised a brass block of 80 mm x 80 mm cross-section and 360 mm length. Three heating bands were arranged along the length of the heating block to make up three heating zones which could individually be set, monitored and controlled to ensure that the temperature along the catalyst bed was isothermal.

In order to optimise the temperature profile along the reactor assembly (i.e., to adjust the individual heating bands of the heating block so that an isothermal zone of sufficient length was formed to eventually place the microchannel reactor in) a thermocouple was moved in small steps from top to bottom inside the central thermowell of the fixed bed reactor by pulling it 1 cm down at a time and measuring the corresponding temperature. The temperature profile was recorded without flow. Temperature profiles obtained at target temperature of 200, 250 and 300 ˚C are shown in Figure 4-11.

The isothermal zone was identified to be located between 20 and 30 cm from the top of the heating block for all of the evaluated target temperatures. This meant that the microchannel reactor was to be placed at this position in the heating block. For operations, the tip of the thermocouple in the microreactor assembly was positioned level with the middle of the microreactor.
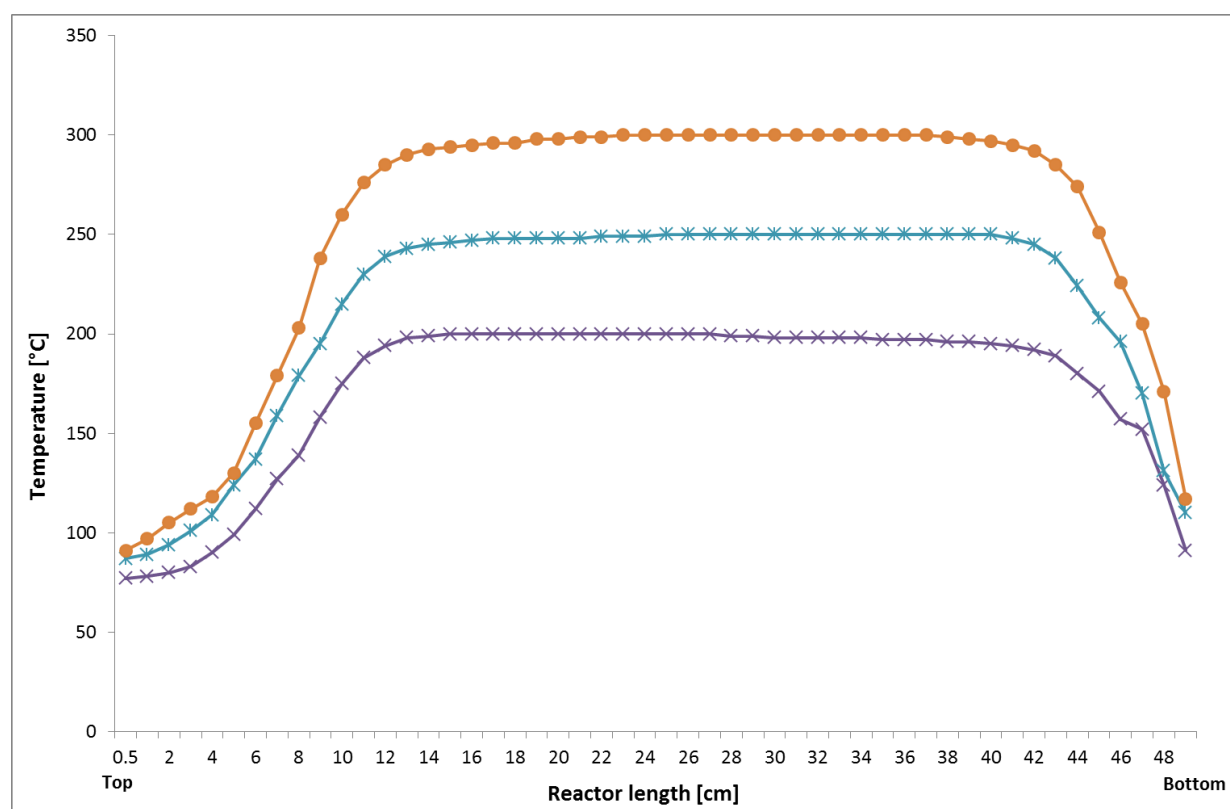
Figure 4-11: **Temperature profiles along the centre of the heating block determined using a SiC packed ¾" standard fixed-bed reactor (Reactor length at 0 cm depicts the top of the reactor preheat tube)**

4.3.2.2 Fitting of microchannel reactor assembly

The head of the assembly consisted of a piece of 3/4'' stainless steel tubing (SS 316) that carried the dry gas feed inlet and water inlet ports. The head was mounted onto another 3/4'' tube by a Swagelok[TA] VCR fitting. This other tube served as the water evaporator (for more details, see Section 4.3.1.2: Steam formation – the evaporator).

The outlet of the evaporator was connected to the microchannel reactor by 1/8'' (OD) tubing. The 1/8'' tubing and the microreactor were fitted into sleeves made from brass. Sleeves S-1 (Figure 4-12, S-1) had a length of 8 cm and a circular, co-axial hole cut to accommodate the 1/8" stainless steel tubes that extended from the ends of the microchannel reactor. The first of the sleeve S-1 encased the line from the evaporator outlet to the reactor inlet. The microchannel reactor (shown in Figure 4-9B) was also fitted into a brass sleeve (Figure 4-12, Sleeve S-2). Sleeve S-2 had a length of 4 cm and a rectangular hole cut to accommodate the microchannel reactor body, to provide good heat conductivity and to ensure an isothermal temperature profile along the microchannel reactor. Two 4 cm long S-2 sleeves were used to enclose the microchannel reactor body.
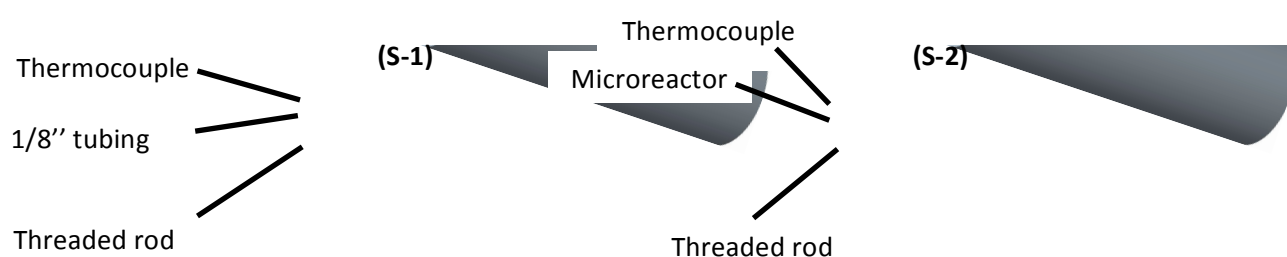
Figure 4-12:   Brass sleeves S-1 and S-2

Another sleeve of shape S-1 accommodated the 1/8" tube that extended from the microreactor outlet to the outlet of the reactor assembly. The sleeves had two additional holes running down their length. Two 25 cm long metal rods, threaded on either end, were placed in these holes and tightened with screws to keep the sleeves in place.

A smaller hole near the centre of the sleeves served as a thermowell which allowed a thermocouple to be moved up and down to determine the temperature profile and measure the working temperature of the microchannel reactor during the experimental runs. During reaction, the tip of the thermocouple was positioned as to be level with the middle of the microchannel reactor. Figure 4-13 shows the overall assembly.

4.3.3   Condenser and knock-out pot

Refer to Figure 4-10. The line after the reactor was heated to 60°C to avoid condensation occurring in this line. The line was followed by a condenser. Unconverted steam was condensed to yield a dry gas for analysis. A 1/8" (OD) stainless steel coil with a length of 2 m and an approximate volume of 10 cm^3, operating in down flow mode inside a cylindrical Teflon shell, circulating a cold (2°C) ethylene glycol-water mixture (volumetric ratio of 3:1) was used to condense and knock out all the unconverted   steam.
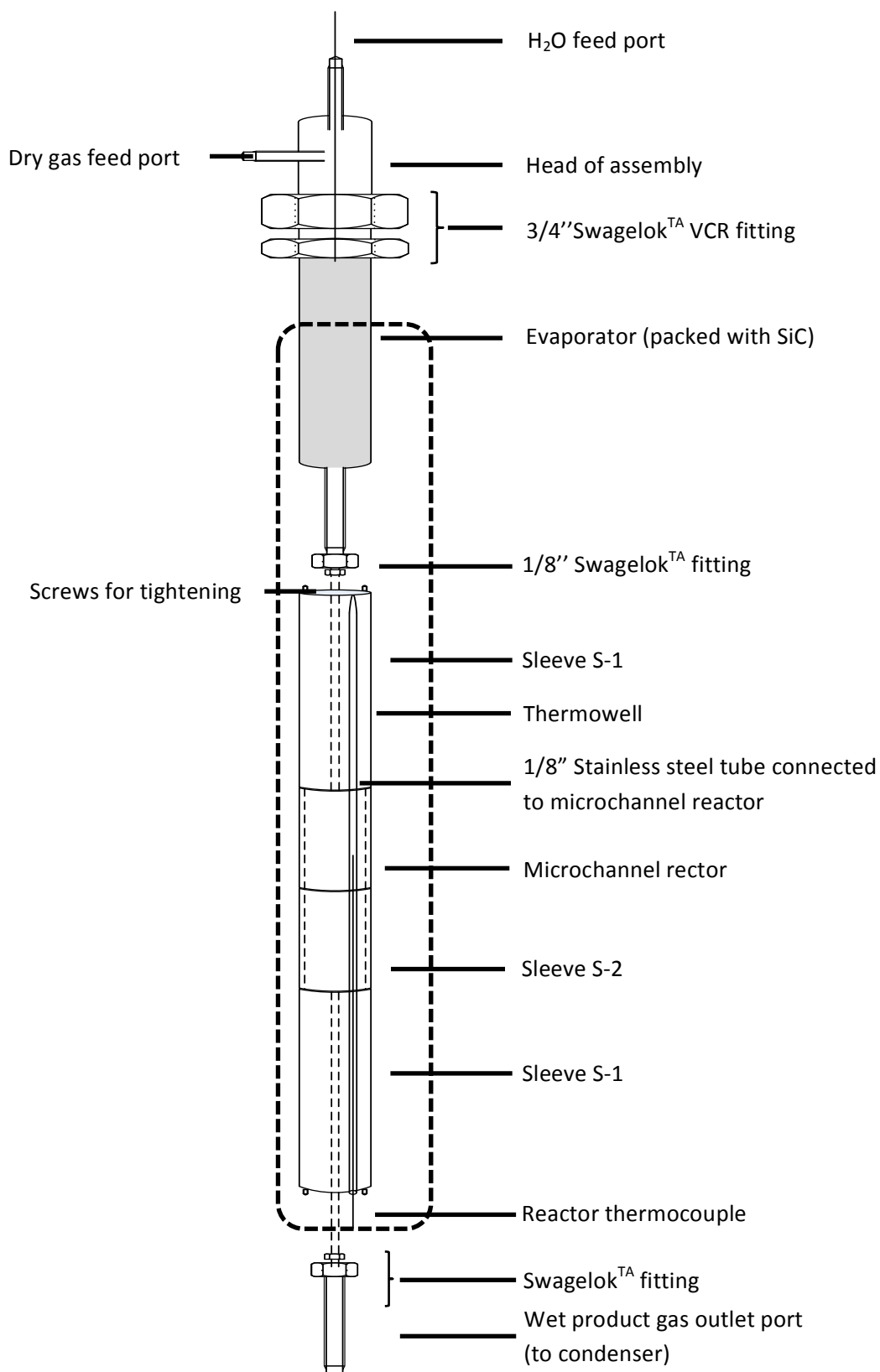
Figure 4-13: **Microchannel reactor assembly (dashed line bold box indicates the heating block)**

(Truter, 2011)

A sealed Perspex vessel that contained a cooling coil with the circulating coolant flowing through acted as the water catch pot. The catch pot was positioned below the condenser and the condensed liquid dripping was collected in this vessel, while allowing the dry product gas to escape into the GC sample line and pass the back pressure regulator at the end. The content of the catch pot was monitored and drained daily.

4.3.4 Back pressure regulator

The system was held at the working pressure (1 barg) by means of a spring loaded back pressure regulator (BPR-2, see Figure 4-10) placed after the water catch pot.

4.3.5 Sampling adaptions

A 4-way crossover valve was positioned after the back pressure regulator to sample the bypass gas (dry feed gas from back pressure regulator BPR-1, see figure 4-10) and the reactor effluent after the water catch pot (dry product gas). The composition of both the dry feed gas and the dry product gas was determined using an on-line gas chromatograph. A complete description of the gas chromatographic device and sampling technique can be found in Section 4.5: Gas chromatography.

4.4 Experimental Operating Conditions

4.4.1 Feed composition

The three different feeds converted by WGS mimicked a Methane Steam Reforming (MSR) product as obtained from a steam reformer whose feeds differed by steam/methane ratio and whose product compositions were close to thermodynamic equilibrium (Zhou et al., 2010). The respective MSR and WGS Feed compositions are given in Table 4-6.

The feeds were chosen with respect to the downstream application, namely the operational conditions of a low temperature proton exchange membrane (LT-PEM) fuel cell (see Sections 2.1.1.1: Polymer Electrolyte Membrane Fuel Cells (PEMFCs)) and 2.1.2: Fuel processing for Fuel cells). It was intended to produce fuel cell feed streams that ranged from wet to dry (i.e. oversaturated to unsaturated at the operational temperature of the fuel cell), see Section 2.1.1.1: Polymer Electrolyte Membrane Fuel Cells (PEMFCs). The different WGS feeds were labeled Feed 1, 2 and 3.

Table 4-6 gives the full details and background of each feed composition. It should be noted that the unconverted methane in the mimicked MSR effluent was substituted for argon in the WGS feed. This was in order to (i) use argon as the internal standard and (ii) identify methane that may have formed during WGS.

Table 4-6: WGS feed composition based on effluent compositions obtained from three different feeds to the methane steam reforming stage[1]

Methane steam reforming feed and CH₄ conversion[1]	Molar S/CH₄ = 2.35 X_{CH_4} = 94.2%	Molar S/CH₄ = 3.02 X_{CH_4}= 86.6%	Molar S/CH₄ = 5.00X_{CH_4}= 95.0%
Composition (%)	**Feed 1**	**Feed 2**	**Feed 3**
Ar[2]	1.11	2.27	0.63
CO	8.95	10.55	3.50
CO₂	8.95	4.10	8.53
H₂	63.19	49.83	44.70
H₂O	17.79	33.25	42.70
Total	100	100	100
Molar S/CO	1.99	3.15	12.2
Fuel cell operation temperature (°C)	**Saturation of feed with water vapour (%)**		
70	64	154[4]	261[4]
85	34	83	141[4]
100	20	47	80
120	10	27	40

MSR effluent= WGS feed / Fuel cell feed resulting[3]

[1](Zhou et al., 2010)

[2]Substitute for unconverted methane, allows tracing of possible methane formation

[3]Assuming WGS stage outlet CO content (wet) = 1 mol% followed by an ideal PROX stage (selective for CO oxidation only)

[4]Condensation, wet feed

4.4.2 Reaction pressure

With regard to the background of the total process (see Section: 2.2 Water-gas shift reaction) and the typically low operational pressure of PEM fuel cells (see Section 2.1.1.1: Polymer Electrolyte Membrane Fuel Cells (PEMFCs)), the operational pressure was low. All experiments were carried out at 1 barg.

4.4.3   Space velocity

In aid of finding the operational window for the WGS stage, space velocity was varied. Section 4.4.5: Overview of experimental runs, gives a list of all space velocities applied for each conditions setting.

4.4.4   Reaction temperature

Different catalysts were tested with different specific working temperature ranges as given by the catalyst suppliers. Section 4.4.5: Overview of experimental runs, gives a detailed list of the temperature ranges applied for each catalyst.

4.4.5   Overview of experimental runs performed

A list of all the experimental runs performed over the various catalysts and the different reaction conditions is given in Table 4-7.

Table 4-7: Overview of experimental runs carried out (the reaction pressure was set to 1 barg for all the experimental runs)

Experiment	Catalyst (see Table 4-2)	Catalyst loading (mg)	Feed	Reaction temperature (°C)	SV_{DRY} [ml/(h.g)] x 10^{-3}
1	X	32.16	2 2	350 325	23, 35, 46, 70, 92 23, 35, 46, 92
2	X	31.81	3	280-325	35, 46, 70, 92, 184
3	WY-1	36.68	1 2 3	300-350 300-350 300-350	23, 46, 92, 184 23, 46, 92, 184, 210, 230 23, 46, 92, 184
4	WY-1	35.98	1 2 3	300-350 275-375 275-375	23, 35, 46, 92 23, 35, 46, 70, 92, 184, 210 23, 35, 46, 70, 92, 184, 210, 230
5	WY-2	25.55	1 2 3	300-350 275-350 275-350	23, 46 23, 35, 46, 92, 184 35, 46, 92, 184
6	WY-2	26.18	1 2 3	275-375 275-375 275-375	23, 46, 92 23, 35, 46, 70, 92, 184 23, 35, 46, 70, 92, 184
7	WY-2	29.40	2 3	275-375 275-350	46 46
8	HTS (G-3C)	25.86	2	375-450	11, 17, 23, 35, 46, 70, 92
9	LTS (C 18-7)	24.7	2 3	180-210 180-210	23 23

4.5 Experimental Operating Procedures

Refer to Figure 4-10.

4.5.1   Leak test

After the reactor assembly was inserted into the reactor heating block and connected to the inlet and outlet lines the system was purged air-free with N_2 via MFC-4. Thereafter the blend pot was pressurized to 10 barg with pure hydrogen using the spring loaded back pressure regulator (BPR-1) before allowing gas to flow through MFC-6/7 to the reactor. Spring loaded back regulator (BPR-2) was used to set the reactor pressure to 6 barg and gas supply from the blend pot was then stopped. Soapy water was used to check for any leaks before leaving the reactor at 6 barg for 2 hours. The reactor pressure was monitored to ensure that there was not any pressure loss, i.e. the system was tight. Thereafter, the system was depressurized back to atmospheric pressure.

4.5.2   Catalyst reduction

Noble metal catalysts (Cat X, WY-1 and 2) were received from the catalyst suppliers in reduced form (see Table 4-2). Base metal catalysts (HTS and LTS) were received in oxidic form (see Table 4-2) and had to be reduced prior to application. This was done in-situ with H_2. For this purpose, the reactor thermocouple was inserted into the thermowell of the microreactor assembly, so that the tip of the thermocouple was located level with the middle the microchannel reactor (Figure 4-13). Once atmospheric pressure was reached after the leak test, the blend pot was pressurized to 8 barg, simultaneously feeding H_2 and Ar at a 1:4 flow ratio via MFCs 2 and 5 in order to obtain a dilute reduction gas mixture of 20 mol% H_2 in inert Ar. Back pressure regulator BPR-2 was set to 1 barg, the reactor was pressurized with the reduction gas mixture to 1 barg and the flowrate of the gas mixture to the reactor was set to 10 ml_{STP}/min, equivalent to *space velocity* of approximately 23,000 ml/(h.g).

The temperature of the reactor was then ramped from ambient temperature to 375 °C at a heating rate of 2 °C per minute and held at this temperature for 12 hours. To complete the reduction process, the reactor feed was subsequently changed to pure H_2, which was fed for 1 hour at the same temperature. Thereafter, the system was purged with N_2, allowed to cool down to the intended starting temperature and eventually left in N_2 atmosphere at working pressure of 1 barg.

4.5.3 Reactor operation

The following description refers to the flow sheet as given by Figure 4-10.

4.5.3.1 Dry gas composition

Feed gases hydrogen, carbon monoxide, carbon dioxide and argon were supplied to the blend pot through MFCs 1, 2, 3 and 5 at different flows in order to make up dry gas mixtures Feeds 1, 2 and 3 (as given in Table 4-8). For more details, see Section 4.3.1.1: Dry gas mixture. A part of the gas mixture was vented through back pressure regulator BPR-1 (the 'bypass'), the point where the stream could be directed through the 4-way crossover valve to the sample line and the gas chromatograph in order to check if the desired composition of the mixture was achieved.

Table 4.8: **Compositions of the different dry gas feed mixtures applied in the experimental runs**

	Feed 1	Feed 2	Feed 3
Constituents	**Composition (mol-%)**	**Composition (mol-%)**	**Composition (mol-%)**
Ar	1.36	3.44	1.10
CO	10.90	16.01	6.10
CO$_2$	10.90	6.22	14.90
H$_2$	76.85	74.33	78.90
Total	100	100	100

Water was added (see Section 4.3.1.2: Steam formation – the evaporator), which produced the 'wet' gas. The composition of the three corresponding wet gas mixtures is given in Table 4-6

4.5.3.2 Start-up procedure

- MFCs 1, 2, 3 and 5 were adjusted so that the desired dry gas mixture was prepared as shown in Table 4-8.

- During this initial phase, all the gas mixture was vented through back pressure regulator BPR-1 and analysed until the desired composition was achieved and constant.

- The three heating bands that heated the heating block around the reactor assembly were switched on and temperature was ramped up at a rate of 1 °C per minute, still under N$_2$ atmosphere, until the desired working temperature was reached.

- The temperature of the microchannel reactor was monitored using the reactor thermocouple, the tip of which was placed level with the middle of the microreactor.

- The thermostat and the circulator of the water/glycol cooling bath were switched on to keep both steam condenser and knocked-out water catch pot at 2 °C.

- After reaction temperature was reached, degassed deionized water was pumped to the water inlet at the top of the evaportor at the desired flowrate until water and water vapour had penetrated the evaporator, tubing and reactor, so that the H_2O partial pressure in the reactor was high enough to prevent coking upon introduction of the syngas.

- Once the H_2O vapour had penetrated these units, the dry gas, at the desired flowrate, was allowed to flow into the reactor via MFC-6 or 7.

- Finally, the 4-way crossover valve was switched from bypass to reactor effluent to allow the reactor outlet stream to flow to the gas sampling device of the gas chromatograph.

4.5.3.3 Change of reaction conditions

The procedures described below were followed when changing reaction conditions.

Feed (all done without stopping neither the gas flow nor water flow to the reactor):

- When changing feed composition, the flowrates of the individual feed gases were adjusted accordingly and the streams were allowed to mix in the blend pot.

- After a period of 1 hour, the 4-way crossover valve was switched to the bypass for feed composition analysis.

- Once the desired dry feed gas composition was achieved and constant, the desired flowrate to the reactor was set on MFC-6 or 7.

- The water pump rate that was required to achieve the desired wet feed composition (as given in Table 4-4) was adjusted after the gas flowrate (without changing the microsplitter setting).

- The 4-way crossover valve was set back to reactor effluent sampling.

Space velocity:

- When changing space velocity, both gas and water feed flowrates were adjusted simultaneously via MFC-6 or MFC-7 and the pump.

- For the dry gas mixture the same procedure was followed as for "Feed"

Temperature:

- When increasing the reaction temperature, temperature was ramped at 1 °C per minute.

- When decreasing the temperature, the new temperature was set and the reactor was allowed to cool naturally.

Pressure:

- Reaction pressure was unchanged as all experimental runs were carried out at 1 barg.

Once operational conditions were changed, a waiting period of approximately 30 minutes was allowed for the system to re-establish steady state before resuming GC analysis of the product stream.

4.5.3.4 Sampling procedure

For analysis, a micro gas chromatograph (Varian CP-4900 micro GC) was used, equipped with a suction pump that drew in a side stream of the stream coming from the 4-way crossing valve (bypass or reactor effluent stream, respectively).

With respect to low space velocity microchannel reaction application, the operation time of the pump had to be limited to 10 seconds. It appeared that, at low space velocities, the suction rate of the pump was higher than the rate of the flow exiting from the microchannel reactor (of about 10 ml/min, as can be derived from Table 4-7), part of the gas sample drawn was in fact pumped back in from the vent line (see Figure 4-10), which carried a mixture of sample, bypass and GC carrier gases.

The GC was a 3 module on-line instrument, equipped with 3 injector sample loops, 3 columns and 3 thermal conductivity detectors. Once the dry gas, either from the bypass feed line or the reactor product line, had reached the sampling line, the sampling valve switched to sampling position and the suction pump drew gas from the sampling line, passed it through the injector sample loops (10 µl devices) and filled them up with gaseous sample. After 10 seconds of flushing the sample loops, the sampling valve switched back to the starting position, whereupon it allowed both argon carrier gas for channel 1 and hydrogen carrier gas for channels 2 and 3 to transport the respective samples to the corresponding columns. The injection time for channel 1 was set to 20 milliseconds, while for channels 2 and 3, it was about 40 milliseconds. Samples (8-10) were taken for every experimental set of conditions during the 2 hours following stabilization of the product composition.

It should be noted that the individual volumes injected were constant and reproducible. This allowed to determine the internal standard on only one of the channels and refer the chromatograms recorded on the other channels to it.

4.5.3.5 Shut-down procedure

- Upon completion of an experimental run, water flow was stopped while the flow of dry gas continued.
- The reactor was depressurized gradually while keeping the working temperature to ensure complete removal of H_2O from the system.
- The supply of dry feed gas was shut off after about 20 minutes.
- Thereafter, the heating bands on the reactor heating block were switched off.
- After the system had cooled down to ambient temperature, the reactor assembly was disconnected from the feed and product lines and removed from the reactor heating block.

4.6 Feed and Product Analysis

4.6.1   Gas chromatography

A micro gas chromatograph (Varian CP-4900 micro GC) was used to sample and analyze both the composition of the dry feed gas and the dry product gas on-line. The instrument was equipped with three modules, each of which consisting of an injector, a column and a thermal conductivity detector. Table 4-9 gives the column types and settings for each of the three channels.

Table 4-9: Gas chromatography conditions

Channel/ module number	1	2	3
Column type	Molsieve 5A	Molsieve 5A	5 CB
Column length (m)	10	10	10
Sampling line and injector temperature (°C)	50	50	40
Column temperature (°C)	50, isothermal	50, isothermal	40, isothermal
Column head pressure (kPa)	150, isobaric	150, isobaric	70, isobaric
Carrier gas used	Ar	H_2	H_2
Compounds analysed	H_2	Ar^1, CH_4 and CO	CO_2

[1] The internal standard, Ar, was analysed on channel 2. It should be noted that the ratios of volumes injected by the system to the individual channels were constant.

4.6.1.1 Gas chromatographic analysis and calibration

A typical chromatogram obtained from channel 2 is shown in Figure 4-14 with Table 4-10 giving the retention times for all the individual components eluted from the different channels.

4.6.1.2 GC calibration

Small percentages of Ar had been added to the WGS feed streams as internal standards (Table 4-6). Ar concentrations were kept the same as unconverted CH4 that would have been detected in the MSR effluent streams. For the calibration of the GC, calibration gas blends were produced via MFCs 1-3 and 5 and sent to the GC via the blend pot vent line (see Figure 4-10). The integrated peak area counts obtained from the gas chromatograms correspond to the flow rates and thus the mole fractions of the respective components in the sample loop.

Table 4-10: Approximate retention times of peak maximums of compounds eluted

Compound	Retention time (min)		
	Channel		
	1	**2**	**3**
H_2	0.5		
Ar		0.9	
CO		2.0	
CO_2			0.5
CH_4		1.5	
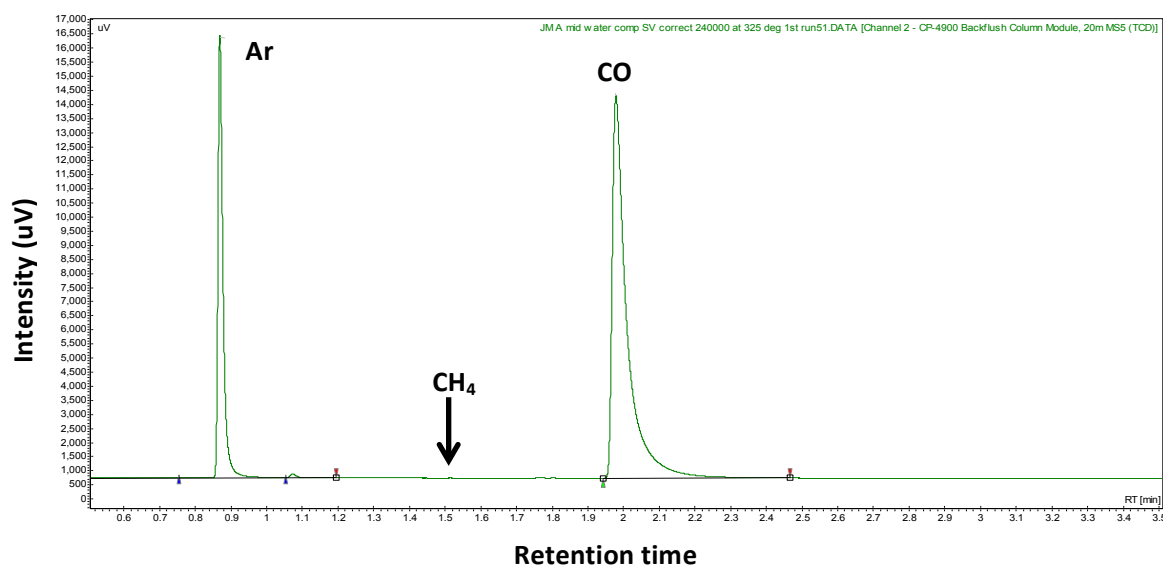
Figure 4-14:   Typical chromatogram obtained from channel 2 for analysis.

Composition data of the calibration gas blends were normalized to Ar concentration to determine the individual gas response factors by means of Equations 4-2 to 4-4 with the following:

A   =   Component A

F_A =   Fraction of A

$R_{f,\ A}$ =   Response factor (slope of the calibration line)

C_A =   Addend (intersection of the calibration line)

$$\frac{peak\ area\ of\ A}{peak\ area\ of\ Ar} = R_{f,\ A} \left(\frac{F_{A,\ calibration\ gas}}{F_{Ar,\ calibration\ gas}} \right) + C_A \qquad \textbf{eqn 4-2}$$

$$R_{f,\ A} = \frac{(peak\ area\ of\ A - C_A) \times F_{Ar,\ calibration\ gas}}{(peak\ area\ of\ Ar - C_A) \times F_{A,\ calibration\ gas}} \qquad \textbf{eqn 4-3}$$

Calibration lines were determined for H_2, CO and CO_2 relative to Ar (see Appendix II, Figures AII-1 to AII-3). From these lines the individual response factors or all feed and product constituents were obtained by linear regression. Equations and factors are given in Table 4.11.

Table 4-11: Individual linear regression equations obtained from gas calibration (relative to Ar)

Component	Channel (equation)			Channel ($R_{f, A}$)			Channel (C_A)		
	1	**2**	**3**	**1**	**2**	**3**	**1**	**2**	**3**
H_2	y = 5.49x			5.49			-		
CO		y = 0.94x + 0.0074			0.94			0.0074	
CO_2			y = 0.93x + 0.0722			0.93			0.0722

The mole fractions of the individual compounds in a product sample were then defined as follows:

$$F_{A, \ product} = \left(\frac{\left(\left(\frac{peak \ area \ of \ A}{peak \ area \ of \ Ar} \right) - C_A \right)}{R_{f, \ A}} \right) \times F_{Ar, \ feed} \qquad \textbf{eqn 4-4}$$

The molar fractions of the individual feed constituents, such as $F_{Ar, \ feed}$, were derived from calibrated mass flow controller settings (see Section 4.3.1.1: Dry gas mixture).

4.6.2 Data work-up

Once the molar fractions of all the individual constituents of the product gas mixture were determined based on Equation 4-4, CO conversion was calculated using Equation 4-5.

$$X_{CO} = \frac{F_{CO, \ feed} - F_{CO, \ product}}{F_{CO, \ feed}} \qquad \textbf{eqn 4-5}$$

The yield and selectivity of methane, small percentages of which were found over some of the catalysts, were not explicitly determined. The slight changes in number of moles of gaseous product by the occasional formation of very small amounts of methane were ignored when calculating X_{CO}. Formation of methane is indicated by a (slight) drop of the carbon balance to below 1.0.

5. RESULTS

In this chapter, the results from catalyst performance testing are given by individual sections for the different catalysts. Results for each catalyst are given in the following order: catalyst stability, performance measurement reproducibility, effect of space velocity and effect of temperature, all compared to thermodynamic equilibrium conversion (ASPEN Plus[TM] process simulation software). Detailed lists of data obtained are given in Appendix V.

Noble metal catalysts WY-1, WY-2 as well as the base metal catalyst LTS were obtained as ready-made catalyst coated microchannel reactors plates (see Table 4.1: List of catalysts used), while noble metal catalyst X and base metal catalyst HTS were obtained in powder form and were coated in-house, as described in Section 4.2.2: Wash-coating method. Therefore, the outcome of the coating procedure is described first.

5.1 Properties of the Catalyst Washcoating

Following the original Zapf method (Zapf et al., 2003), except for the addition of acetic acid, since there was no need for pH adjustment (see Section 2.3.1.5: Uniformity of the coating), resulted in uniform wash-coats with good adhesion to the channel walls.

5.1.1 Uniformity of catalyst coating

For the top view and cross sectional images of the coated test plates (Figures 5-1 A and B and 5-2 A), the uniform distribution of the coated catalyst between and along the individual channels can clearly be seen. Furthermore, it can also be seen that the catalyst layer is closely packed onto the walls.

(A)   **(B)**
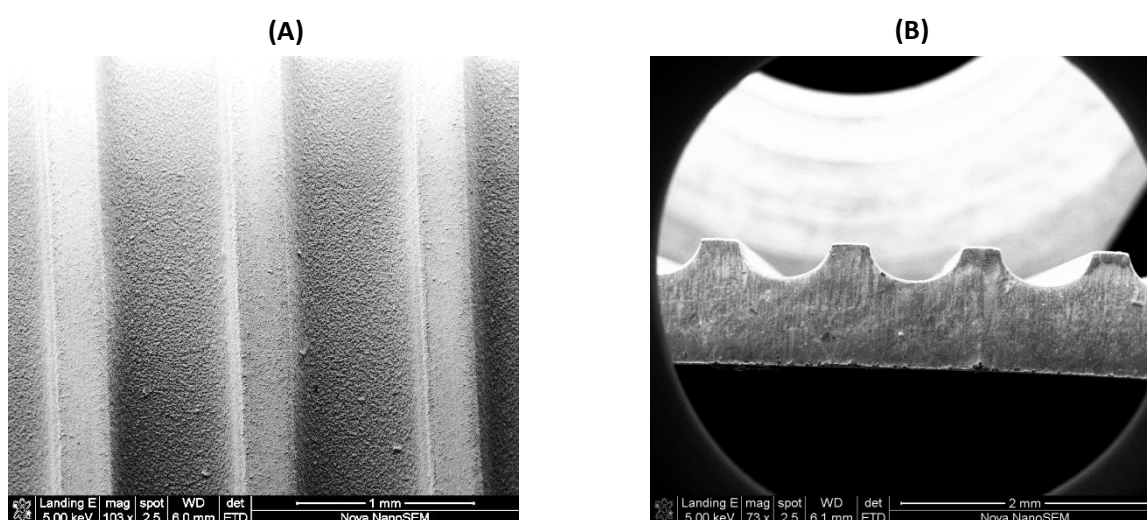
Figure 5-1: **Top view and cross-sectional image of a microchannel test plate showing a uniform distribution of the catalyst washcoat between and along channels (A) and on the channel walls and bottoms (B)**

5.1.2   Catalyst adhesion on microchannel walls

With 6 different microchannel test plates, coated with catalyst X (one of the two catalysts that were coated in-house), the 'drop test' (see Section 4.2.6.1: Catalyst adhesion) was performed. From 'drop test' analyses, it was found that only negligible weight loss had occurred after each plate was subjected to 10 tests. The average loss suffered for all the test plates dropped was 0.3 % of the original mass of the catalyst coating and for individual plates, the weight loss was always below 1%. A full detailed compilation of the 'drop test' results can be found in Appendix IV in Table IV-1. The coating was found to be still closely packed and uniformly distributed onto the microchannel channel walls after adhesion test ('drop test'), with the washcoating not showing any discontinuities, cracks or peeling-off the wall. An example is shown in Figure 5-2 (B).

(A)

(A)

(B)

(B)
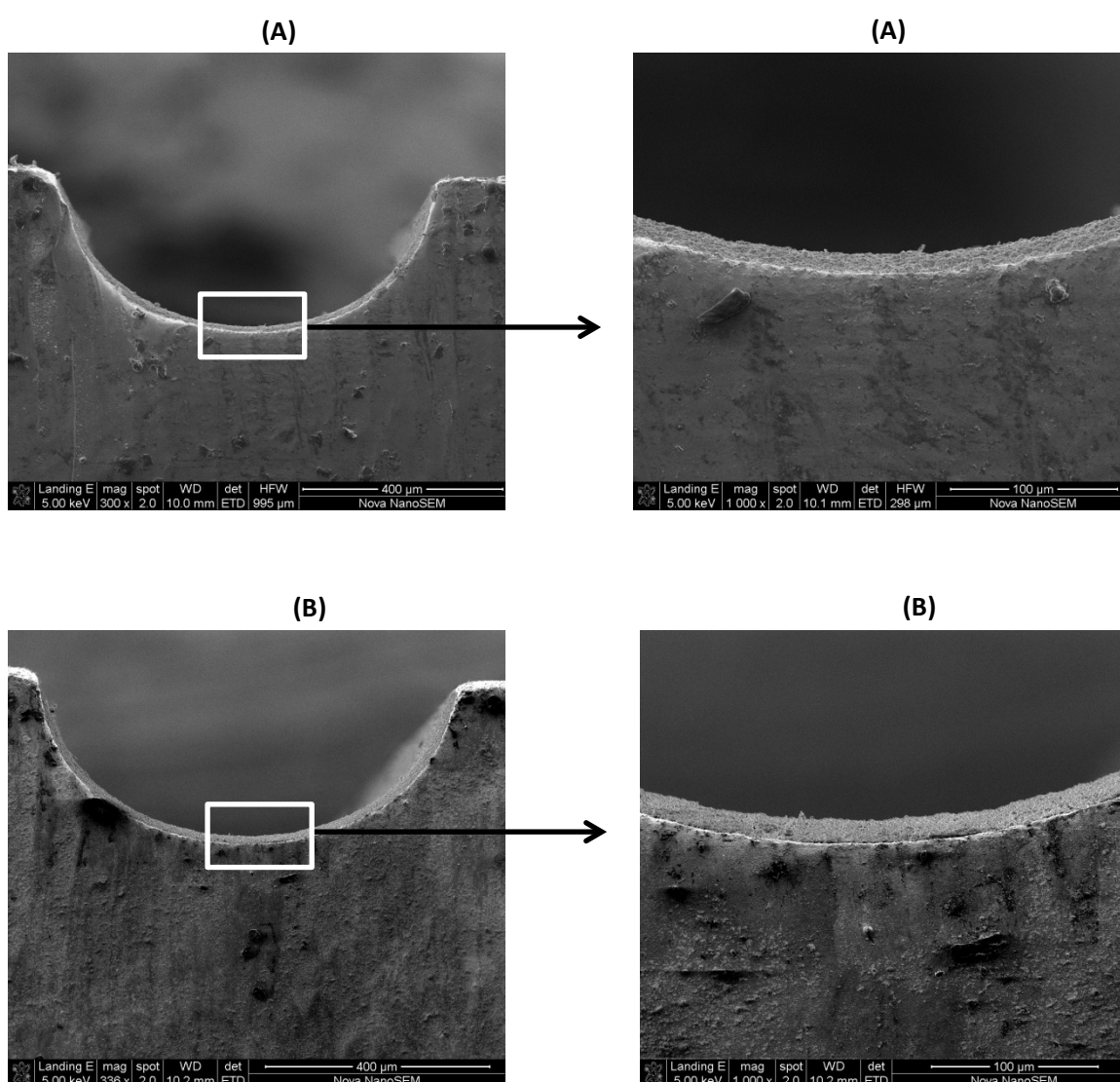
Figure 5-2:   Cross-sectional image of microchannel test plates showing a uniform distribution and a close packing of the washcoat on the channel walls before (A) and after the drop test (B)

5.2 Performance of Catalyst WY-1

5.2.1 Catalyst stability

Experiment 4 was run for more than 550 hours, varying feeds and reaction conditions (see Table 4-6 in Section 4.4.1: Feed composition and Table 4-7 in Section 4.4.5: Overview of experimental runs). Catalyst performance was monitored over prolonged time on stream at all the conditions tested and was found to be stable for the entire duration of the experiment, as shown in Figure 5-3. The same CO conversion of slightly above 50% was obtained during the first 20 hours on stream and upon repeating the initial reaction condition after approximately 550 hours on stream, showing that activity was still retained.
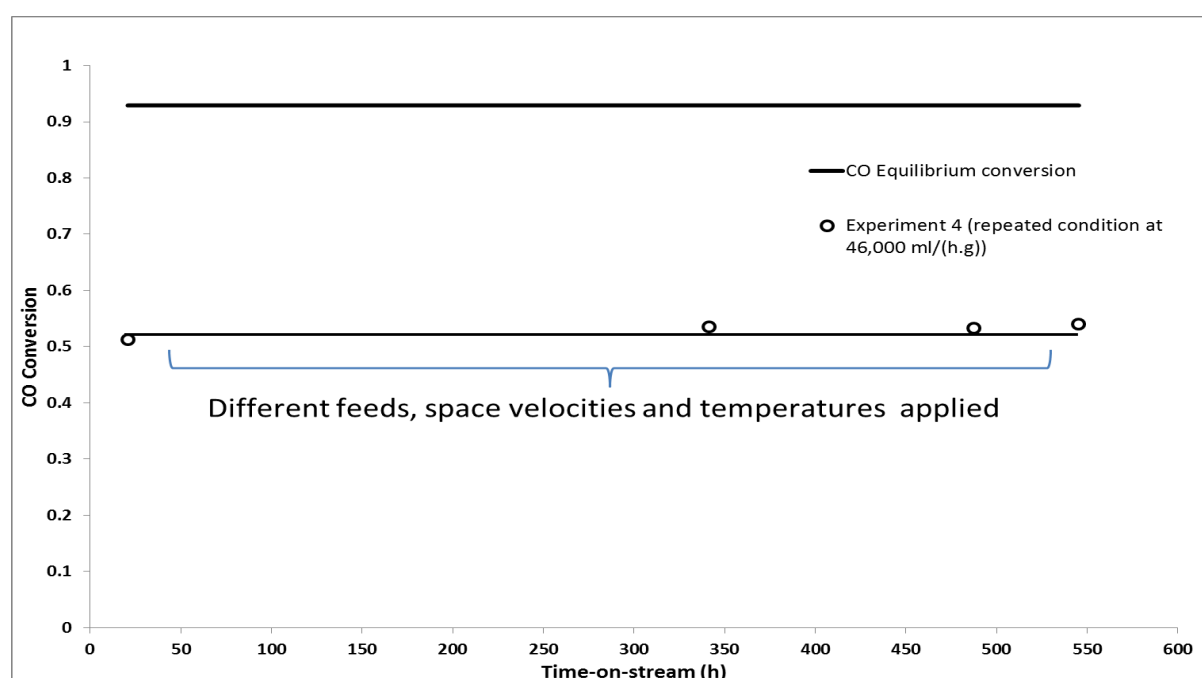
Figure 5-3: **Time-on-stream performance of catalyst WY-1. Data points shown were obtained with Feed 3 at SV_{DRY} of 46,000 ml/(h.g$_{cat}$), 275 °C and 1 barg (Experiment 4). (The Individual data points represent averages of 10 samples each, taken over periods of 2 hours)**

5.2.2 Catalyst performance reproducibility

Figures 5-4 to 5-6 show CO conversion (i.e. catalyst activity) for repeated experimental runs using different reactors, i.e., fresh coatings (Table 4-7 in Section 4.4.5: Overview of experimental runs) coated with catalyst WY-1, namely experiments 3 and 4 with feeds 1, 2 and 3 (Table 4-6 in Section 4.4.1: Feed composition) at varying space velocities and temperatures. Only small deviations, i.e., acceptable reproducibility for both the reactors with each of the feeds were observed (Section 5.3.2: Catalyst performance reproducibility for the analysis of the deviation in catalyst WY-2 reproducibility tests).

Figure 5-4: Experimental performance reproducibility and effect of temperature for catalyst WY-1 with Feed 1 (Table 4-6 in Section 4.4.1: Feed composition) at different dry gas *space velocities.* Experiments 3 (open symbols) and 4 (full symbols)

Figure 5-5: Experimental performance reproducibility and effect of temperature for catalyst WY-1 with Feed 2 (Table 4-6 in Section 4.4.1: Feed composition) at different dry gas *space velocities.* Experiments 3 (open symbols) and 4 (full symbols)

Figure 5-6: Experimental performance reproducibility and effect of temperature for catalyst WY-1 with Feed 3 (Table 4-6 in Section 4.4.1: Feed composition) at different dry gas *space velocities*. Experiments 3 (open symbols) and 4 (full symbols).

5.2.3 Effect of space velocity

The three different feeds were also used to investigate the effect of space velocity on catalyst performance. *Dry gas space velocities* applied ranged from 23,000 to 230,000 ml/(h.g$_{cat}$) at temperatures between 275 and 375 °C. Figures 5-7 to 5-8 show CO conversion generally decreased with increasing space velocity, as expected, especially and proportionally for low CO conversions far from equilibrium conversion.
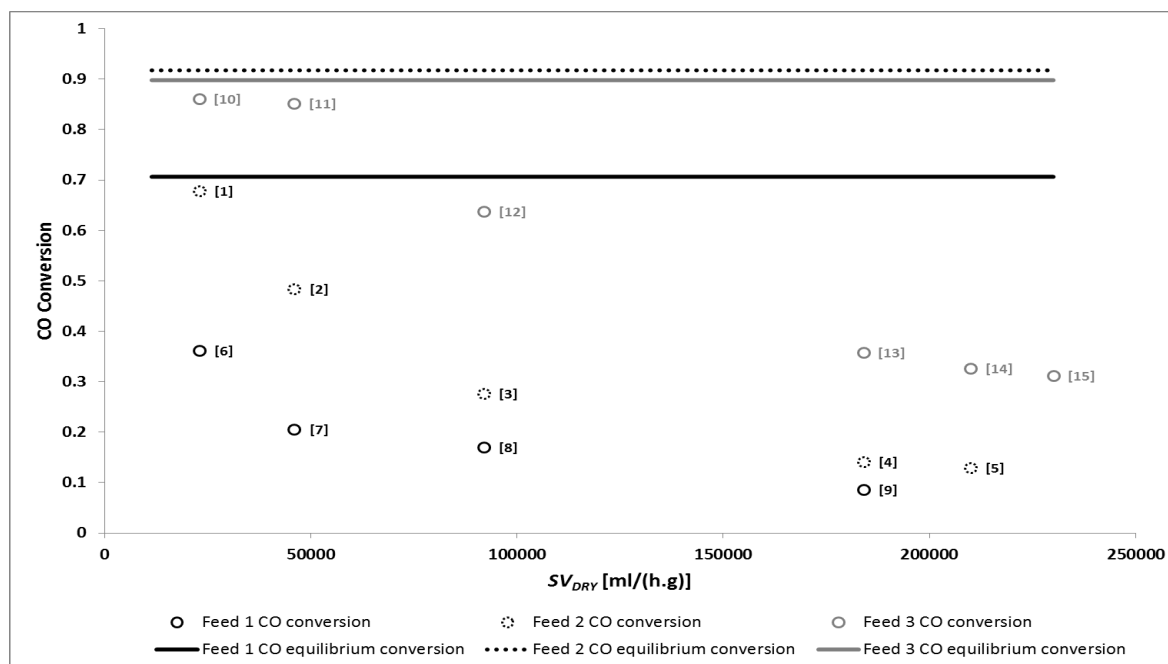
Figure 5-7: CO conversion over catalyst WY-1 as a function of space velocity with Feeds 1, 2 and 3 (Table 4-6 in Section 4.4.1: Feed composition) at 300 °C (Experiment 3). [] values in square brackets indicate the testing sequence.
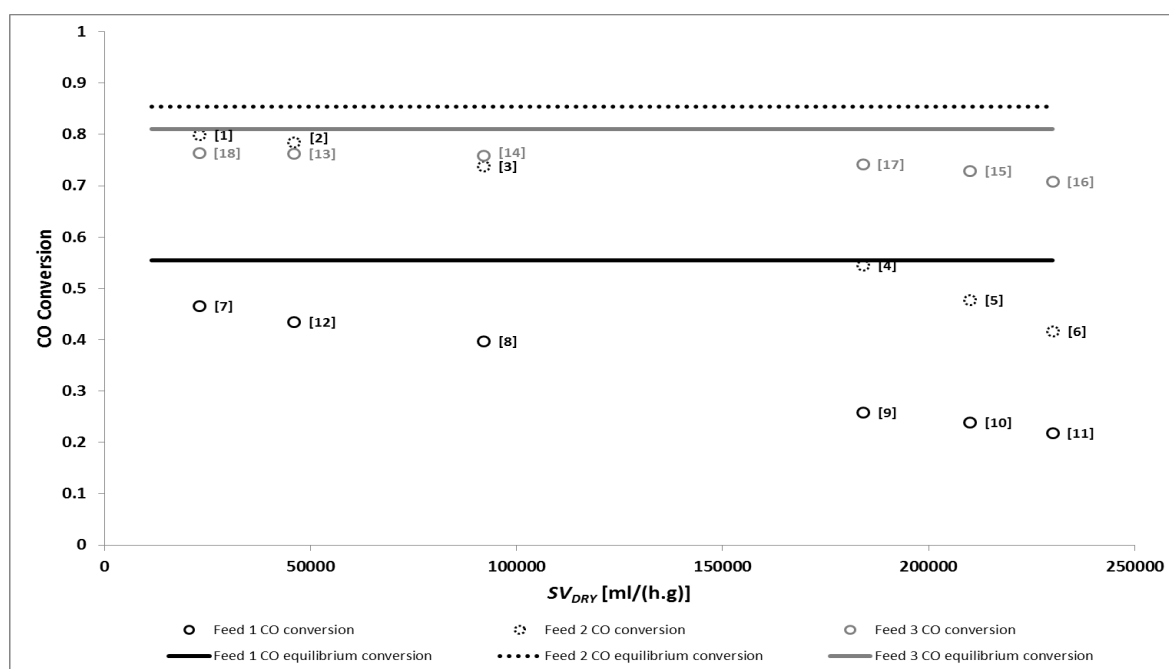
Figure 5-8: CO conversion over catalyst WY-1 as a function of space velocity with Feeds 1, 2 and 3 (Table 4-6 in Section 4.4.1: Feed composition) at 350 °C (Experiment 3). [] values in square brackets indicate the testing sequence.

5.2.4 Effect of temperature

Temperature effect was evaluated by increasing temperature from 275 °C to 375 °C in increments of 25 °C. Results from using different feeds are shown in Figures 5-4 to 5-6. As long as equilibrium conversion was not reached (or closely approached), CO conversion increased with increasing temperature as expected. It was also observed that under all conditions CO conversion decreased with increasing temperature after having reached equilibrium conversion. This is as expected, since equilibrium CO conversion declines with increasing temperature, as the figures show. For Feed 1, as indicated in Figure 5-4, equilibrium conversion was reached at temperatures around 350 °C for SV_{DRY} of 46,000 ml/(h.g_{cat}) and below while, for higher SV_{DRY} above 92,000 ml/(h.g_{cat}), CO conversion at 350 °C was still far from equilibrium conversion.

For Feed 2 as shown in Figure 5-5, equilibrium conversion was reached at temperatures around 350 °C for SV_{DRY} of 92,000 ml/(h.g_{cat}) and below while, for SV_{DRY} higher than 92,000 ml/(h.g_{cat}), CO conversion at 350 °C was still far from equilibrium conversion.

A similar trend of an increase in CO conversion with increasing temperature was also observed with Feed 3 (Figure 5-6), the feed with the highest S/CO ratio. CO conversion reached equilibrium conversion at 300 °C already for SV_{DRY} of 46,000 ml/(h.g_{cat}) and below, at 325 °C for SV_{DRY} of 92,000 ml/(h.g_{cat}) and almost so at 350 °C for SV_{DRY} of 184,000 ml/(h.g_{cat}).

The reason for the differences between calculated and measured CO equilibrium conversions are addressed in section 5.3.2: Catalyst performance reproducibility (for catalyst WY-2).

5.3 Performance of Catalyst WY-2

5.3.1 Catalyst stability

Experiment 6 was run for approximately 750 hours varying reaction conditions and feeds (Table 4-6 in Section 4.4.1: Feed composition and Table 4-7 in Section 4.4.5: Overview of experimental runs). CO conversion for feed 2 and 3 at different times on stream is shown in Figure 5-9. For Feed 2, at SV_{DRY} of 23,000 ml/(h.g$_{cat}$) and a temperature of 275 °C, CO conversion of approximately 46% was observed during the first 28 hours on stream and upon repeating the initial reaction condition after approximately 650 hours on stream, activity was still retained. However, a decrease in activity to approximately 41% was observed after 750 hours on stream. This was after the catalyst had been exposed to low S/CO ratio Feed 1 (Table 4-6 in section 4.4.1: Feed composition) at a temperature of 375 °C between 650 hours and 750 hours on stream. For feed 3 at SV_{DRY} of 184,000 ml/(h.g$_{cat}$) and a temperature of 275 °C, CO conversion of approximately 35% was observed during the first 81 hours on stream and no deactivation was found upon repeating the initial reaction condition after 620 hours on stream.
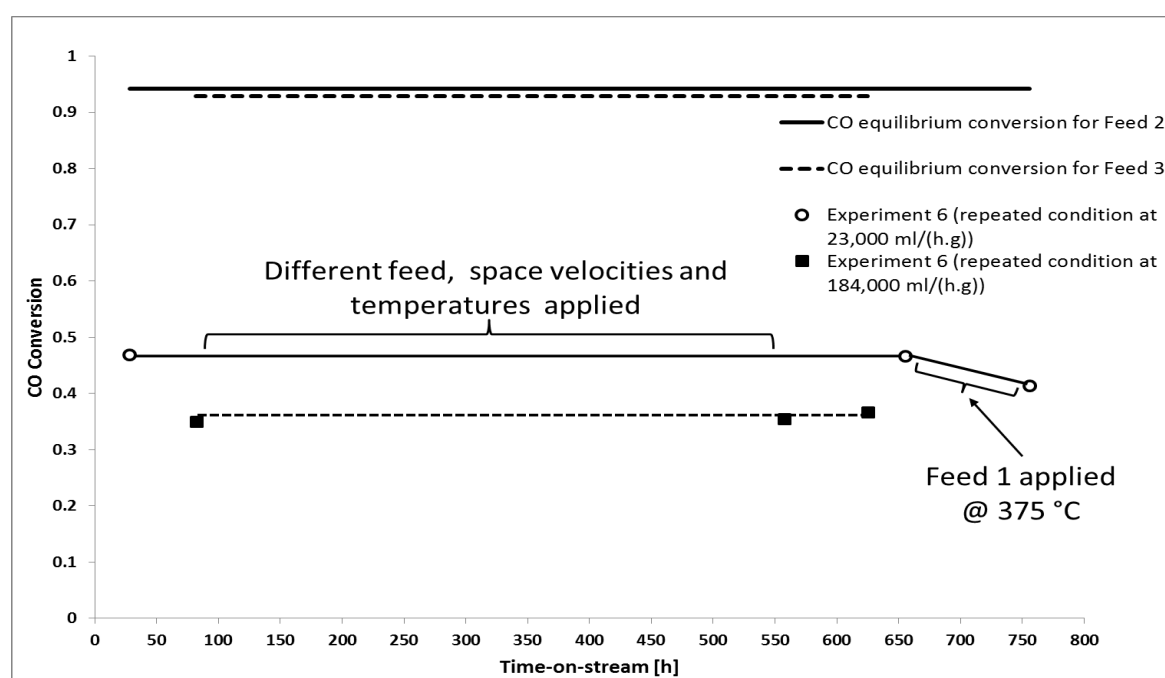
Figure 5-9: **Time-on-stream performance of catalyst WY-2. Data points shown were obtained with Feed 2 and 3 at SV_{DRY} of 23,000 ml/(h.g$_{cat}$) and 184,000 ml/(h.g$_{cat}$), respectively, 275 °C and 1 barg (Experiment 6). (The individual data points represent averages of 10 samples each, taken over periods of 2 hours).**

5.3.2   Catalyst performance reproducibility

Figures 5-10 to 5-12 show CO conversion (i.e. catalyst activity) for repeated experimental runs using different reactors, i.e., fresh coatings (Table 4-7 in Section 4.4.5: Overview of experimental runs) coated with catalyst WY-2, namely experiments 5, 6 and 7 with Feeds 1, 2 and 3 (Table 4-6 in section 4.4.1: Feed composition) at varying space velocities and temperatures. After experiment 5 and the repeat, experiment 6 had been carried out, it appeared that catalyst activity was not reproducible for any of the 3 different feeds at the temperatures and space velocities applied. This is evidently clear for experiments 5 and 6 from Figures 5-10 to 5-12.
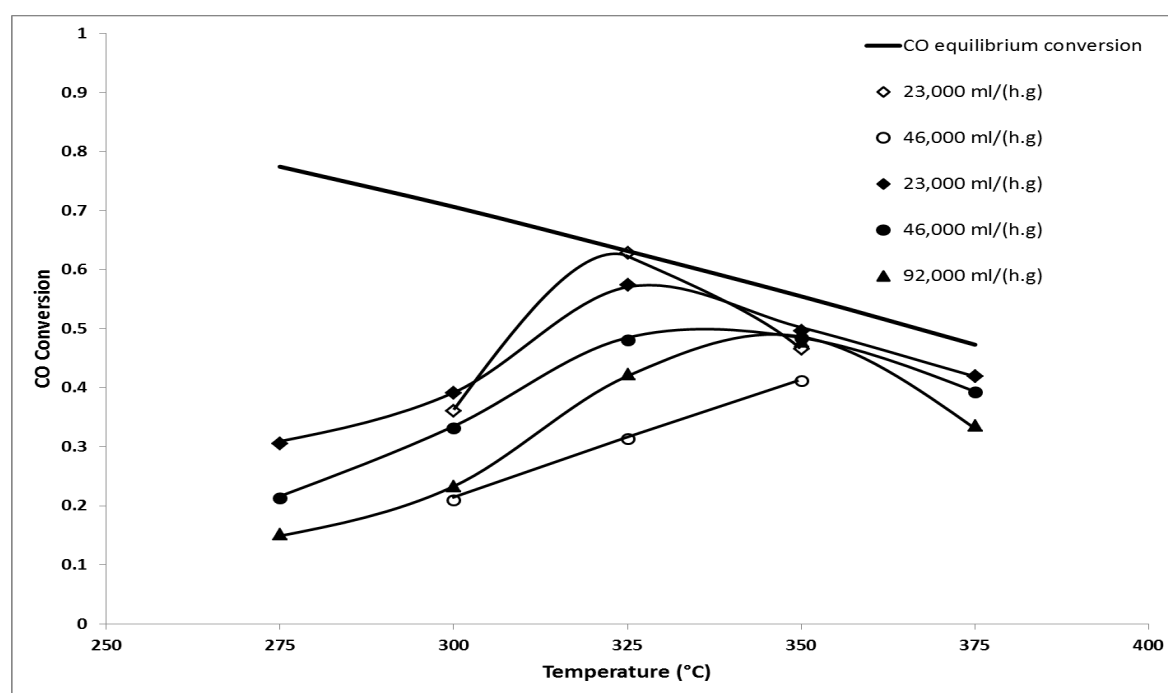
Figure 5-10:   Experimental performance reproducibility and effect of temperature for catalyst WY-2 with Feed 1 (Table 4-6 in Section 4.4.1: Feed composition) at different dry gas *space velocities*. Experiments 5 (open symbols) and 6 (full symbols).

Consequently, a third run with catalyst WY-2 was carried out, experiment 7. The results from experiment 7 were similar to those from experiment 5, indicating that experiment 6 was flawed.

Section 5.3.2.1 is an attempt to analyze and identify the cause of this fail.
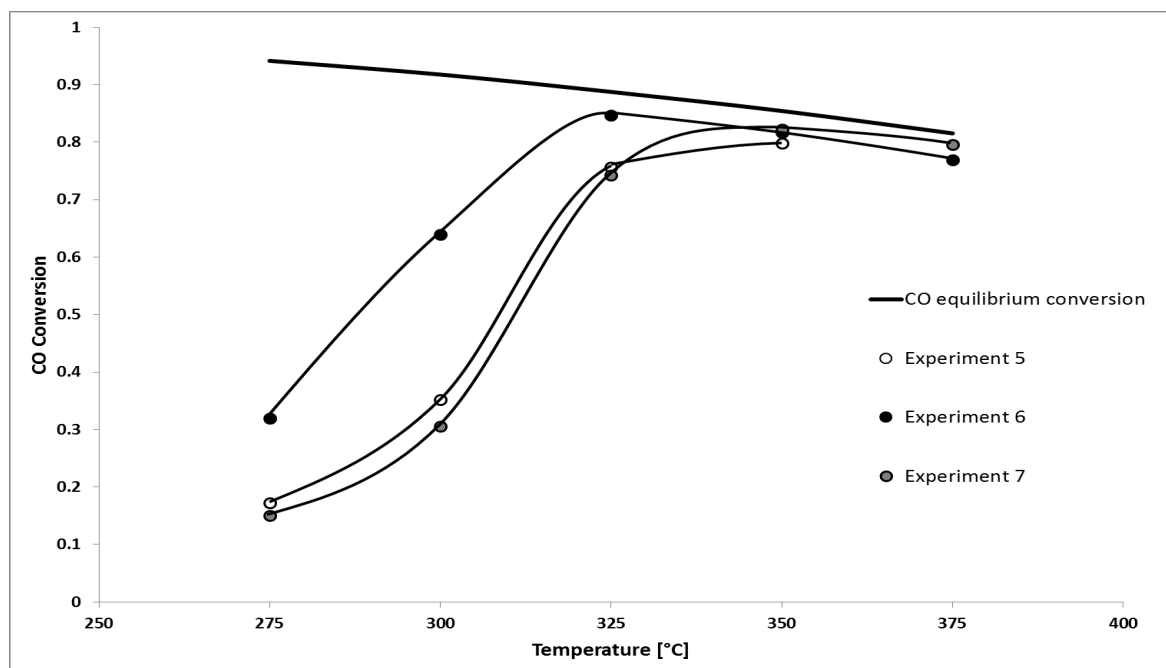
Figure 5-11: Experimental performance reproducibility and effect of temperature for catalyst WY-2 with Feed 2 (Table 4-6 in Section 4.4.1: Feed composition) at SV_{DRY} of 46,000 ml/(h.g_{cat}). Experiments 5 (open symbols), 6 (full symbols) and 7 (grey symbols).
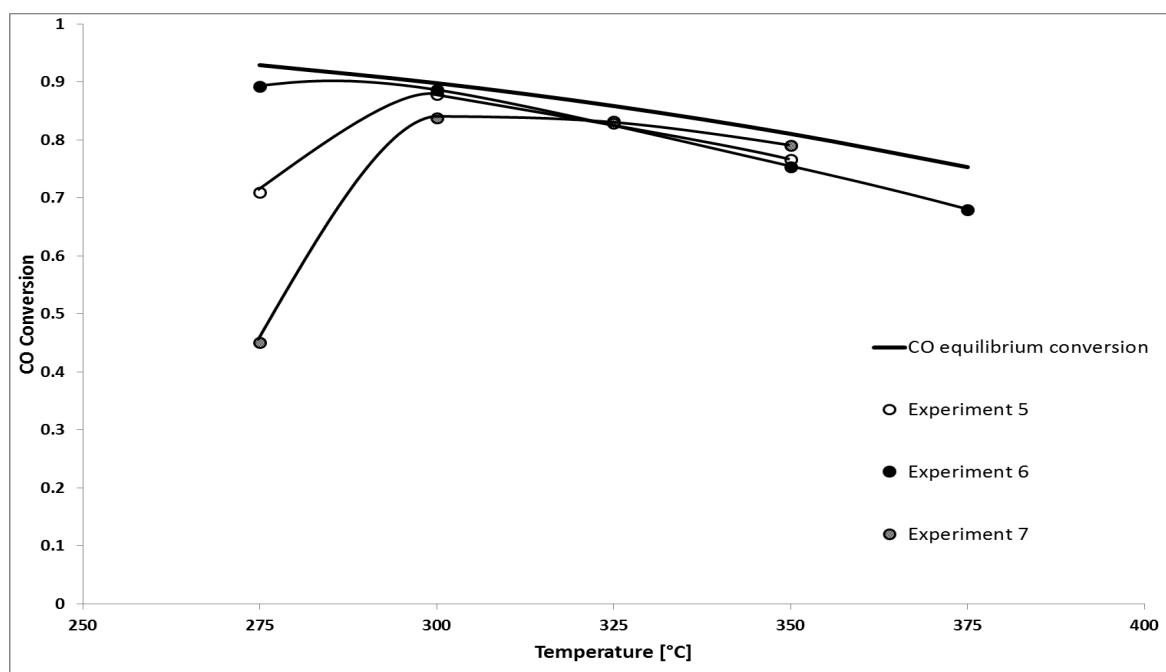
Figure 5-12: Experimental performance reproducibility and effect of the temperature for catalyst WY-2 with Feed 3 (Table 4-6 in Section: 4.4.1 Feed composition) at SV_{DRY} of 46,000 ml/(h.g_{cat}). Experiment 5 (open symbols), 6 (full symbols) and 7 (grey symbols).

More results of CO conversion for repeated experimental runs using the different reactors coated with catalyst WY-2, namely experiments 5, 6 and 7 with Feed 3 and carried out at different space velocities and temperatures (Table 4-7 in section 4.4.5: Overview of experimental runs and Table 4-6 in Section 4.4.1: Feed composition) are given in Appendix VI, Figure VI–2.

5.3.2.1 Non-optimal configuration of the microreactor environment

A closer look at the curves for CO conversion versus temperature reveals a general trend, which suggest and indicates towards the possible cause of the poor reproducibility: Figures 5-10 to 5-12 (for Feeds 1 to 3) show the following ranking of catalysts activities/ reactors/ experimental setups in experiments 5, 6 and 7 (Table 5–1):

Table 5–1: Seeming ranking of catalyst WY-2 activities in repeat experiments

Figure	Low temperature	T [°C]	High temperature	T [°C]
5-10	Exp 6 > Exp 5	300	n/a	
5-11	Exp 6 > Exp 5 > Exp 7	275, 300	Exp 7 > Exp 6	375
5-12	Exp 6 > Exp 5 > Exp 7	275	Exp 7 > Exp 5 > Exp 6	350

For all of the figures, the trend in conversion at low and high temperature is identical, but exactly reversed. Also, the curves for the high temperatures branches are running in parallel to the equilibrium conversion curve but at a distance below it. The trend in distance to the equilibrium conversion curve follows the trend at low temperature, namely:

$$Exp\ 6\ \gg\ Exp\ 5\ >\ Exp\ 7$$

In the experimental setup utilized (Figure 4-7: Brass sleeves, in Section 4.3.2: Microchannel reactor assembly), the thin, long plate of the microreactor was housed in a slit of a cylindrical sleeve. This sleeve was then placed in the round through-hole of the heating block. The thermocouple that measured the reaction temperature was located in a narrow hole in the sleeve, parallel and close to the microreactor.

Assuming, as a working hypothesis, that the configuration of the microchannel reactor assembly was not optimal and that the temperature measured by the said thermocouple did not reflect the correct actual temperature of the catalyst bed, the deviations in activity (CO conversion) observed under supposedly identical reaction conditions, may be attributed to incorrect catalyst temperature measurement due to the tip of the thermocouple not being placed correctly on level with the middle of the microreactor, see Figure 4-13, but erroneously outside the isothermal zone (Figure 4-11).

Indeed, for experiments 5, 6 and 7, with feeds 2 and 3, shifting the data points for experiment 6 (full black symbols) by 20 °C to the right (i.e. to a higher temperature as indicated by the reactor thermocouple during experiment 6) results in a good match of the individual sets of data points obtained from the three experiments and also the equilibrium curve. This working hypothesis is proved to be correct by both Figures 5-13 and 5-14 (for Feeds 2 and 3, respectively) that show that the irreproducibility of performances during these experiments was due to incorrect temperature measurements indeed, probably caused by an incorrectly positioned thermocouple.
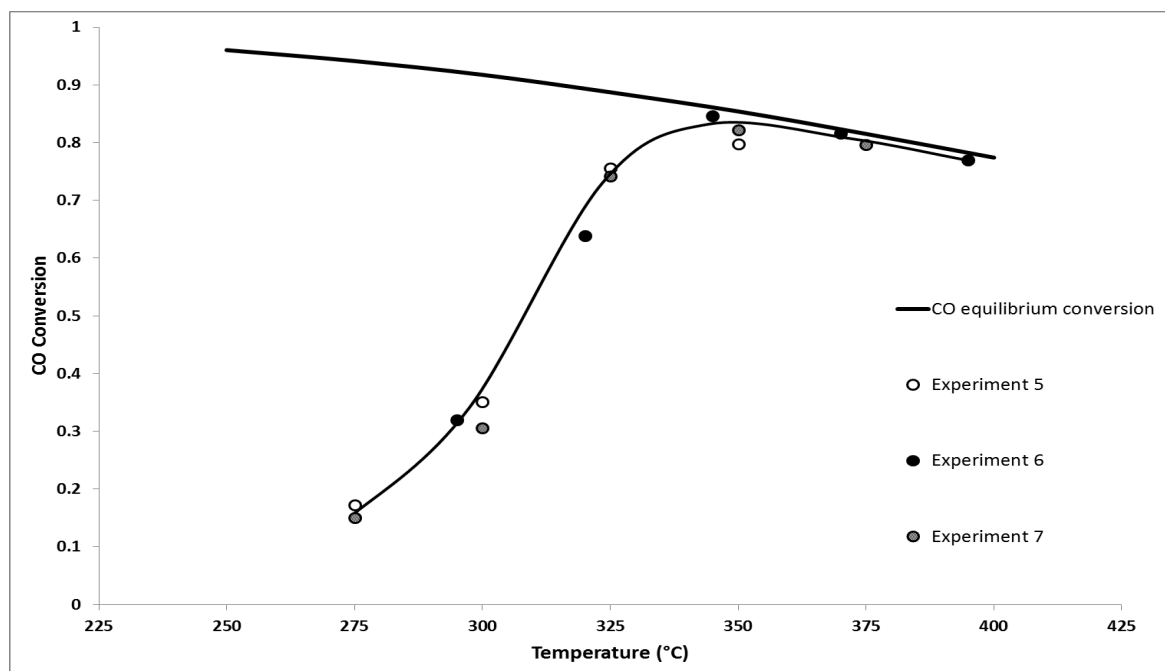
Figure 5-13: **Modified experimental performance reproducibility plot for catalyst WY-2 with Feed 2 (Table 4-6 in Section 4.4.1 Feed composition) at SV_{DRY} of 46,000 ml/(h.g$_{cat}$). Data points for experiment 6 are shifted to the right by 20 °C compared to Figure 5-11. Experiment 5 (open symbols), 6 (full symbols) and 7 (grey symbols).**
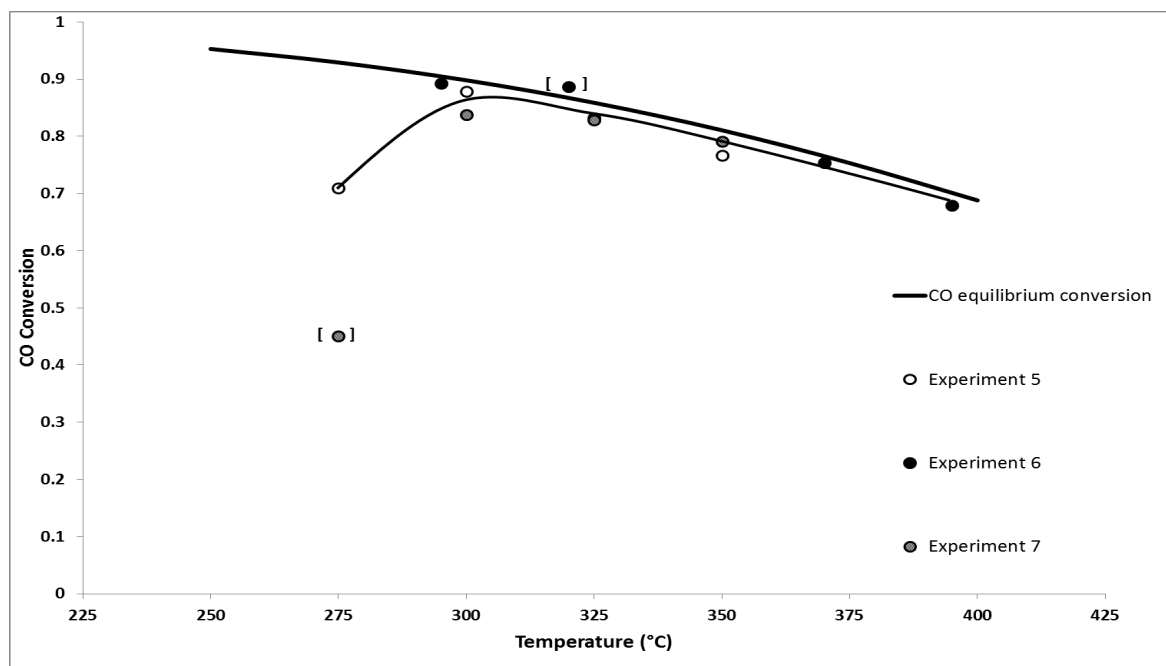
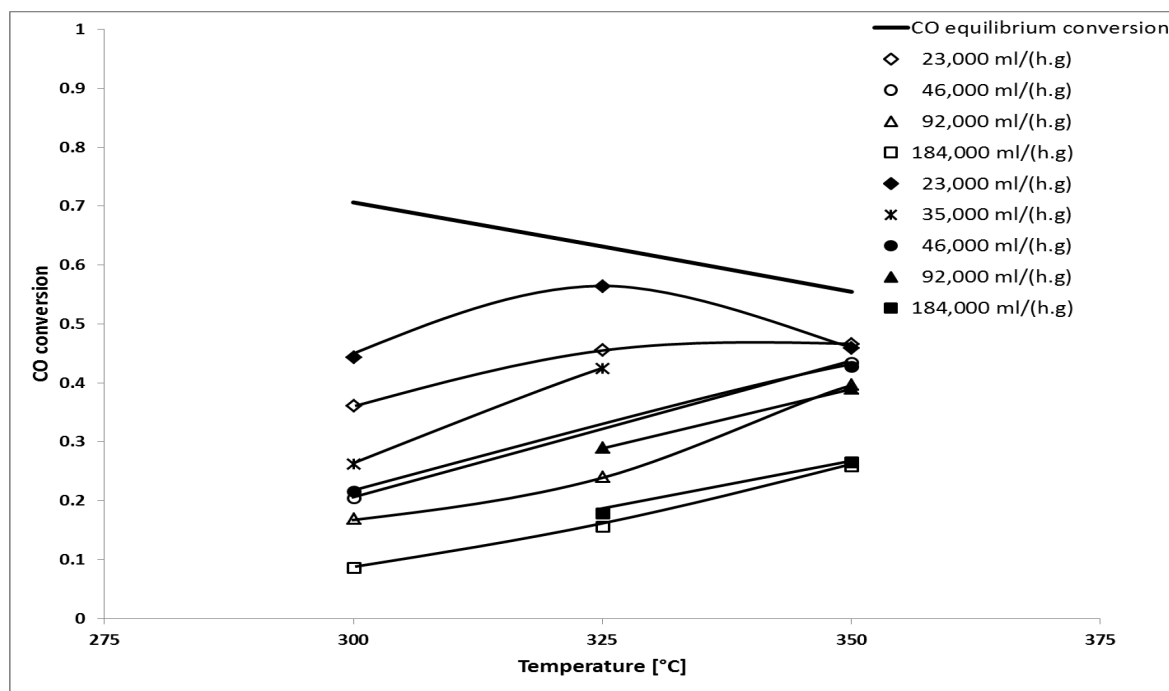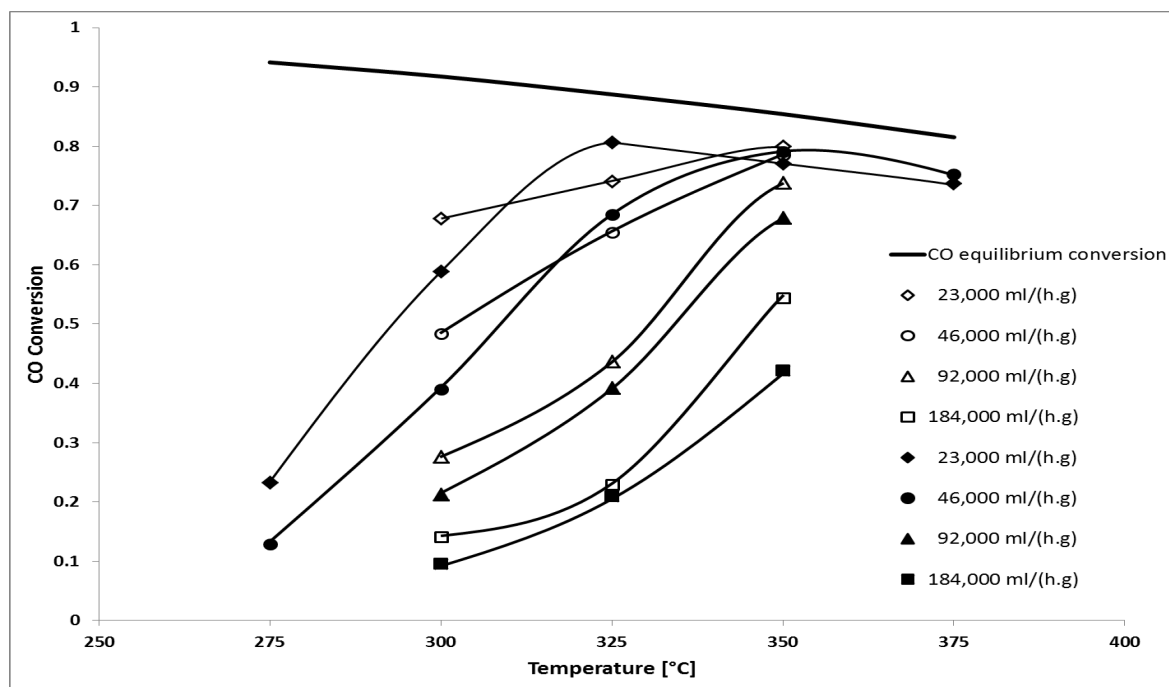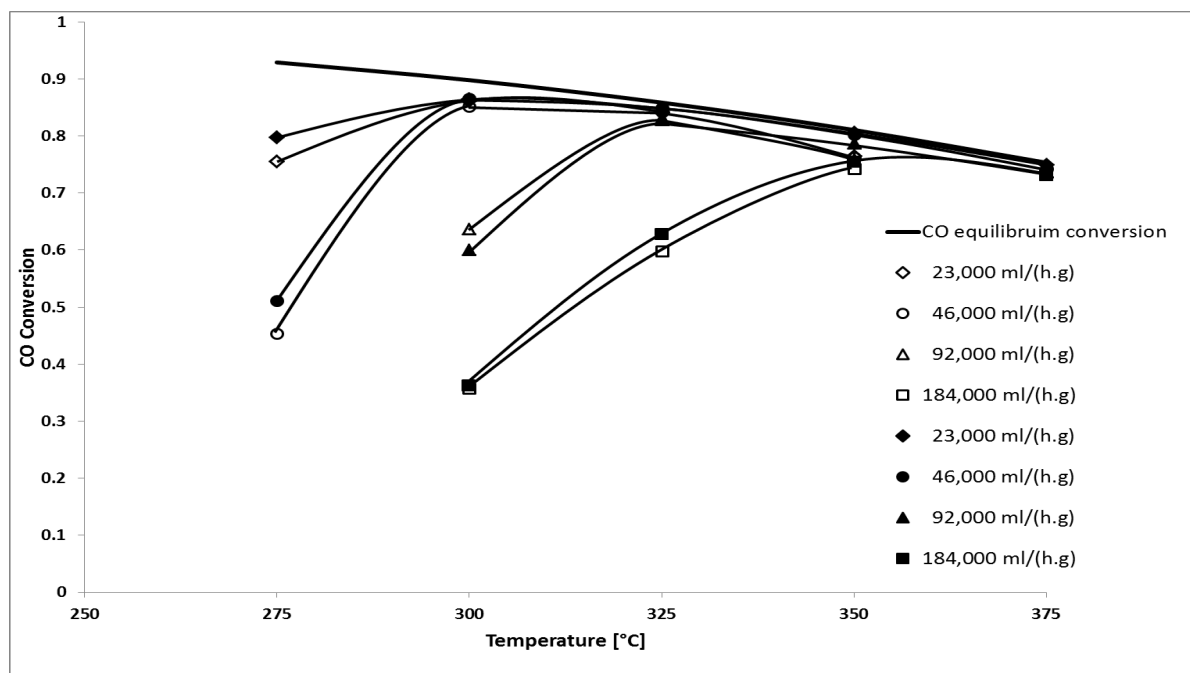**Figure 5-14:** **Modified experimental performance reproducibility plot for catalyst WY-2 with Feed 3 (Table 4-6 in Section 4.4.1: Feed composition) at SV_{DRY} of 46,000 ml/(h.g$_{cat}$). Data points for experiment 6 are shifted to the right by 20 °C compared to Figure 5-12. Experiment 5 (open symbols), 6 (dotted symbols) and 7 (grey symbols).**

5.3.3 Effect of space velocity

The three different feeds (Feeds 1, 2 and 3) were also used to investigate the effect of space velocity on catalyst WY-2 performance. Results for catalyst WY-2 activity determination were not sufficiently reproducible (section 5.3.2.1: Non-optimal configuration of the microreactor environment). Therefore, only Feeds 2 and 3 results from experiments 5, varying dry gas space velocity (ranging from 23,000 to 230,000 ml/(h.g$_{cat}$)) at a temperature of 300 °C were used to show the effect of space velocity. Figures 5-15 (averaged CO conversions) show CO conversion generally decreased with increasing space velocity, as expected, especially and proportionally for CO conversions far from equilibrium conversion.
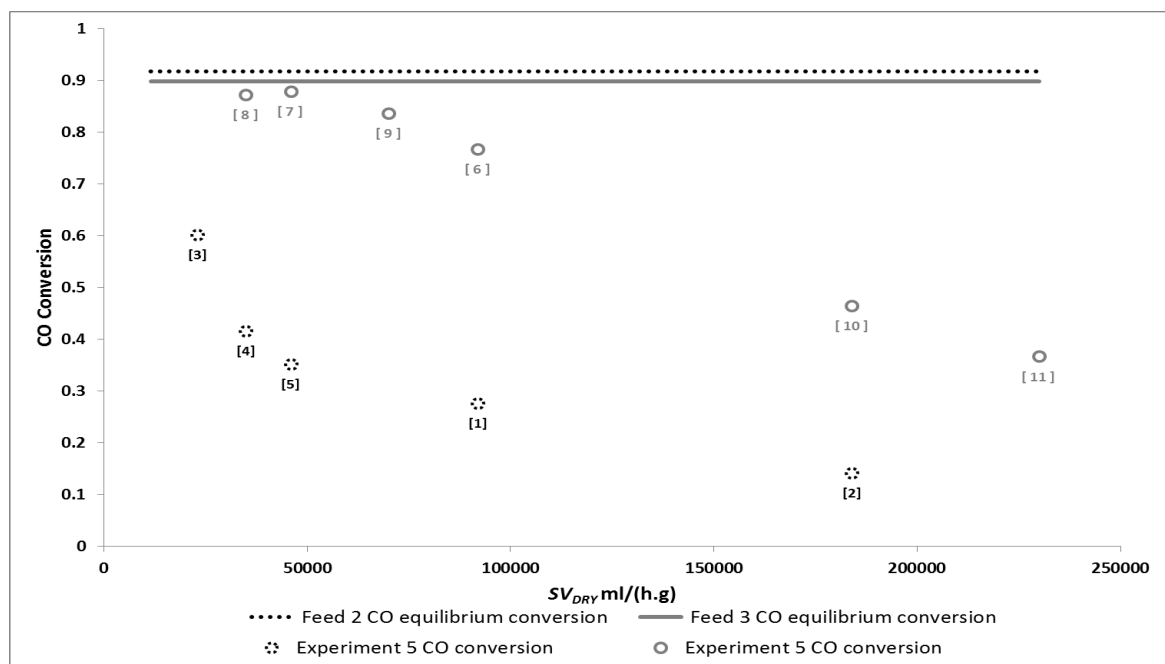
Figure 5-15: CO conversion over catalyst WY-2 as a function of space velocity with Feeds 2 and 3 (Table 4-6 in Section: 4.4.1 Feed composition) at 300 °C (Experiments 5). [] values in square brackets indicate the testing sequence

5.3.4   Effect of temperature

Temperature effect was evaluated by increasing temperature from 275 °C to 375 °C in increments of 25 °C. Results from different feeds are shown in Figures 5-10 to 5-12 and with temperature corrected data points for experiment 6 shown in Figure 5-13. As long as equilibrium conversion was not reached, CO conversion increased with increasing temperature as expected. For Feed 2 as observed in Figure 5-11 and 5-13, equilibrium conversion was reached at temperatures around 350 °C for dry gas *space velocity* of 46,000 ml/(h.g_{cat}).

A similar trend of an increase in temperature resulting in an increase in CO conversion was also observed with Feed 3 (Figure 5-14). CO conversion approached equilibrium conversion at 300 °C for dry gas *space velocity* of 46,000 ml/(h.g_{cat}). It was also observed, as expected, that at all conditions CO conversion decreased with further increasing temperature after equilibrium conversion was reached.

5.4 Performance of Catalyst X

5.4.1 Catalyst stability

Experiment 2 was run for approximately 180 hours with Feeds 2 and 3, varying reaction temperature and space velocity (Table 4-6 in Section 4.4.1: Feed composition and Table 4-7 in Section 4.4.5: Overview of experimental runs). Rapid catalyst deactivation was observed. CO conversion as a function of time-on-stream for Feed 3 is shown in Figure 5-16. Prior to that, the catalyst has lost one third of its initial activity, while exposed to a temperature of only 325 °C at various space velocities.
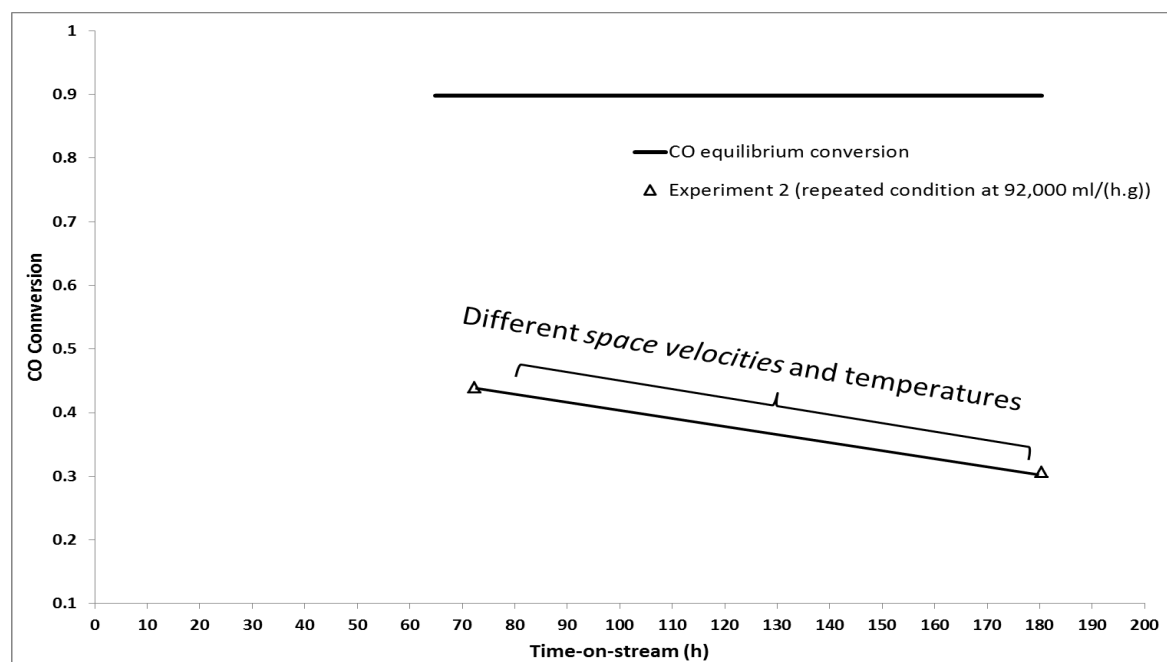
Figure 5-16: Time-on-stream performance of catalyst X. Data points shown were attained with Feed 3 at SV_{DRY} of 92,000 ml/(h.g$_{cat}$), 300 °C and 1 barg (Experiment 2). (The individual data points represent averages of 10 samples each, taken over periods of 1 hour)

5.4.2 Catalyst performance reproducibility

Performance reproducibility experiments were not carried out for catalyst X.

5.4.3 Effect of space velocity

Since Catalyst X was not stable, only two experiments were carried out to investigate the effect of space velocity on catalyst performance. Results from experiment 1 with Feed 2 at temperatures of 325 and 350 °C and dry gas *space velocities* ranging from 23,000 to 92,000 ml/(h.g) are shown in Figure 5-17. Results from experiment 2 with Feed 3 at temperatures of 280, 300 and 325 °C, and dry gas *space velocities* of 35,000 to 184,000 ml/(h.g$_{cat}$) are shown in Figure 5.18. From both figures it follows that CO conversion generally decreased with increasing space velocity, as expected, especially and proportionally for CO conversion if far from equilibrium conversion.
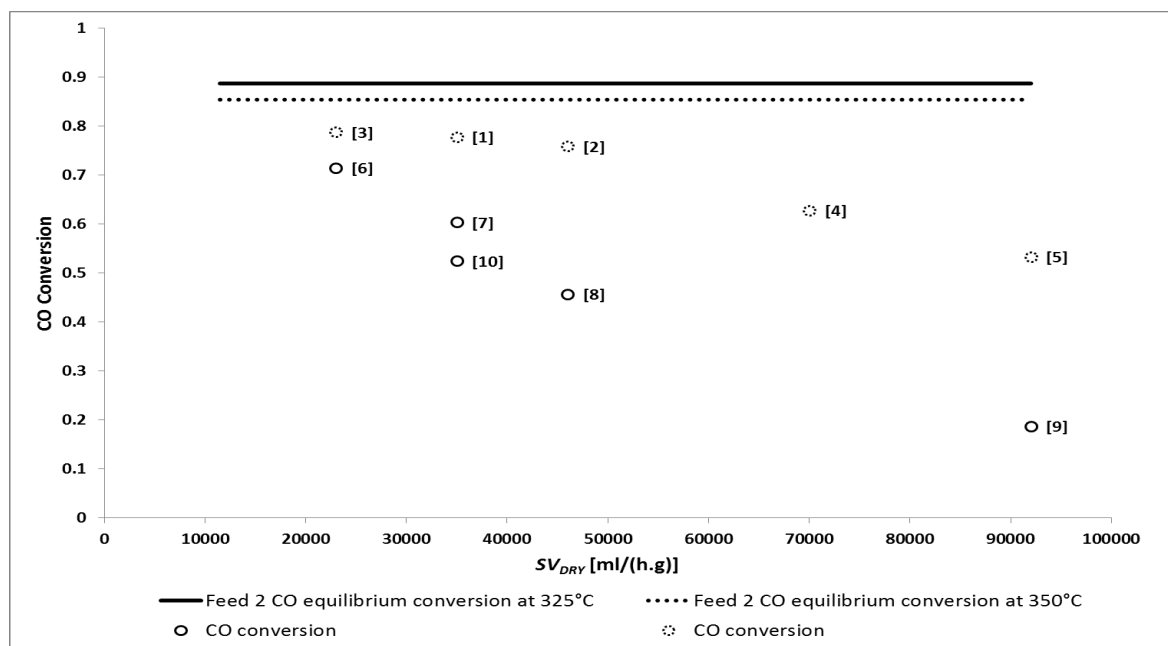
Figure 5-17: CO conversion over catalyst X as a function of space velocity with Feed 2 (Table 4-6 in Section 4.4.1: Feed composition) at 325 and 350 °C (Experiment 1). [] values in square brackets indicate the testing sequence. Data point pair [7] /[10] reflects the rather rapid deactivation observed for catalysts X (Section 5.4.1: Catalyst stability)
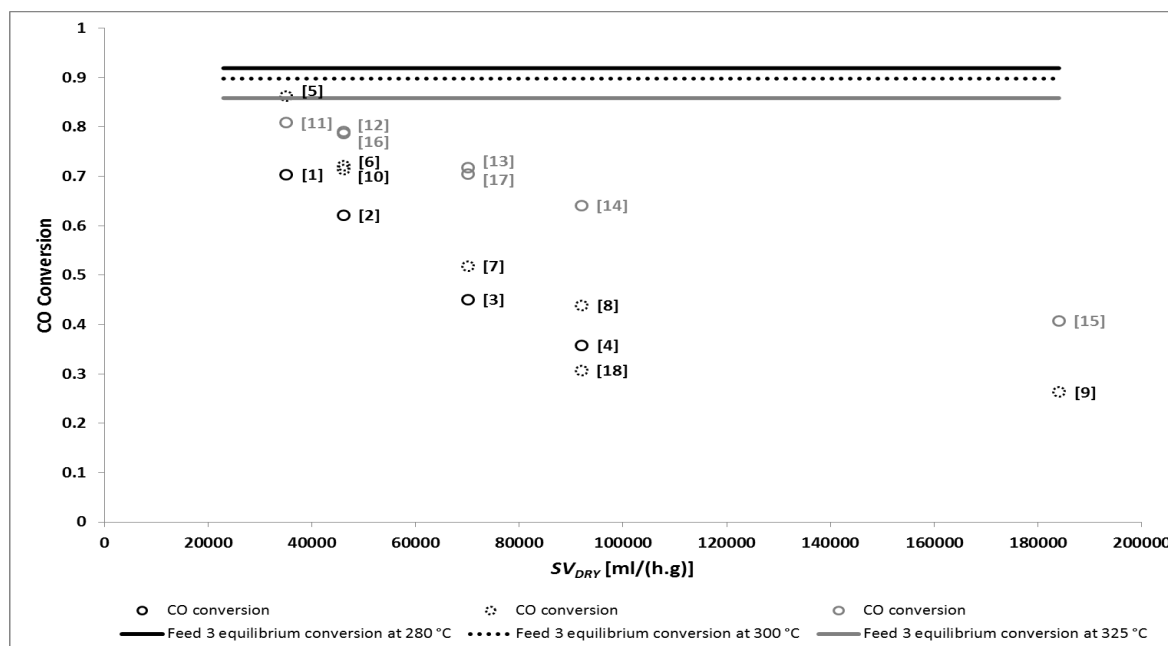
Figure 5-18: CO conversion over catalyst X as a function of space velocity with Feed 3 (Table 4-6 in Section 4.4.1 Feed composition) at 280, 300 and 325 °C (Experiment 2). [] values in square brackets indicate the testing sequence. For data point pairs [6]/[10] and [13]/[17] reflect a rather stable activity while data points [8] and [18] reflect the rather rapid deactivation observed for catalyst X (Section 5.4.1: Catalyst stability)

5.4.4   Effect of temperature

Temperature effect with Feed 2 was evaluated by increasing temperature from 325 °C to 350 °C in one step. Figure 5-19 shows CO conversion as a function of temperature at different space velocities. CO conversion increased with increasing temperature as expected. Equilibrium conversion was reached at 350 °C for all the space velocities applied as indicated.
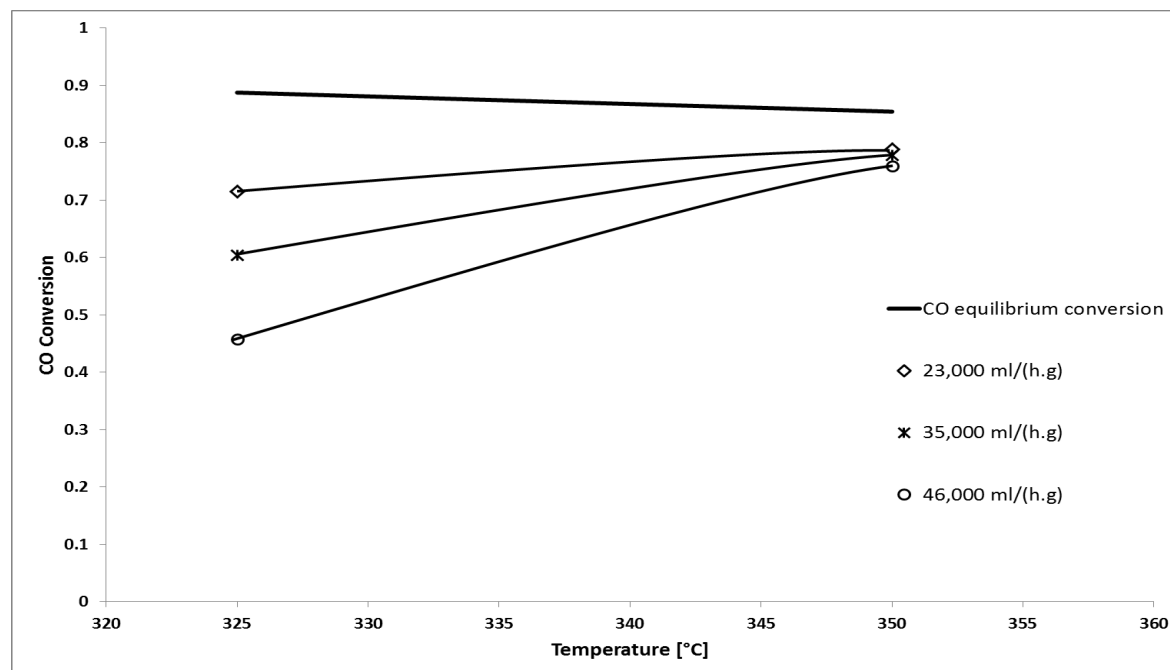
Figure 5-19: CO conversion over catalyst X as a function of temperature with Feed 2 (Table 4-6 in Section 4.4.1: Feed composition) at different dry gas *space velocities* (Experiment 1)

Temperature effect with Feed 3 was evaluated at 3 different temperatures, namely 280, 300 and 325 °C. Figure 5-20 shows CO conversion X as a function of temperature at different space velocities. As long as equilibrium conversion was not reached (particularly for the lowermost space velocity), CO conversion increased with increasing temperature as expected. Equilibrium conversion was reached at a temperature of around 300 °C for SV_{DRY} of 35,000 ml/(h.g$_{cat}$) and for SV_{DRY} of 46,000 ml/(h.g$_{cat}$) at 325 °C, but at the highest SV_{DRY} applied of 92,000 ml/(h.g$_{cat}$), CO conversion at 325 °C was still far from equilibrium.
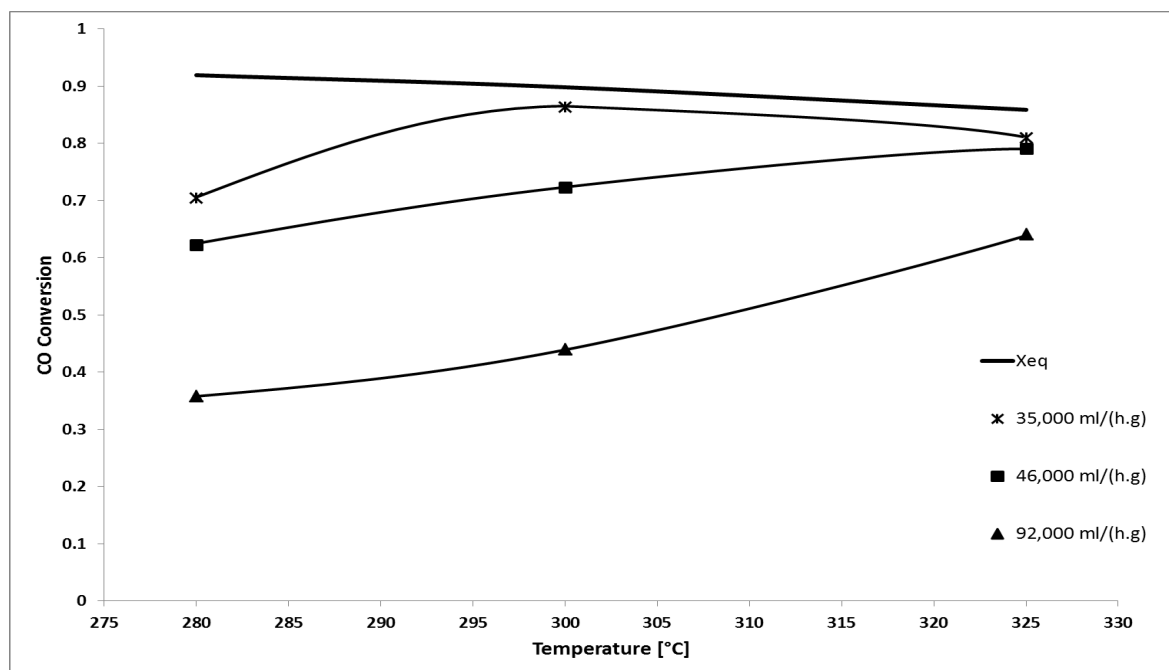
Figure 5-19: **CO conversion over catalyst X as a function of temperature with Feed 3 (Table 4-6 in Section 4.4.1: Feed composition) at different dry gas *space velocities* (Experiment 2)**

5.5 Performance of Catalyst HTS (G-3C)

5.5.1   Catalyst stability

Experiment 8 was run for approximately 130 hours with Feed 2 (Table 4-6 in Section 4.4.1: Feed composition) varying reaction temperature and space velocity. Catalyst performance was found to be unchanged for the comparatively short duration of this experiment, as shown in Figure 5-21. Identical CO conversion of approximately 29% was observed after the first 30 hours on stream and upon repeating the initial reaction condition after approximately 130 hours on stream.
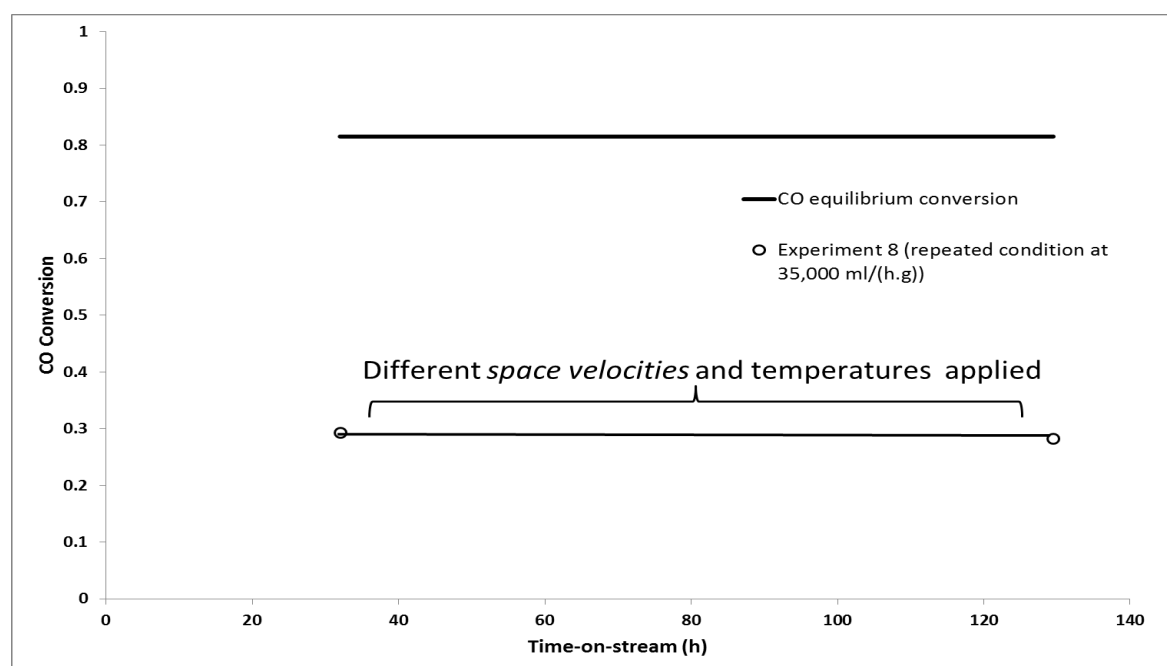
Figure 5-201: Time-on-stream performance of catalyst HTS (G-3C). Data points shown were obtained with Feed 2 at SV_{DRY} of 35,000 ml/(h.g$_{cat}$), 375 °C and 1 barg (Experiment 8). (The individual data points represent averages of 10 samples each, taken over periods of 2 hours)

5.5.2   Catalyst performance reproducibility

Performance reproducibility experiments were not carried out for catalyst HTS (G-3C), as only one experimental run was done with for this catalyst.

5.5.3   Effect of space velocity

Feed 2 was used to investigate the effect of space velocity on catalyst performance. *Dry gas space velocities* applied ranged from 11,500 to 92,000 ml/(h.g) at a temperatures of 375°C. As Figure 5-22 shows, CO conversion generally decreased with increasing space velocity, as expected.
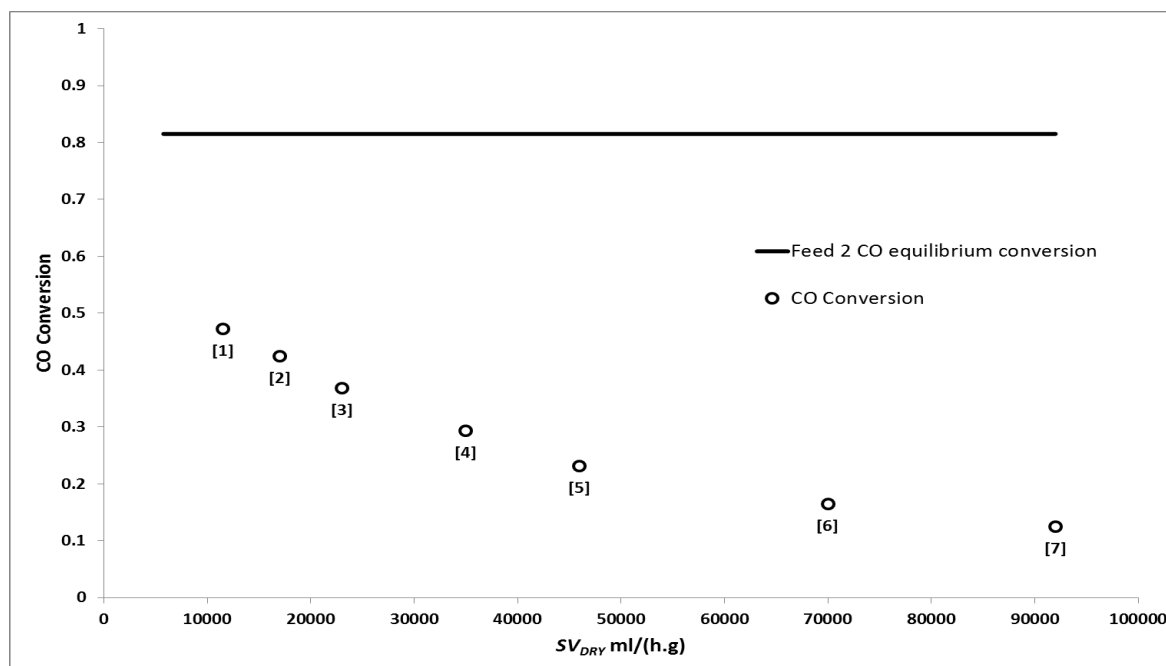
Figure 5-22: CO conversion over catalyst HTS (G-3C) as a function of space velocity with Feed 2 (Table 4-6 in section 4.4.1 Feed gas composition) at 375 °C (Experiment 8). [] values in square brackets indicate the testing sequence.

5.5.4 Effect of temperature

Temperature effect was evaluated by increasing temperature from 375 °C in increments of 25 °C to 450 °C using Feed 2. Figure 5-23 shows CO conversion as a function of temperature at different space velocities. As long as equilibrium conversion was not reached (or closely approached), CO conversion increased with increasing temperature as expected.

For temperatures below 400 °C and SV_{DRY} below 46,000 ml/(h.g_{cat}) traces of methane were detected. However, Methanation (indicated by a significant methane peak in the chromatograms) was dominant at temperatures above 400 °C. It was also observed that the catalyst coked while operating under these conditions (indicated by an increasing pressure drop that build up between reactor inlet and outlet).
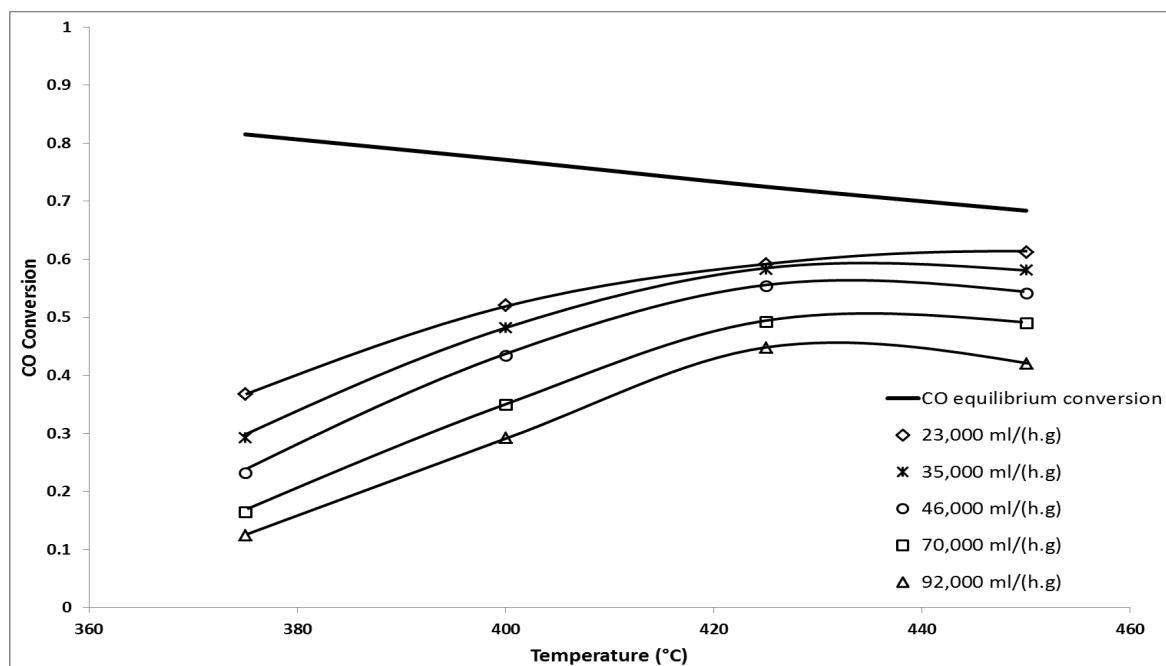
Figure 5-213: CO conversion over catalyst HTS (G-3C) as a function of temperature with Feed 2 (Table 4-6 in section 4.4.1: Feed composition) at different space velocities (Experiment 8)

5.6 Performance of Catalyst LTS (C 18-7)

The microreactor coated with catalyst LTS (C 18-7) was operated with Feeds 2 and 3 at low SV_{DRY} of 23,000 ml/(h.g$_{cat}$) and typical LTS temperatures of between 180 and 210 °C (Wheeler et al., 2004; Ladebeck & Wagner, 2003; Rhodes et al., 1995). No catalyst activity was observed. It was revealed later that, erroneously, the coated reactor plates had been calcined at too high a temperature for the delicate LTS catalyst to survive, namely at the same temperature of 450 °C as the HTS catalyst (Figure 4-6). This temperature was too high, since the Cu-Zn oxide catalyst coated (Table 4-1) rapidly sinters at temperatures > 240 °C (Rhodes et al., 1995).

5.7 Summary of Results

WGS catalysts coated on microreactors are active for the WGS reaction. Washcoating of catalyst powder onto microreactor walls also performed successfully, producing active catalysts.

Catalyst activity, on mass of catalyst-basis, ranked as follows:

WY-2 slightly > WY-1 > X >> HTS (G-3C)

Low temperature shift catalyst C 18-7 could not be evaluated, since it was inactive due to the high pre-treatment temperature that was erroneously applied.

Two of the noble metal catalysts namely, WY-1 and WY-2 showed stable performance in the temperature range applied (up to 350 °C), while noble metal catalyst X deactivated. Base metal high temperature shift catalyst G-3C was also stable over the temperature range studied (up to 450 °C).

The highest CO conversion and best performance was achieved for Feed 3, which had the highest steam/carbon ratio of the feeds applied.

For all catalysts tested (except LTS (C 18-7)), CO conversion increased steadily with increasing temperature, as long as equilibrium conversion was not reached (or close). This was expected and consistent with text books on chemical reaction engineering (Fogler, 1999).

CO conversion over all catalysts tested (except LTS (C 18-7)) was found to decrease with increasing space velocity (especially and proportionally for CO conversions far from equilibrium conversion). This is due to a decrease of 'contact time' of the reacting gas species on the catalyst surface when space velocity is increased. This was expected and consistent with text books on chemical reaction engineering (Fogler, 1999).

6. DISCUSSION

Noble and base metal WGS catalyst in powder form can be washcoated onto steel plate microreactors. WGS over noble metal and conventional base metal high temperature WGS catalysts can be carried out with these washcoated microreactors operating at high space velocities, which are in the range of several hundred thousand ml/(h.gcat) for the noble metal catalysts.

Of the noble metal catalysts tested in the microreactor, two (WY-2 and WHY-1) were stable (not X).

6.1 Effect of Reaction Variables

The one objective of this study was comparison of the performance of commercial noble metal supported catalysts for WGS with that of industrial state-of-the-art base metal WGS catalysts, applied as wall-coated microreactors. The noble metal catalysts were found to be significantly more active per unit catalyst mass than a Fe/Cr high temperature WGS catalyst. Comparison with a Cu/Zn low temperature WGS catalyst failed due to, as it finally revealed, due to applying too high a temperture during the calcination procedure of the washcoated microreactor plates.

The other, the major objective of this study was to identify feasible operating conditions for the noble metal catalysts (range of space velocity and temperature) for use in the fuel processing device of an integrated PEM fuel cell power system that works under transient conditions and with frequent on/off operation, since operational modes and conditions for industrial state-of-the-art WGS shift catalysts are not suitable for this application.

1 mol% (wet) of CO remaining was chosen as the target effluent level for the WGS stage, since this level can be tolerated by HT-PEM fuel cells and since removing this last percent of CO by a subsequent PROX or SELMETH stage in order to produce a 'CO-free' LT-PEM feed does not affect the final hydrogen yield too much. Different feeds for the WGS reaction were chosen on the basis of the final application, namely low temperature PEM fuel cells. Feeds differed essentially by steam/carbon (S/C) ratio, which finally resulted in either a non-water-saturated or a water saturated or 'over'-saturated stream suitable to feed a high temperature or low temperature fuel cell, respectively (Table 4-6 in Section 4.4.1: Feed composition).

The windows within which it was thermodynamically possible to achieve CO concentrations in the WGS stage effluent stream of ≤ 1 mol% (wet) were determined for the different feeds. Figure 6-1 shows the three different such areas for each of the three feeds tested, within which a 1 vol% (wet) CO effluent stream is thermodynamically possible and which minimum conversion of the CO in the feed to the WGS is required. From Figure 6-1, the following can be extrapolated: For low S/C Feed 1 (molar steam to methane ratio of the respective steam reformer feed = 2.35, Table 4-6), a reaction

temperature lower than 230 °C would be required in order to thermodynamically allow achieving a CO effluent stream from the WGS stage of 1 mol% CO (wet), meaning a CO conversion of more than 89% for this specific feed.

For medium S/C Feed 2 (molar steam to methane ratio of the respective steam reformer feed = 3, Table 4-6), a reaction temperature lower than 310 °C is required in order to thermodynamically allow achieving a CO effluent stream from WGS stage of 1 mol% CO (wet), meaning a CO conversion of more than 91% for this specific feed.

For high S/C Feed 3 (molar steam to methane ratio of the respective steam reformer feed = 5 , Table 4-6), a reaction temperature lower than 395 °C is required in order to thermodynamically allow achieving a CO effluent stream from WGS stage of 1 mol% CO (wet), meaning a CO conversion of more than 71% for this specific feed.
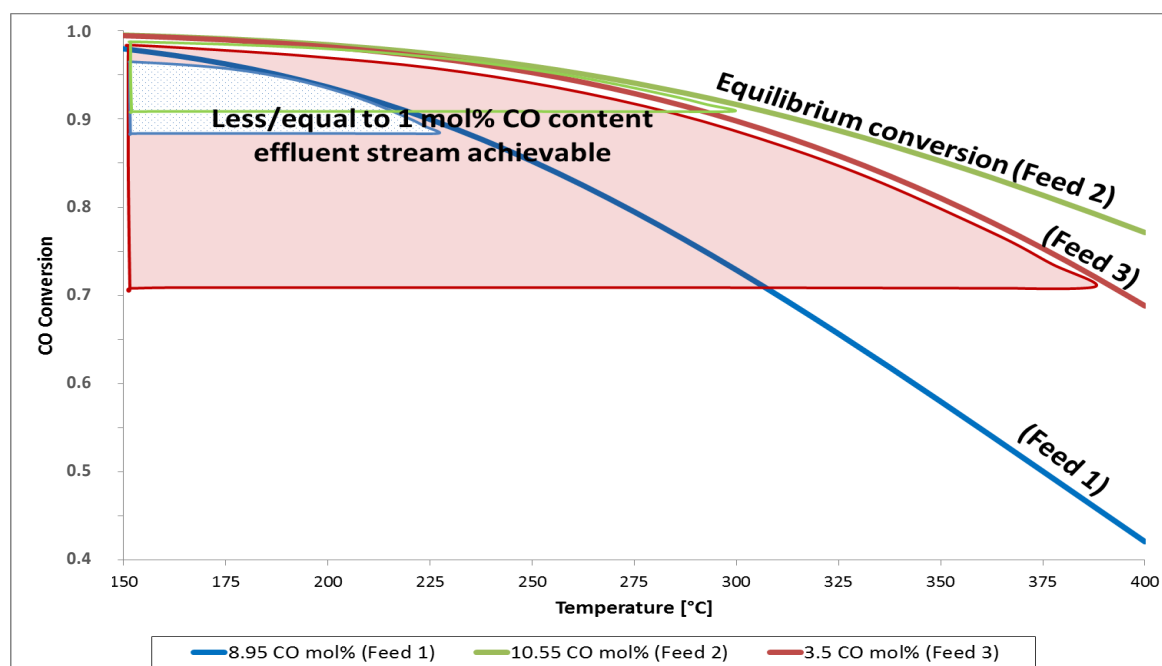
Figure 6-1: Operational windows (three colour shaded areas) for Feeds 1 to 3 (Table 4-6 in Section 4.4.1: Feed composition) within which it is thermodynamically possible to achieve high enough a conversion of CO to for a less or equal than 1 mol% CO (wet) effluent stream of the WGS stage.

With Feed 1 (corresponding to the comparatively low molar steam /methane steam reformer feed ratio of 2.35), operating at 230 °C, close to the lower edge of the typical operational temperature window for LT-WGS catalysts, would be required in order to overcome thermodynamic limitations.

6.2 Operational Windows for the WGS Stage for Different Catalysts and Feeds

Figures 6-2 to 6-10 give an overview over the outcome of the experiments varying reaction temperature, space velocity and feed with the individual catalysts. Full symbols indicate that an equal to or less than 1 mol% (wet) CO WGS effluent stream was not achieved for the respective feed and under the respective conditions (SV and T), while the open symbols indicate that less than or equal to 1 mol% (wet) CO have been achieved.

It can be seen for Feed 3 (5:1 SR feed molar steam/methane ratio), Figures 6-4, 6-7 and 6-9, that the thermodynamic limitation is on high level, at 395°C, and that the targeted CO concentration of ≤ 1 mol% (wet) could be achieved at 325 ^{o}C and *space velocities* (wet) of up to 100,000 ml/(h.g$_{cat}$) over catalyst X and 350 ^{o}C and 400,000 ml/(h.g$_{cat}$) over the other noble metal catalysts. Space velocities could even be higher at higher reaction temperatures (but below the thermodynamic limit of 395 ^{o}C) or the target CO concentration could be lower, respectively, when operating at lower temperatures and space velocities.

It can be seen from Figures 6-3, 6-6, 6-8 and 6-10 that for Feed 2 (3:1 SR feed molar steam/methane ratio), in order to achieve the targeted WGS effluent concentration of less than 1 mol% CO (wet), very low space velocities are required (lower than 31 000 ml/(h.g$_{cat}$) wet for the noble metal catalysts and much lower than these for HTS catalyst G-3C). This is because of the rather low thermodynamic limitation temperature of 310 ^{o}C and the, therefore, low operational temperatures required.
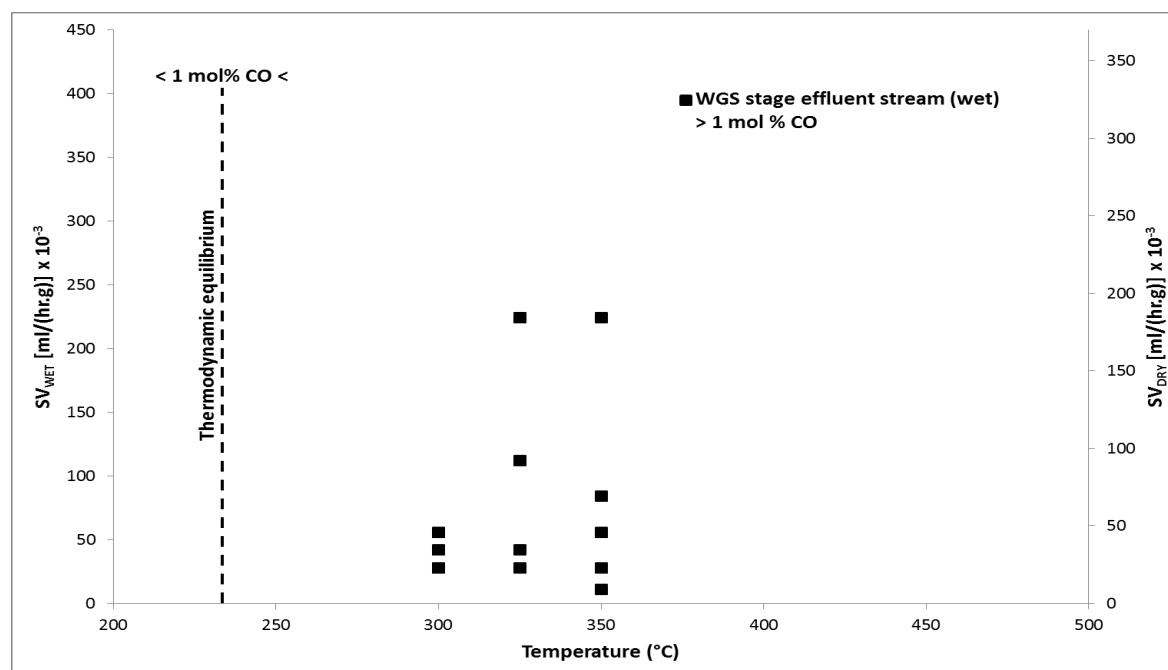
Figure 6-2: **Performance of Catalyst WY-1 with Feed 1 (SR feed H$_2$O/CH$_4$ ratio = 2.35, Table 4-6) from experiments 3 and 4 (Table 4-7)**
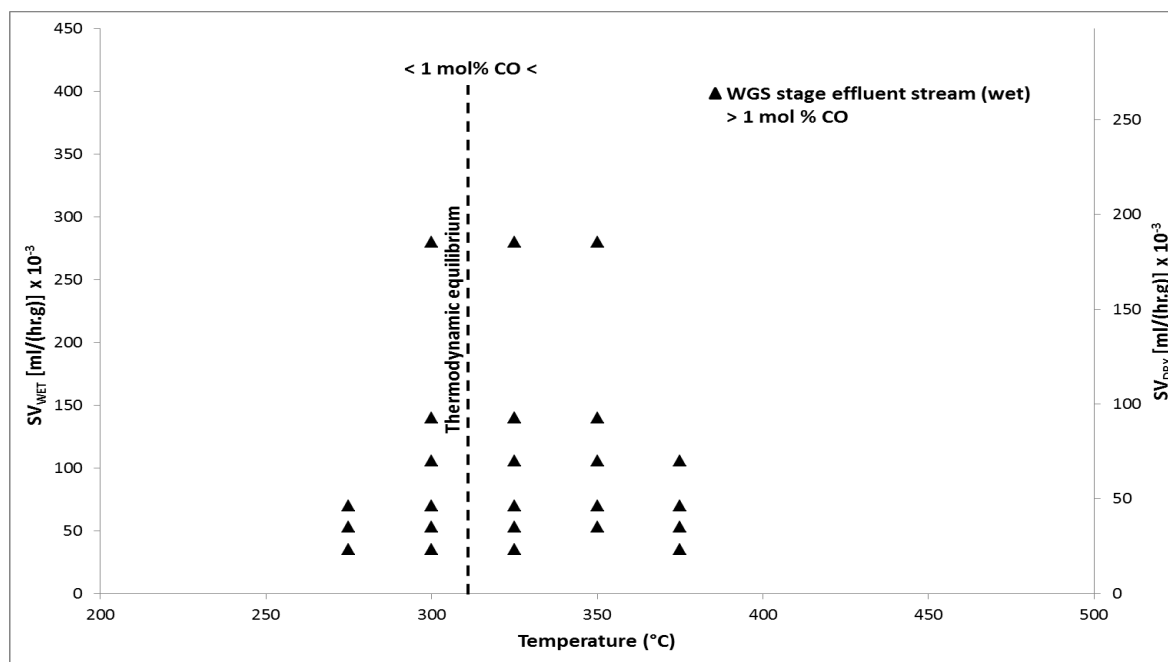
Figure 6-3: **Performance of Catalyst WY-1 with Feed 2 (SR feed H$_2$O/CH$_4$ ratio = 3, Table 4-6) from experiments 3 and 4 (Table 4-7)**
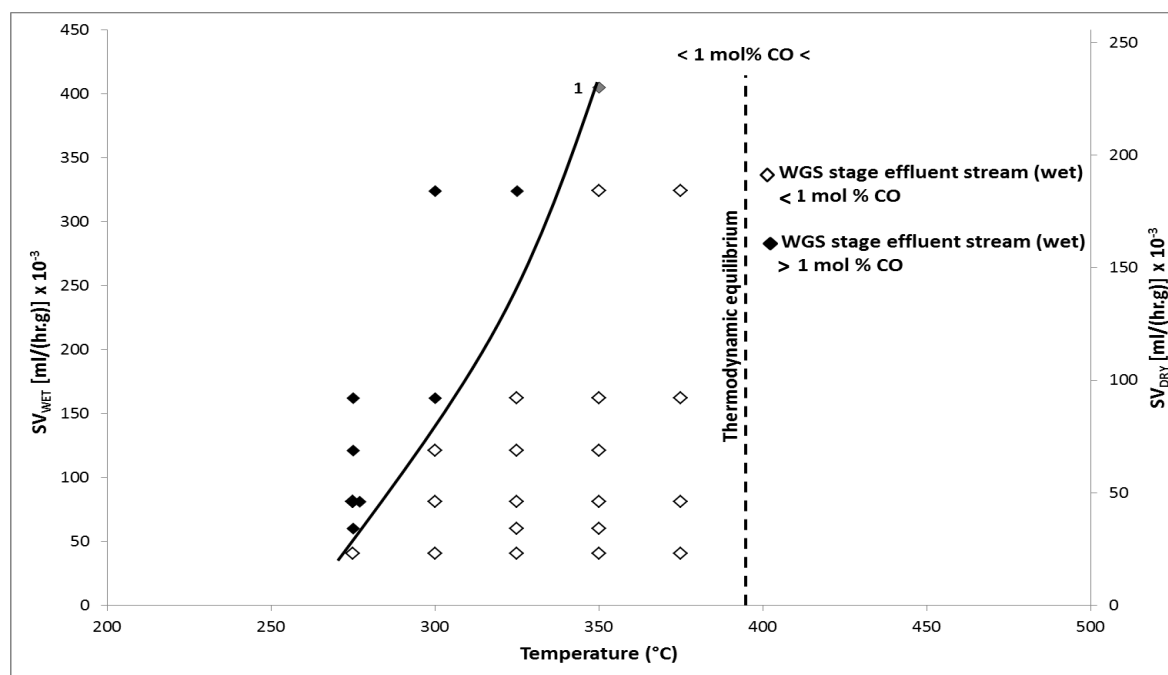
[1] The grey data point indicates that for the respective experiments, the one produced a result slightly above 1 vol% CO (wet) and the other one a result slightly below 1 vol% CO (wet).

Figure 6-4: **Performance of Catalyst WY-1 with Feed 3 (SR feed H$_2$O/CH$_4$ ratio = 5, Table 4-6) from experiments 3 and 4 (Table 4-7)**
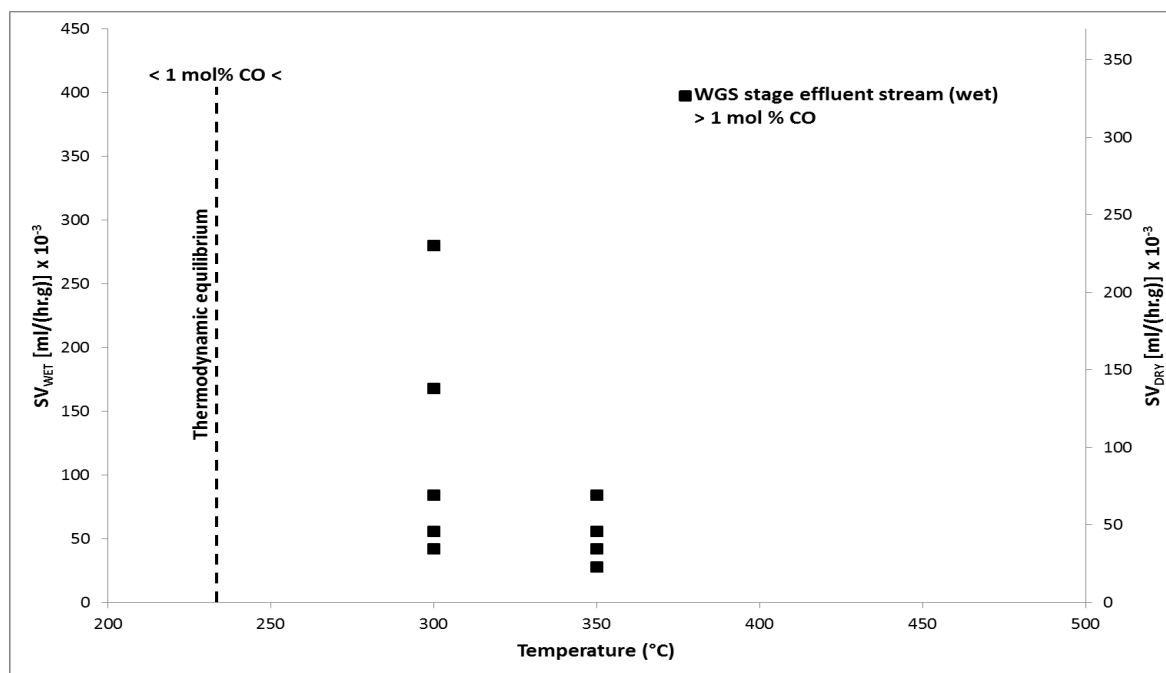
Figure 6-5: **Performance of Catalyst WY-2 with Feed 1 (SR feed H$_2$O/CH$_4$ ratio = 2.35, Table 4-6) from experiment 5 (Table 4-7)**
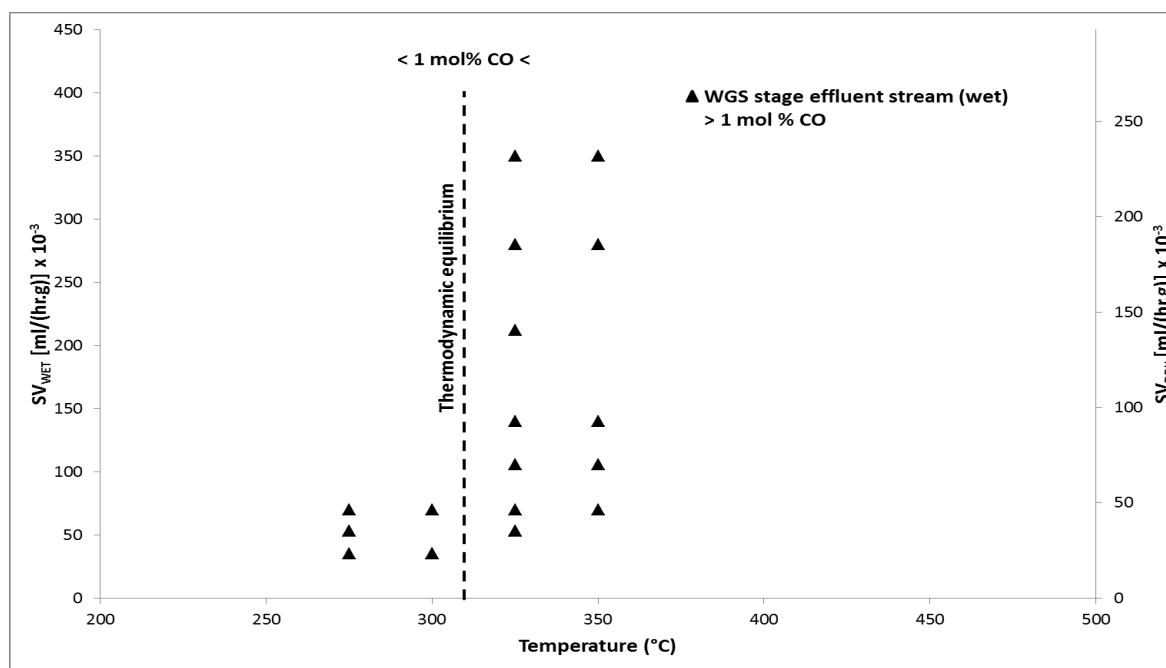
Figure 6-6: **Performance of Catalyst WY-2 with Feed 2 (SR feed H$_2$O/CH$_4$ ratio = 3, Table 4-6) from experiments 5 and 7 (Table 4-7)**
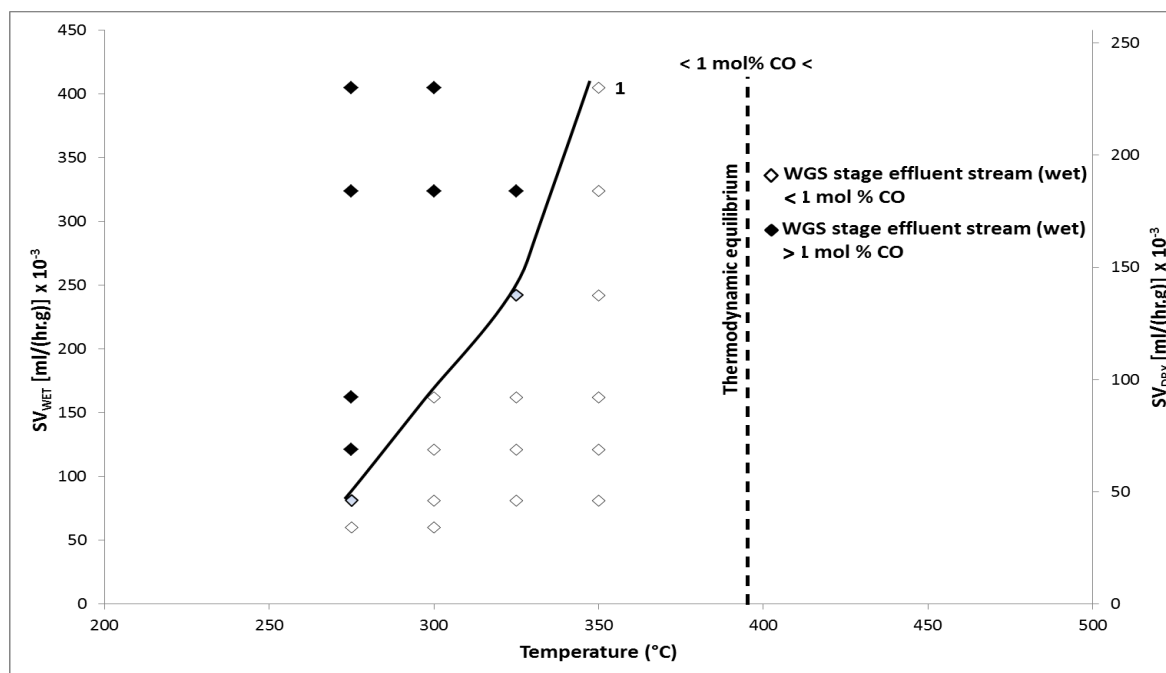
¹ The grey data points indicate that for the respective experiments, the one produced a result slightly above 1 vol% CO (wet) and the other one a result slightly below 1 vol% CO (wet).

Figure 6-7: Performance of Catalyst WY-2 with Feed 3 (SR feed H₂O/CH₄ ratio = 5, Table 4-6) from experiments 5 and 7 (Table 4-7)
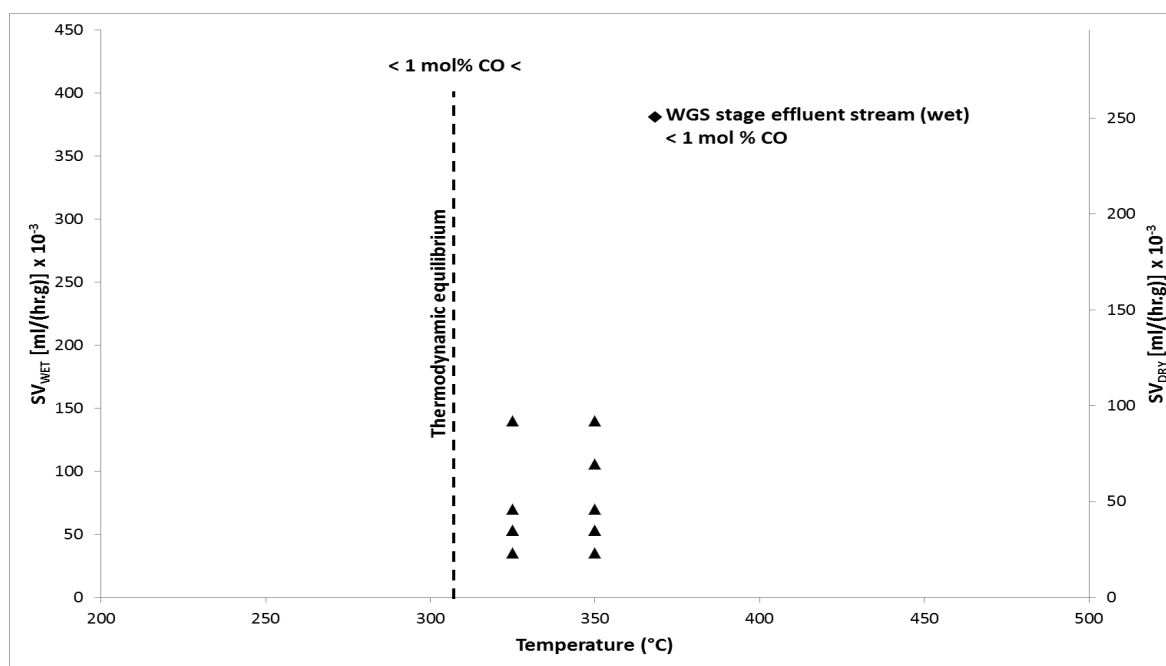
Figure 6-8: Performance of Catalyst X with Feed 2 (SR feed H₂O/CH₄ ratio = 3, Table 4-6) from experiment 1 (Table 4-7)
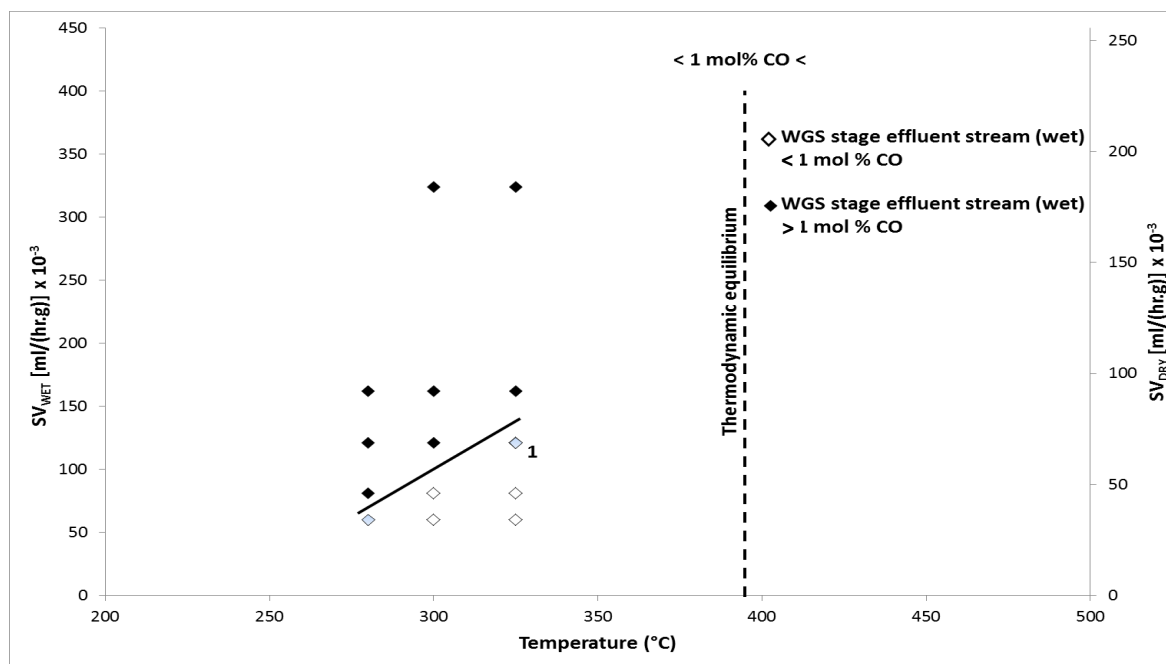
[1] The grey data points indicate that for the respective experiments, the one produced a result slightly above 1 vol% CO (wet) and the other one a result slightly below 1 vol% CO (wet).

Figure 6-9: Performance of Catalyst X with Feed 3 (SR feed H_2O/CH_4 ratio = 5, Table 4-6) from experiment 2 (Table 4-7)
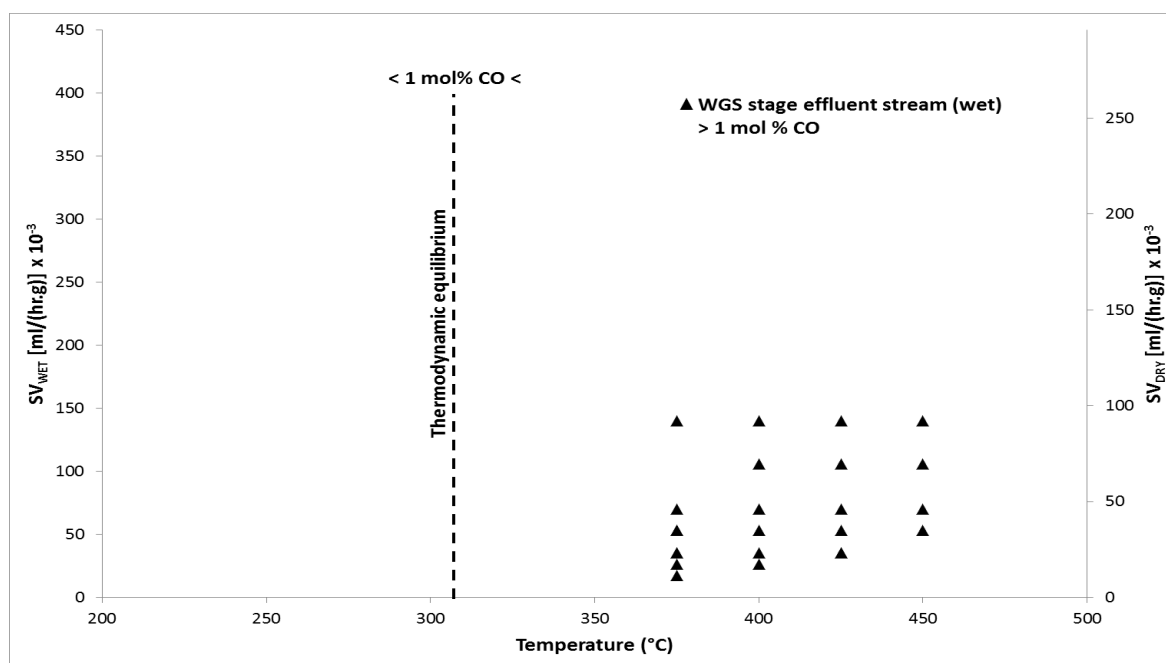
Figure 6-10:   Performance of Catalyst HTS (G-3C) with Feed 2 (SR feed H_2O/CH_4 ratio = 3, Table 4-6) from experiment 8 (Table 4-7)

6.3 Comparison of the Operational Windows for the WGS Stage for Different Catalysts

Catalyst activities in terms of the kinetic limits, i.e., the highest space velocities that allow achieving the target of 1 mol% (wet) of unconverted CO remaining over the three noble metal catalysts (catalysts WY-1, WY-2 and X) with feed 3 are compared in Figure 6-11. The following ranking of activity was found in the high temperature range (around 350 °C):

WY-2 slightly > WY-1 >> X

And in the low temperature range (around 275 °C):

WY-2 slightly > WY-1 = X

Catalysts WY-1 and WY-2 do not differ much in performance, while the activity of catalyst X is only similar in the low temperature range but much lower in the high temperature range. However, this trend may, if extrapolated to a lower temperature range than investigated during this study, suggest that catalyst X is the most active catalyst of the samples tested at very low temperatures.

The said deviations in trend would also mean that the activation energy for the WGS reaction over catalysts WY-1 and WY-2 is higher than that over catalyst X. (One may speculate that this indicates towards different catalyst carriers). However, despite this favourable aspect, the crucial handicap of catalyst X compared to the two other noble metal catalysts is its instability under typical WGS conditions (Figures 5-16, 5-9 and 5-3).
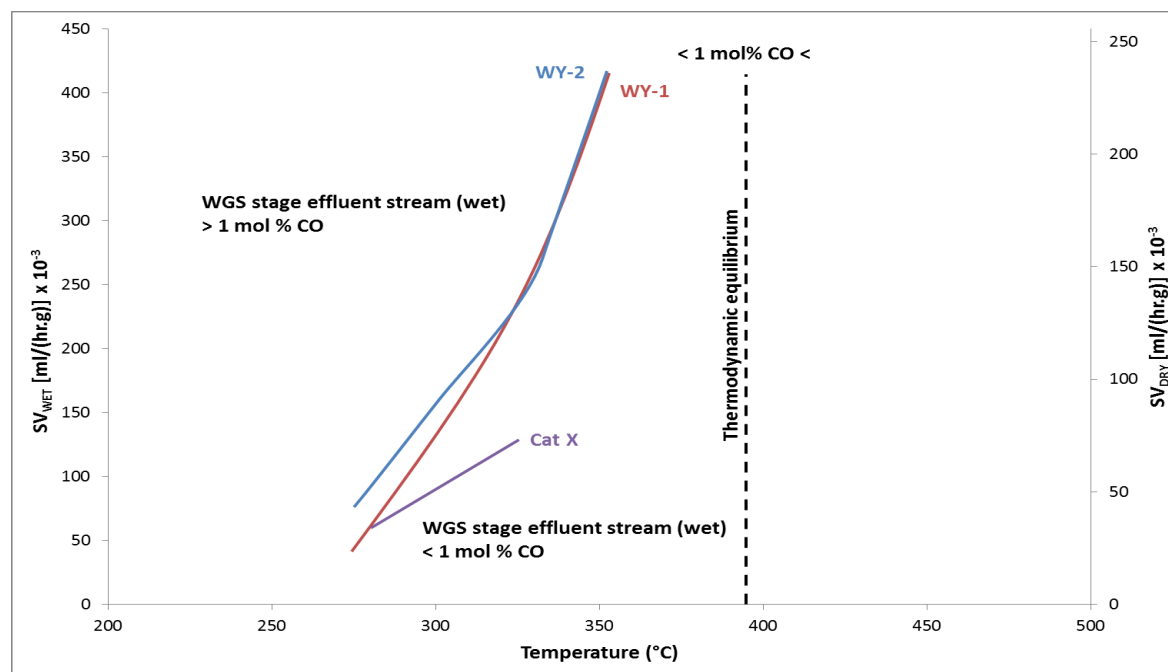
Figure 6-11: **Kinetic edges of the operational windows for catalysts WY-1, WY-2 and X with Feed 3 in comparison**

7.   CONCLUSIONS

Washcoating of the catalyst onto microchannel plates is a promising way of manufacturing highly efficient WGS microreactors.

For the feed to the SR stage upstream the WGS reactor a molar steam to methane ratio of around 5 to 1 or higher is required in order to:

1.   Provide sufficiently wide an operational window for the WGS reaction to achieve less than 1 mol% (wet) CO in the reactor effluent stream (Figure 6-11).

2.   Shift the thermodynamic equilibrium limit of the WGS for the 1 mol% (wet) CO level to temperatures where the noble metal catalysts are sufficiently active, such as to >350 °C (Figures 6-2 to 6-10).

3.   Shift the WGS kinetic limit to attractively high space velocities (Figures 6-4, 6-7 and 6-9).

4.   Ensure that the humidity of the feed stream is high enough to meet the requirements of a downstream low temperature PEM fuel cell (Table 4-6 in Section 4.4.1: Feed composition).

The reasons for the comparatively rapid deactivation of catalyst X in microreactor (washcoating) application should be investigated, since this was not observed when this catalyst was applied in a fixed bed reactor under identical reaction conditions (Tsui, 2014).

8. REFERENCES

Atkinson, D. and McDaniel, J. (2010). Microchannel reactors in fuel production. Eptq.com, edition 2010/Q2, http://www.eptq.com/view_article.aspx?intAID=1024 www.eptq.com (accessed 14 Jan 2011).

Bayer, T., Jenck, J. and Matlosz, M. (2005). Impulse – A new approach to reactor design. *Chemical Engineering & Technology*, *28*(4), 431-438. doi:10.1002/cite.200403417.

Brandner, J. J. (2012). Microfabrication in metals, ceramics and polymers. *Russian Journal of General Chemistry*, *82*(12), 2025-2033. doi:10.1134/S1070363212120249.

Brooks, K., Davis, J., Fischer, C., Heintzelman, A., King, D., Pederson, L., Stenkamp, S., Tegrotenhuis, W., Wegeng, B. and Whyatt, G. (2002). Microchannel fuel processing. Fuel cells for transportation/fuels for fuel cells. *Annual Program/Lab R&D Review 2002. Pacific Northwest National Laboratory, U.S. Department of Energy.*

Bunluesin, T., Gorte, R. J. and Graham, G. W. (1998). Studies of the water-gas-shift reaction on ceria-supported Pt , Pd , and Rh : implications for oxygen-storage properties. *Applied Catalysis B: Environmental*, *15*, 107-114.

Conrad, O. (2010), Director: HySA/Catalysis Competence Centre, Centre for Catalysis Research, Department of Chemical Engineering, University of Cape Town (personal communication).

Choung, S. Y., Ferrandon, M., and Krause, T. (2005). Pt-Re bimetallic supported of CeO_2-ZrO_2 mixed oxides as water-gas shift catalysts. *Catalysis Today*, *99*, 257-262.

Dicks, A. (2003). Proton exchange membrane fuel cells. In *Fuel Cell Systems Explained* (Larmanie, J. and Dicks, A., editors), 2nd edition. Wiley, New York.

Farrauto, R., Hwang, S., Shore, L., Ruettinger, W., Lampert, J., Giroux, T., Liu, Y. and Ilinich, O. (2003). New material needs for hydrocarbon fuel processing: generating hydrogen for the PEM fuel cell. *Annual Review of Materials Research, 33*, 1-27. doi:10.1146/annurev.matsci.33.022802.091348.

Fogler, H. S. (1999). *Elements of Chemical Reaction Engineering*. Prentice-Hall, Upper Saddle River, New Jersey, chpts. 1.4 and 3.1.

Germani, G., Alphonse, P., Courty, M., Schuurman, Y. and Mirodatos, C. (2005). Platinum/ ceria/ alumina catalysts on microstructures for carbon monoxide conversion. *Catalysis Today, 110*, 114-120. doi:10.1016/j.cattod.2005.09.017.

Germani, G. and Schuurman, Y. (2006). Water-gas shift reaction kinetics over μ-structured $Pt/CeO_2/Al_2O_3$ catalysts. *AIChE Journal*, *52*, 1806-1813. doi:10.1002/aic 10764.

Ghenciu, A. F. (2002). Review of fuel processing catalysts for hydrogen production in PEM fuel cell systems. *Current Opinion in Solid State and Materials Science*, *6*, 389-399.

Hilaire, S., Wang, X., Luo, T., Gorte, R. J. and Wagner, J. (2001). A comparative study of water-gas-shift reaction over ceria supported metallic catalysts. *Applied Catalysis A: General*, *215*, 271-278.

Hessel, V., Löwe, H., Müller, A. and Kolb, G. (2005). *Chemical Micro Process Engineering: Processing and Plants*. Wiley-VCH, Weinheim, 380-399.

Holladay, J. D., Wang, Y. and Jones, E. (2004). Review of developments in portable hydrogen production using microreactor technology. *Chemical Reviews, 104,* 4767-4790.

Katikaneni, S., Gaffney, A. M. and Song, C. (2002). Fuel processing for fuel cell applications. *Catalysis Today*, 77, 99-106.

Kolb, G., Schürer, J., Tiemann, D., Wichert, M., Zapf, R., Hessel, V. and Löwe, H. (2007). Fuel processing in integrated micro-structured heat-exchanger reactors. *Journal of Power Sources*, *171*, 198-204. doi:10.1016/j.jpowsour.2007.01.006.

Kolb, G., Cominos, V., Hofmann, C., Pennemann, H., Schürer, J., Tiemann, D., Wichert, M., Zapf, R., Hessel, V. and Löwe, H. (2005a). Integrated microstructured fuel processors for fuel cell applications. *Chemical Engineering Research and Design*, *83*(A6), 626-633. doi:10.1205/cherd.04357.

Kolb, G. (2008). *Fuel processing for fuel cells*. Wiley-VCH, Weinheim.

Kolb, G. and Hessel, V. (2004). Micro-structured reactors for gas phase reactions. *Chemical Engineering Journal, 98,* 1-38. doi:10.1016/j.cej.2003.10.005.

Kolb, G., Pennemann, H. and Zapf, R. (2005b). Water-gas shift reaction in micro-channels — results from catalyst screening and optimisation. *Catalysis Today*, *110*, 121-131. doi:10.1016/j.cattod.2005.09.012.

Ladebeck, J. R. and Wagner, J. P. (2003). Catalyst development for water-gas shift. In *Handbook of Fuel Cells – Fundamentals, Technology and Applications* (Vielstich, W., Lamm, A. and Gasteiger, H. A., eds.), Wiley, Chichester, vol. *3(2)*, 190-201.

Liu, X., Ruettinger, W., Xu, X. and Farrauto, R. (2005). Deactivation of Pt/CeO_2 water-gas shift catalysts due to shutdown/startup modes for fuel cell applications. *Applied Catalysis B: Environmental, 56*, 69-75.

Lloyd, L., Ridler, D.E. and Twigg, M.V. (1996). The water-gas shift reaction. In: *The Catalyst Handbook*, 2nd ed., Twigg, M.V. (ed.), Manson, London.

Meille, V. (2006). Review on methods to deposit catalysts on structured surfaces. *Applied Catalysis A: General*, *315*, 1-17. doi:10.1016/j.apcata.2006.08.031.

O'Connell, M., Kolb, G., Schelhaas, K.-P., Wichert, M., Tiemann, D., Pennemann, H. and Zapf, R. (2012). Towards mass production of microstructured fuel processors for application in future distributed energy generation systems: A review of recent progress at IMM. *Chemical Engineering Research and Design*, *90*(1), 11–18. doi:10.1016/j.cherd.2011.08.002.

Parak, M. (2011). A collocation-based 3-dimensional microchannel reactor model applied to the water-gas shift reaction, MSc thesis, Centre for Catalysis Research, Department of Chemical Engineering, University of Cape Town, 1–19.

Pintauro, P. and Wycisk, R. (2008). Fuel Cell Membranes. in: *Advancde Membrane Technology and Applications* (Li, N. N., Fane, A. G., Ho, W. S. W. and Matsuura, T, eds.), Wiley, New York, Chapter 29.

Radhakrishnan, R., Willigan, R. R., Dardas, Z. and Vanderspurt, T. H. (2006). Water gas shift activity of noble metals supported on ceria-zirconia oxides. *AIChE Journal, 52*(5) 1888-1894. doi:10.1002/aic.10785

Rhodes, C., Hutchings, G. J. and Ward, A. M. (1995). Water-gas shift reaction: finding the mechanistic boundary. *Catalysis Today*, *23*, 43-58.

Rhodes, C. and Hutchings, G. J. (2003). Studies of the role of the copper promoter in the iron oxide/chromia high temperature water gas shift catalyst. *Physical Chemistry Chemical Physics, 5*(12), 2719-2723. doi:10.1039/b303236c.

Rosa, F., López, E., Briceño, Y., Sopeña, D., Navarro, R. M., Alvarez-Galván, M. C., Fierro, J. L. G. and Bordons, C. (2006). Design of a diesel reformer coupled to a PEMFC. *Catalysis Today*, *116*, 324-333. doi:10.1016/j.cattod.2006.05.061.

Sun, J., DesJardins, J., Buglass, J. and Liu, K. (2005). Noble metal water gas shift catalysis: Kinetics study and reactor design. *International Journal of Hydrogen Energy, 30,* 1259-1264. doi:10.1016/j.ijhydene.2005.02.013.

Swartz, S., Azad, A.-M. and Seabaugh, M. (2003). Ceria-based water-gas-shift catalysts. *Proceedings of the 2002 fuel cell seminar and exposition, Palm Springs, CA, Nov 18-21*, 587-590.

Truter, L. (2011). Development of a zeolite washcoating technique for microchannel reactors. MSc thesis, Centre for Catalysis Research, Department of Chemical Engineering, University of Cape Town.

Tsui, L.-H. (2014). MSc thesis (in preparation), Centre for Catalysis Research, Department of Chemical Engineering, University of Cape Town.

Wheeler, C., Jhalani, A., Klein, E. J., Tummala, S. and Schmidt, L. D. (2004). The water-gas-shift reaction at short contact times. J*ournal of Catalysis, 223*, 191-199. doi:10.1016/j.jcat.2004.01.002.

Winter, C.-J. (2009). Hydrogen energy — abundant, efficient, clean: a debate over the energy-system-of-change. *International Journal of Hydrogen Energy*, *34*(14, suppl. 1), S1-S52. doi:10.1016/j.ijhydene.2009.05.063.

Xue, E., O'Keeffe, M. and Ross, J. R. H. (1996). Water-gas shift conversion using a feed with a low steam to carbon monoxide ratio and containing sulphur. *Catalysis Today*, *30*, 107–118.

Yuan, X.-Z. and Wang, H. (2008). PEM fuel cell fundamentals. In: *PEM fuel cell electrocatalysts and catalysts layers – fundamentals and applications* (Zhang, J., ed.), Springer, London 2-25.

Zalc, J. M., Sokolovskii, V. and Löffler, D. G. (2002). Are noble metal-based water-gas-shift catalysts practical for automotive fuel processing? *Journal of Catalysis*, *206*, 169-171. doi:10.1006/jcat.2001.3465.

Zalc, J. M., and Löffler, D. G. (2002). Fuel processing for proton exchange membrane fuel cells: transport and kinetic issues of system design. *Journal of Power Sources, 111*, 58–64.

Zapf, R., Becker-Willinger, C., Berresheim, K., Bolz, H., Gnaser, H., Hessel, V., Kolb, G., Löb, P., Pannwitt, A.-K. and Ziogas, A. (2003). Detailed characterization of various porous alumina-based catalyst coatings within microchannels and their testing. *Chemical Engineering Research and Design, 81(A7),* 721-729.

Zapf, R., Kolb, G., Pennemann, H. and Hessel, V. (2006). Basic study of adhesion of several alumina-based washcoats deposited on stainless steel microchannels. *Chemical Engineering & Technology*, *29*(12), 1509-1512. doi:10.1002/ceat.200600204.

Zhou, Y., Böhringer, W. and Fletcher J.C.Q. (2010). Preliminary laboratory data, Centre for Catalysis Research, Department of Chemical Engineering, University of Cape Town, unpublished.

Appendix I

Tabulated summary of catalysts tested and experimental operating conditions

Table AI-1: List of catalysts used (copy of Table 4-1)

Catalyst code	Origin of catalyst	Active metal	Carrier	Form received	Shape as received	Applied as
X	Commercial (undisclosed)	Noble metal	Undisclosed	Pre-reduced	Powder	Coated
WY-1	Commercial (undisclosed)	Noble metal	Undisclosed	Pre-reduced	Coated	Coated
WY-2	Commercial (undisclosed)	Noble metal	Undisclosed	Pre-reduced	Coated	Coated
HTS	Süd-Chemie (G-3C)	Fe-Cr	Alumina	Oxide	Pallets[1]	Coated
LTS	Süd-Chemie (C 18-7)	Cu-Zn	Alumina	Oxide	Pallets[1]	Coated

[1] Milled using a pestle and mortar and sieved to 200-250 µm

Table AI-2: Overview over all experimental runs carried out (copy of Table 4-7). The reaction pressure was set to 1 barg for all the experimental runs

Experiment	Catalyst (Table 4-2)	Catalyst loading (mg)	Feed	Reaction temperature (°C)	SV_{DRY} [ml/(h.g$_{cat}$)] x 10^{-3}
1	X	32.16	2	350	23, 35, 46, 92
			2	325	23, 35, 46, 70, 92
2	X	31.81	3	280-325	35, 46, 70, 92, 184
3	WY-1	36.68	1	300-350	23, 46, 92, 184
			2	300-350	23, 46, 92, 184, 210, 230
			3	300-350	23, 46, 92, 184
4	WY-1	35.98	1	300-350	23, 35, 46, 92
			2	275-375	23, 35, 46, 70, 92, 184, 210
			3	275-375	23, 35, 46, 70, 92, 184, 210, 230
5	WY-2	25.55	1	300-350	23, 46
			2	275-350	23, 35, 46, 92, 184
			3	275-350	35, 46, 92, 184
6	WY-2	26.18	1	275-375	23, 46, 92
			2	275-375	23, 35, 46, 70, 92, 184
			3	275-375	23, 35, 46, 70, 92, 184
7	WY-2	29.40	2	275-375	46
			3	275-350	46
8	HTS (G-3C)	25.86	2	375-450	11, 17, 23, 35, 46, 70, 92
9	LTS (C 18-7)	24.7	2	180-210	23
			3	180-210	23

Table AI-3: WGS feed composition based on effluent compositions from three different feeds of the methane steam reforming stage (copy of Table 4-6)

Methane steam reforming feed and CH₄ conversion[1]		Molar S/CH₄ = 2.35 X_{CH_4} = 94.2%	Molar S/CH₄ = 3.02 X_{CH_4} = 86.6%	Molar S/CH₄ = 5.00 X_{CH_4} = 95.0%
MSR effluent= WGS feed	Composition (%)	Feed 1	Feed 2	Feed 3
	Ar[2]	1.11	2.27	0.63
	CO	8.95	10.55	3.50
	CO2	8.95	4.10	8.53
	H_2	63.19	49.83	44.70
	H_2O	17.79	33.25	42.70
	Total	100	100	100
	Molar S/CO	1.99	3.15	12.2
Fuel cell feed resulting[3]	Fuel cell operation temperature (°C)	Saturation of feed with water vapour (%)		
	70	64	154[4]	261[4]
	85	34	83	141[4]
	100	20	47	80
	120	10	27	40

Appendix II

Gas calibration factors

Binary mixtures of H_2, CO and CO_2 with Argon at different molar ratios, produced by main flow controllers MFC-1 to MFC-3 and MFC-5 (Figure 4-10), were used to obtain the individual GC gas calibration factors for these gases, as shown in Figures AII-1 to AII-3.

Calibration factors were determined relative to Ar. The individual pairs of gas calibration factors, $R_{f,A}$ C_A were calculated according to the equations shown in Section 4.6.1.3: GC calibration.

H₂ calibration gas factor, channel 1

y = 5.4886x
R² = 0.9786
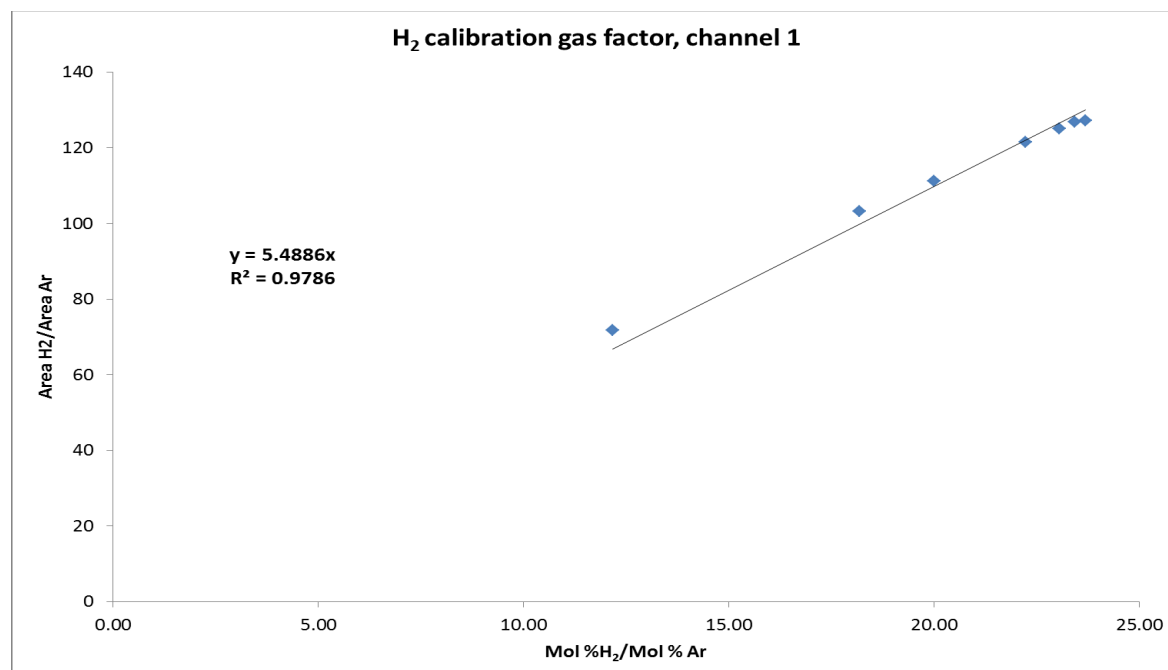
Figure AII-1: Hydrogen gas calibration factor: R_{f,H_2} = 5.49. Since, due to technical limitations, no calibration was possible for H_2/Ar molar ratios <12, the trend line was forced through the origin.
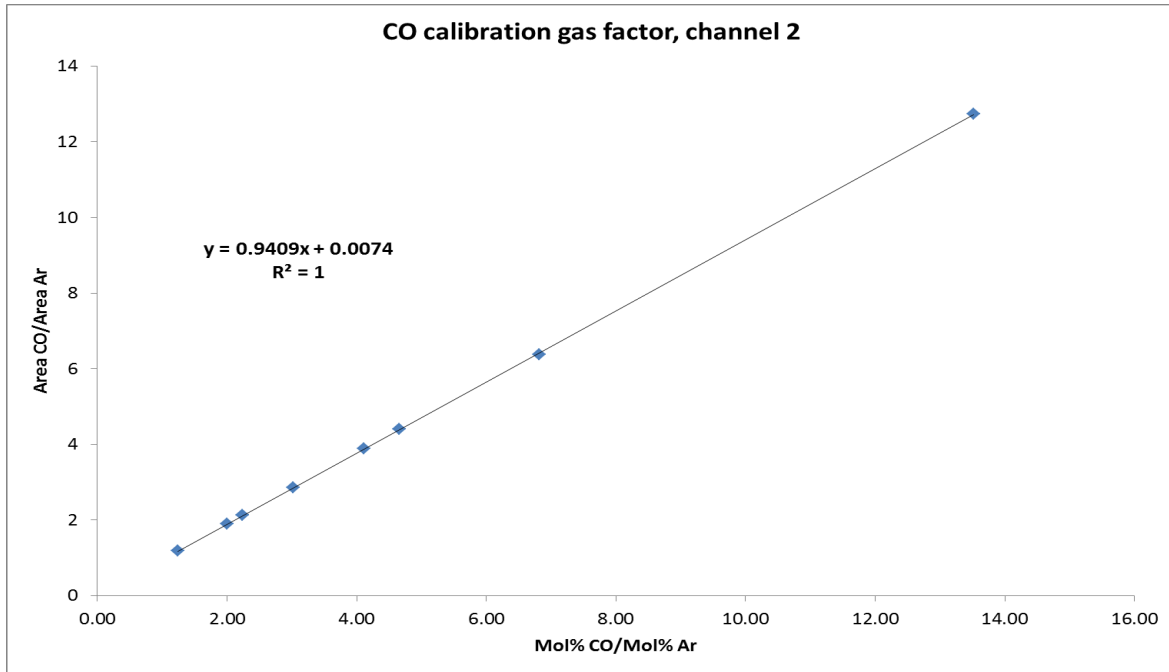
Figure AII-2: Carbon monoxide gas calibration factor. $R_{f,CO}$ = 0.94 ; C_{CO} = 0.0074
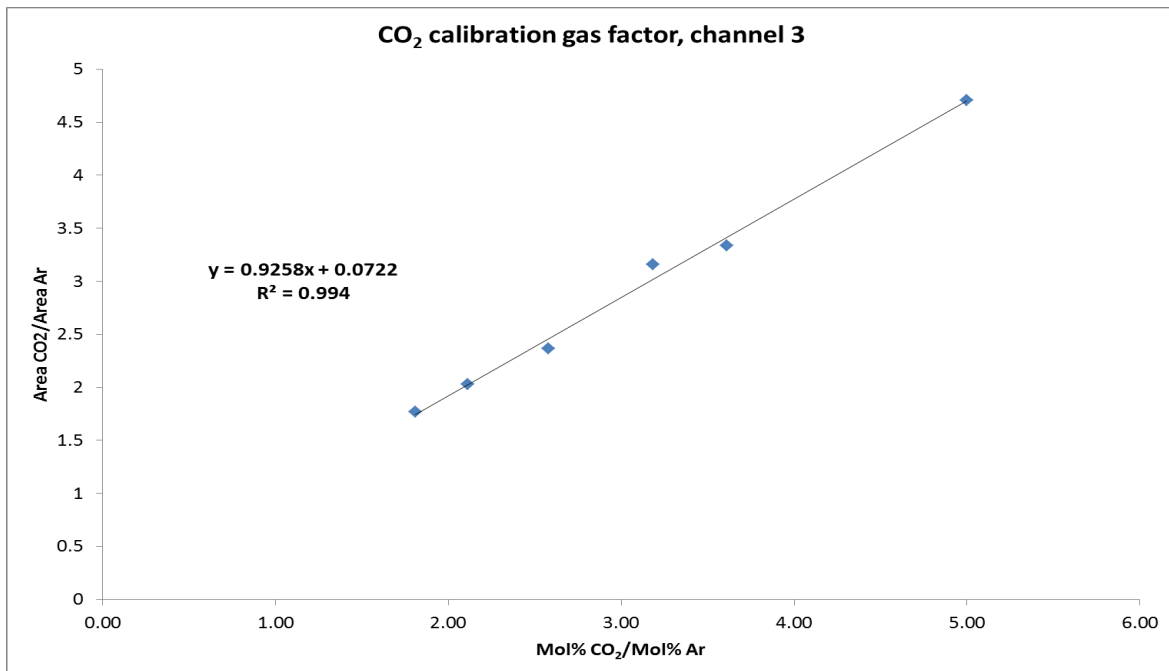
Figure AII-3: Carbon dioxide gas calibration factor. R_{f,CO_2} = 0.93; C_{CO} = 0.0722

Appendix III

Pump split ratio calibration (refers to section 4.3.1.2: Steam formation – the evaporator)

Vial no	Empty vial (g)	Full vial (g)	Weight (g)	Time (min)	F (ml/min)	T_{flow} (ml/min)	Split ratio
A1	6.915	7.188	0.274	60	0.005		0.099
A2	64.742	67.227	2.485	60	0.041	0.046	0.901
B1	7.494	7.735	0.242	60	0.004		0.098
B2	4.142	6.358	2.217	60	0.037	0.041	0.902
C1	7.312	10.622	3.311	827	0.004		
C2	15.857	38.754		827			
E1	2.496	3.079	0.583	143	0.004		0.095
E2	7.595	13.116	5.521	143	0.039	0.043	0.905
F1	2.712	3.079	0.366	170	0.002		0.062
F2	7.566	13.116	5.550	170	0.033	0.035	0.938
G1	2.700	3.107	0.407	172	0.002		0.096
G2	7.341	11.189	3.848	172	0.022	0.025	0.904
H1	2.694	3.014	0.320	149	0.002		0.096
H2	7.253	10.254	3.001	149	0.020	0.022	0.904
I1	2.701	2.920	0.219	60	0.004		0.097
I2	7.406	9.437	2.031	60	0.034	0.038	0.903
J1	7.573	11.011	3.438	809	0.004		
J2	15.293			809			
L1	2.714	3.097	0.383	112	0.003		0.097
L2	7.196	10.755	3.559	112	0.032	0.035	0.903
M1	2.698	3.443	0.745	233	0.003		0.095
M2	7.432	14.558	7.125	233	0.031	0.034	0.905
A1	2.510	2.764	0.255	60	0.004		0.099
A2	7.532	9.855	2.323	60	0.039	0.043	0.901
B1	2.509	2.726	0.217	52	0.004		0.097
B2	7.534	9.560	2.026	52	0.039	0.043	0.903
D1	2.490	3.050	0.560	134	0.004		0.096

D2	7.721	12.974	5.253	134	0.039	0.043	0.904
0.027							
E1	2.535	2.783	0.247	93	0.003		0.098
E2	7.544	9.816	2.273	93	0.024	0.027	0.902
0.024							
B	2.698	4.011	1.313	60	0.022		0.911
H_2O feed to reactor					0.002	0.024	0.089
0.024							
G	7.521	11.658	4.137	189	0.022		0.912
H_2O feed to reactor					0.002	0.024	0.088
0.024							
K	7.527	9.916	2.389	109	0.022		0.913
H_2O feed to reactor					0.002	0.024	0.087
0.048							
H	7.475	13.980	6.505	149	0.044		0.910
H_2O feed to reactor					0.004	0.048	0.090
0.058							
J	7.360	11.313	3.953	75	0.053		0.909
H_2O feed to reactor					0.005	0.058	0.091
0.058							
I	7.599	12.921	5.322	101	0.053		0.909
H_2O feed to reactor					0.005	0.058	0.091
0.058							
A	7.610	14.281	6.671	128	0.052		0.899
H_2O feed to reactor					0.006	0.058	0.101
0.117							
B	7.564	13.872	6.308	60	0.105		0.899
H_2O feed to reactor					0.012	0.117	0.101

0.235							
C	7.349	15.555	8.206	39	0.210		0.895
H$_2$O feed to reactor					0.025	0.235	0.105
0.029							
F	7.501	9.822	2.321	88	0.026		0.909
H$_2$O feed to reactor					0.003	0.029	0.091
0.014							
D	7.502	9.054	1.553	119	0.013		0.932
H$_2$O feed to reactor					0.001	0.014	0.068

Appendix IV

This appendix refers to the numbers mentioned in Section 4.2.6.1: Catalyst adhesion on microchannel walls. Percentage weight loss was calculated using equation 4-1 given in Section 4.2.6.1: Catalyst adhesion on microchannel walls.

Table AIV-1: Adhesion test results

TEST PLATE	Weight of the uncoated plate (mg)	Weight of the coated plate (mg)	Weight after adhesion test (mg)	Weight loss (mg)	Weight loss (%)
1	11957	11978	11978	0.1	0.6
3	12127	12152	12152	0.1	0.4
4	12318	12337	12337	0.0	0.1
5	12180	12205	12205	0.1	0.3
2	11884	11914	11914	0.2	0.5
6	12042	12066	12066	0.0	0.1

Appendix IV

Appendix V

Experimental data

(For other details see Table 4-1, 4-6 and 4-7, or AI-1 to AI-3, respectively)

Experiment 1   - Catalyst X   (32.16 mg loading)

Experiment 2   - Catalyst X   (31.81 mg loading)

Experiment 3   - Catalyst WY-1   (36.68 mg loading)

Experiment 4   - Catalyst WY-1   (35.98 mg loading)

Experiment 5   - Catalyst WY-2   (25.55 mg loading)

Experiment 6   - Catalyst WY-2   (26.18 mg loading)

Experiment 7   - Catalyst WY-2   (29.40 mg loading)

Experiment 8   - Commercial HTS (G-3C) catalyst   (25.86 mg loading)

Experiment 9   - Commercial LTS (C 18-7) catalyst   (24.7 mg loading)

Explanation of data in tables:

The data was worked up according to the equations shown in Section 4.6.2, Data work-up.

Only the averages from the gas chromatographic analysis of the 10 samples obtained during 2 hours steady state sampling periods (Section 4.5.3.4: Sampling procedure) are given in tables below.

Carbon balance was calculated on the basis of all carbon containing compounds excluding methane (CH_4). For conditions tested, a carbon balance of 1 was typically obtained, except for the cases were CH_4 was detected (HTS catalyst G3-C testing), in which a carbon balance < 1.0 was achieved.

It should be noted the data in the following tables is given as molar flows rates F_A' of the individual compounds. These translate into molar fractions F_A (Section 4.6.1.3: GC calibrations and 4.6.2: Data work-up) by normalising to 100%.

Experiment 1: Catalyst X under Feed 2

Time-on-stream (h)	X_{CO}	$C_{balance}$	F'_{H_2} (mol/min)	F'_{CO_2} (mol/min)	F'_{Ar} (mol/min)	F'_{CO} (mol/min)	Temperature (°C)	SV$_{DRY}$ [ml/(hr.g)]
12.1	0.778	1.0	63.5	14.9	2.6	2.7	350	35,000
17.2	0.759	1.0	63.4	14.9	2.6	2.8	350	46,000
20.3	0.788	1.0	60.7	14.4	2.6	2.6	350	23,000
23.4	0.533	1.0	60.3	11.8	2.6	5.8	350	92,000
26.2	0.777	1.0	63.2	14.9	2.6	2.7	350	35,000
28.2	0.628	1.0	61.8	13.3	2.6	4.4	350	70,000
59.8	0.715	1.0	60.1	13.3	2.6	3.4	325	23,000
64.4	0.604	1.0	62.2	12.9	2.6	4.7	325	35,000
72.3	0.458	1.0	60.4	11.0	2.6	6.5	325	46,000
98.3	0.525	1.0	61.1	11.8	2.6	5.8	325	35,000

Experiment 2: Catalyst X under Feed 3

Time-on-stream (h)	X_{CO}	$C_{balance}$	F'_{H_2} (mol/min)	F'_{CO_2} (mol/min)	F'_{Ar} (mol/min)	F'_{CO} (mol/min)	Temperature (°C)	SV_{DRY} [ml/(hr.g)]
16.5	0.704	1.0	167.8	40.9	2.5	4.1	280	35,000
20.2	0.622	1.0	173.0	41.5	2.5	5.3	280	46,000
23.6	0.451	1.0	171.7	39.7	2.5	7.5	280	70,000
26.5	0.358	1.0	170.3	38.4	2.5	8.8	280	92,000
65.9	0.723	1.0	171.5	42.0	2.5	4.0	300	46,000
69.7	0.519	1.0	171.0	40.1	2.5	6.6	300	70,000
72.8	0.440	1.0	169.0	38.7	2.5	7.8	300	92,000
75.3	0.264	1.0	167.8	36.7	2.5	10.2	300	184,000
93.5	0.809	1.0	165.7	41.8	2.5	2.8	325	35,000
95.5	0.791	1.0	171.4	43.1	2.5	2.9	325	46,000
97.8	0.718	1.0	171.4	42.4	2.5	3.9	325	70,000
100.1	0.641	1.0	169.7	41.4	2.5	4.6	325	92,000
103.0	0.408	1.0	169.7	38.4	2.5	8.2	325	184,000
109.2	0.705	1.0	170.1	42.0	2.5	4.0	325	70,000

Experiment 3: Catalyst WY-1 under Feed 1, 2 and 3

Time-on-stream (h)	X_{CO}	$C_{balance}$	F'_{H_2} (mol/min)	F'_{CO_2} (mol/min)	F'_{Ar} (mol/min)	F'_{CO} (mol/min)	Temperature (°C)	SV_{DRY} ml/(hr.g)
18.9	0.787	1.0	62.8	14.1	2.6	2.6	350	23,000
28.0	0.796	1.0	63.1	14.4	2.6	2.5	350	23,000
37.4	0.784	1.0	63.2	14.3	2.6	2.6	350	23,000
53.9	0.794	1.0	63.5	14.6	2.6	2.5	350	23,000
73.9	0.790	1.0	64.7	14.8	2.6	2.7	350	46,000
79.3	0.745	1.0	64.9	14.3	2.6	3.2	350	92,000
92.5	0.545	1.0	62.5	11.9	2.6	5.5	350	184,000
98.8	0.478	1.0	61.5	11.0	2.6	6.3	350	210,000
104.7	0.418	1.0	61.2	10.3	2.6	7.1	350	230,000
141.7	0.678	1.0	62.4	13.3	2.6	3.9	300	23,000
154.9	0.483	1.0	61.6	11.1	2.6	6.3	300	46,000
161.3	0.276	1.0	59.3	8.5	2.6	8.8	300	92,000
168.9	0.141	1.0	57.6	6.7	2.6	10.4	300	184,000
201.2	0.129	1.0	57.8	6.6	2.6	10.6	300	210,000
261.1	0.457	1.0	121.7	24.2	2.3	9.9	350	23,000
285.7	0.397	1.0	130.5	25.3	2.3	11.0	350	92,000
291.4	0.259	1.0	129.5	23.0	2.3	13.5	350	184,000
295.4	0.239	1.0	128.7	22.6	2.3	13.8	350	210,000
298.3	0.218	1.0	128.2	22.2	2.3	14.2	350	230,000
312.9	0.767	1.0	170.2	41.9	2.5	3.2	350	46,000
318.2	0.765	1.0	170.5	41.9	2.5	3.2	350	92,000
327.6	0.730	1.0	167.7	40.8	2.5	3.7	350	210,000

334.9	0.706	1.0	167.7	40.7	2.5	4.0	350	230,000
338.7	0.742	1.0	168.2	41.2	2.5	3.5	350	184,000
392.5	0.769	1.0	151.9	37.5	2.5	3.2	350	23,000
408.5	0.866	1.0	156.7	39.7	2.5	1.9	300	23,000
433.2	0.854	1.0	167.5	42.5	2.5	2.0	300	46,000
436.8	0.637	1.0	167.2	40.1	2.5	4.9	300	92,000
440.9	0.354	1.0	165.1	36.4	2.5	8.7	300	184,000
444.8	0.326	1.0	164.7	36.0	2.5	9.1	300	210,000
447.7	0.312	1.0	164.5	35.8	2.5	9.3	300	230,000
477.6	0.362	1.0	119.6	22.6	2.3	11.6	300	23,000
488.6	0.204	1.0	118.0	21.8	2.3	14.5	300	46,000
491.3	0.170	1.0	127.4	21.5	2.3	15.1	300	92,000
493.6	0.089	1.0	126.3	20.0	2.3	16.6	300	184,000
504.2	0.456	1.0	127.7	25.9	2.3	9.9	325	23,000
507.1	0.240	1.0	128.3	22.6	2.3	14.0	325	96,000
510.3	0.157	1.0	127.8	21.4	2.3	15.3	325	184,000
530.8	0.842	1.0	172.5	43.1	2.5	2.1	325	46,000
534.7	0.598	1.0	171.6	40.6	2.5	5.4	325	184,000
537.2	0.513	1.0	171.2	39.5	2.5	6.6	325	230,000
544.5	0.842	1.0	156.8	39.2	2.5	2.1	325	23,000
561.7	0.832	1.0	173.4	43.5	2.5	2.3	325	92,000
569.3	0.437	1.0	60.7	10.7	2.6	6.8	325	92,000
577.1	0.230	1.0	58.2	8.1	2.6	9.3	325	184,000
581.5	0.740	1.0	63.3	14.2	2.6	3.2	325	23,000
589.6	0.654	1.0	63.2	13.4	2.6	4.2	325	46,000
601.3	0.798	1.0	63.8	15.0	2.6	2.5	350	23,000

Experiment 4: Catalyst WY-1 under Feed 1, 2 and 3

Time-on-stream (h)	X_{CO}	$C_{balance}$	F'_{H_2} (mol/min)	F'_{CO_2} (mol/min)	F'_{Ar} (mol/min)	F'_{CO} (mol/min)	Temperature (°C)	SV_{DRY} [ml/(hr.g)]
22.3	0.523	1.0	154.9	36.4	2.5	6.6	275	46,000
24.3	0.670	1.0	135.2	32.9	2.5	4.5	275	35,000
29.5	0.793	1.0	134.3	33.7	2.5	2.9	275	23,000
42.6	0.366	1.0	153.8	34.6	2.5	8.7	275	70,000
44.9	0.301	1.0	152.4	33.4	2.5	9.6	275	92,000
62.9	0.172	1.0	55.2	7.0	2.6	10.1	275	35,000
67.6	0.236	1.0	53.8	7.3	2.6	9.3	275	23,000
70.6	0.129	1.0	54.9	6.6	2.6	10.5	275	46,000
78.3	0.448	1.0	100.7	18.7	2.3	10.2	300	23,000
97.7	0.264	1.0	119.8	21.3	2.3	13.6	300	35,000
99.3	0.212	1.0	118.7	20.3	2.3	14.6	300	46,000
113.1	0.443	1.0	98.7	18.5	2.3	10.3	300	23,000
119.3	0.876	1.0	122.4	31.2	2.5	1.7	300	23,000
122.1	0.865	1.0	161.7	41.8	2.5	1.9	300	46,000
124.4	0.745	1.0	155.7	39.1	2.5	3.5	300	70,000
126.1	0.606	1.0	153.7	37.1	2.5	5.4	300	92,000
128.9	0.363	1.0	156.3	35.2	2.5	8.8	300	184,000
134.0	0.590	1.0	57.4	11.9	2.6	5.0	300	23,000
142.0	0.425	1.0	57.7	10.3	2.6	7.0	300	35,000
146.2	0.242	1.0	55.9	8.1	2.6	9.2	300	70,000
149.7	0.092	1.0	54.2	6.2	2.6	11.0	300	184,000
157.2	0.390	1.0	58.0	9.9	2.6	7.4	325	92,000

161.7	0.210	1.0	55.7	7.6	2.6	9.6	325	184,000
166.2	0.809	1.0	60.5	14.6	2.6	2.3	325	23,000
170.3	0.772	1.0	61.6	14.5	2.6	2.8	325	35,000
173.4	0.679	1.0	60.8	13.3	2.6	3.9	325	46,000
175.0	0.529	1.0	59.3	11.6	2.6	5.7	325	70,000
176.8	0.421	1.0	58.1	10.2	2.6	7.0	325	92,000
183.0	0.852	1.0	168.7	43.5	2.5	2.0	325	70,000
187.4	0.827	1.0	171.7	44.4	2.5	2.4	325	92,000
189.5	0.621	1.0	161.8	39.8	2.5	5.2	325	184,000
204.3	0.290	1.0	119.0	20.4	2.3	15.0	325	92,000
208.0	0.176	1.0	119.4	20.3	2.3	15.2	325	184,000
213.2	0.566	1.0	106.9	22.5	2.3	8.0	325	23,000
220.8	0.427	1.0	126.5	25.6	2.3	10.6	325	35,000
263.7	0.796	1.0	168.2	43.3	2.5	2.8	350	35,000
268.1	0.810	1.0	132.0	33.6	2.5	2.6	350	23,000
276.4	0.804	1.0	163.6	42.5	2.5	2.7	350	46,000
282.0	0.789	1.0	168.7	43.4	2.5	2.9	350	70,000
284.5	0.795	1.0	164.2	42.3	2.5	2.8	350	92,000
286.8	0.774	1.0	163.4	42.0	2.5	3.1	350	184,000
290.2	0.702	1.0	163.4	41.2	2.5	4.1	350	230,000
300.8	0.680	1.0	61.1	13.6	2.6	3.9	350	92,000
305.7	0.420	1.0	58.1	10.5	2.6	7.0	350	184,000
317.4	0.793	1.0	61.9	14.9	2.6	2.5	350	35,000
330.8	0.795	1.0	62.7	15.2	2.6	2.5	350	46,000
333.8	0.754	1.0	62.7	14.7	2.6	3.0	350	70,000
341.4	0.529	1.0	159.8	39.5	2.5	4.7	275	46,000

349.7	0.429	1.0	122.9	25.2	2.3	10.5	350	46,000
356.0	0.459	1.0	105.4	21.0	2.3	10.0	350	23,000
387.5	0.401	1.0	122.9	25.0	2.3	11.1	350	70,000
424.0	0.395	1.0	121.8	24.6	2.3	11.2	350	92,000
445.2	0.266	1.0	119.8	22.3	2.3	13.6	350	184,000
474.5	0.841	1.0	153.4	40.4	2.5	2.2	325	35,000
478.1	0.845	1.0	161.3	42.4	2.5	2.1	325	46,000
481.1	0.845	1.0	124.3	32.4	2.5	2.1	325	23,000
487.2	0.532	1.0	158.0	38.3	2.5	6.5	275	46,000
491.9	0.385	1.0	57.5	10.0	2.6	7.4	300	46,000
499.0	0.213	1.0	55.3	7.7	2.6	9.6	300	92,000
510.7	0.739	1.0	59.8	13.9	2.6	3.2	375	23,000
512.6	0.767	1.0	61.2	14.5	2.6	2.8	375	35,000
514.7	0.757	1.0	61.5	14.6	2.6	2.9	375	46,000
516.2	0.769	1.0	61.6	14.7	2.6	2.8	375	70,000
521.9	0.743	1.0	130.8	32.7	2.5	3.5	375	23,000
526.5	0.737	1.0	159.3	40.5	2.5	3.6	375	46,000
528.5	0.750	1.0	160.3	41.2	2.5	3.4	375	92,000
533.9	0.731	1.0	161.7	42.1	2.5	3.4	375	184,000
545.3	0.543	1.0	160.9	39.6	2.5	6.3	277	46,000

Experiment 5: Catalyst WY-2 under Feed 1, 2 and 3

Time-on-stream (h)	X_{CO}	$C_{balance}$	F'_{H_2} (mol/min)	F'_{CO_2} (mol/min)	F'_{Ar} (mol/min)	F'_{CO} (mol/min)	Temperature (°C)	SV_{DRY} [ml/(hr.g)]
19.9	0.765	1.0	170.1	42.6	2.5	3.2	300	92,000
34.0	0.880	1.0	165.1	42.5	2.5	1.7	300	46,000
39.2	0.878	1.0	153.9	40.1	2.5	1.7	300	35,000
45.1	0.838	1.0	162.4	41.5	2.5	2.2	300	70,000
47.3	0.465	1.0	158.1	36.3	2.5	7.4	300	184,000
50.7	0.367	1.0	159.9	35.7	2.5	8.7	300	230,000
61.1	0.818	1.0	160.0	40.6	2.5	2.5	325	92,000
63.8	0.834	1.0	170.2	43.4	2.5	2.3	325	70,000
66.5	0.834	1.0	163.3	41.6	2.5	2.3	325	46,000
69.8	0.628	1.0	169.9	41.5	2.5	4.8	325	230,000
95.5	0.762	1.0	161.5	40.5	2.5	3.2	325	140,000
113.3	0.663	1.0	164.0	40.3	2.5	4.7	325	184,000
128.2	0.775	1.0	169.2	42.6	2.5	3.1	350	92,000
134.0	0.759	1.0	162.4	41.1	2.5	3.1	350	140,000
136.7	0.729	1.0	162.4	40.6	2.5	3.7	350	230,000
140.3	0.742	1.0	168.1	42.3	2.5	3.6	350	184,000
150.7	0.743	1.0	169.4	42.3	2.5	3.5	350	70,000
158.8	0.790	1.0	150.0	38.0	2.5	2.9	350	46,000
167.3	0.409	1.0	161.3	37.3	2.5	7.7	275	92,000
174.8	0.709	1.0	170.0	42.2	2.5	3.8	275	46,000
179.7	0.172	1.0	159.3	34.1	2.5	10.8	275	230,000
181.9	0.222	1.0	157.6	34.1	2.5	10.1	275	184,000

185.1	0.476	1.0	160.8	37.5	2.5	6.8	275	70,000
187.2	0.784	1.0	161.7	41.0	2.5	3.0	275	35,000
189.7	0.397	1.0	165.7	38.0	2.5	7.9	275	92,000
206.7	0.105	1.0	57.9	6.3	2.6	11.0	275	92,000
209.1	0.172	1.0	59.4	7.4	2.6	10.1	275	46,000
212.5	0.245	1.0	59.3	8.1	2.6	9.3	275	35,000
213.6	0.360	1.0	52.0	7.2	2.6	7.8	275	23,000
224.3	0.414	1.0	60.8	10.0	2.6	7.2	300	35,000
228.0	0.352	1.0	60.4	9.2	2.6	8.1	300	46,000
231.9	0.601	1.0	55.0	10.2	2.6	5.1	300	23,000
234.5	0.786	1.0	55.4	11.7	2.6	2.6	325	23,000
236.7	0.223	1.0	59.3	7.8	2.6	9.5	325	230,000
238.7	0.279	1.0	59.8	8.4	2.6	8.9	325	184,000
246.1	0.774	1.0	64.6	14.3	2.6	2.8	325	35,000
254.9	0.320	1.0	60.0	9.0	2.6	8.3	325	140,000
257.2	0.450	1.0	61.4	10.6	2.6	6.8	325	92,000
259.3	0.549	1.0	62.4	11.8	2.6	5.5	325	70,000
261.1	0.759	1.0	55.4	11.9	2.6	3.0	325	46,000
274.2	0.788	1.0	62.8	14.3	2.6	2.6	350	35,000
280.9	0.355	1.0	60.4	9.5	2.6	7.9	350	230,000
284.9	0.619	1.0	62.9	12.6	2.6	4.7	350	92,000
287.6	0.435	1.0	61.0	10.3	2.6	7.1	350	184,000
296.2	0.796	1.0	64.5	14.7	2.6	2.5	350	46,000
301.2	0.713	1.0	63.5	13.6	2.6	3.6	350	70,000
304.2	0.786	1.0	53.4	11.7	2.6	2.6	350	23,000
323.7	0.332	1.0	119.3	21.1	2.3	12.4	350	35,000

327.0	0.366	1.0	126.8	23.3	2.3	11.7	350	70,000
334.2	0.411	1.0	126.6	23.9	2.3	10.9	350	46,000
371.5	0.205	1.0	126.9	21.3	2.3	14.7	300	46,000
374.5	0.149	1.0	126.3	20.4	2.3	15.7	300	70,000
377.7	0.101	1.0	124.8	19.4	2.3	16.7	300	140,000
381.0	0.055	1.0	125.2	19.1	2.3	17.1	300	230,000
384.1	0.335	1.0	121.6	21.8	2.3	12.3	300	35,000
391.4	0.777	1.0	172.4	39.5	2.5	6.2	350	23,000

Experiment 6: Catalyst WY-2 under Feed 1, 2 and 3

Time-on-stream (h)	X_{CO}	$C_{balance}$	F'_{H_2} (mol/min)	F'_{CO_2} (mol/min)	F'_{Ar} (mol/min)	F'_{CO} (mol/min)	Temperature (°C)	SV_{DRY} [ml/(hr.g)]
24.1	0.652	1.0	59.4	12.4	2.6	4.2	275	11,500
28.3	0.469	1.0	59.7	11.2	2.6	6.3	275	23,000
32.7	0.410	1.0	59.5	10.4	2.6	7.1	275	35,000
35.7	0.316	1.0	58.6	9.3	2.6	8.3	275	46,000
44.5	0.891	1.0	172.3	44.5	2.5	1.5	275	46,000
47.2	0.898	1.0	169.3	43.7	2.5	1.4	275	23,000
64.4	0.739	1.0	171.8	43.5	2.5	3.6	275	70,000
71.2	0.590	1.0	170.3	41.7	2.5	5.5	275	92,000
81.9	0.350	1.0	160.9	36.1	2.5	9.1	275	184,000
91.5	0.306	1.0	125.5	24.1	2.3	12.8	275	23,000
113.4	0.392	1.0	118.6	23.3	2.3	11.2	300	23,000
152.1	0.879	1.0	64.1	16.0	2.6	1.5	300	23,000
158.3	0.774	1.0	63.3	15.1	2.6	2.6	300	35,000
165.1	0.639	1.0	61.7	13.4	2.6	4.3	300	46,000
167.3	0.486	1.0	60.3	11.4	2.6	6.2	300	70,000
169.6	0.381	1.0	59.2	10.0	2.6	7.6	300	92,000
173.3	0.210	1.0	59.3	10.1	2.6	7.5	300	184,000
190.8	0.871	1.0	160.6	36.1	2.5	9.0	300	23,000
194.5	0.888	1.0	171.8	44.5	2.5	1.5	300	35,000
196.1	0.883	1.0	172.4	44.8	2.5	1.6	300	46,000
199.1	0.887	1.0	171.9	44.9	2.5	1.6	300	70,000
202.4	0.878	1.0	171.8	44.9	2.5	1.6	300	92,000

237.6	0.843	1.0	62.8	15.4	2.6	1.9	325	23,000
260.9	0.847	1.0	63.7	15.7	2.6	1.9	325	35,000
277.9	0.845	1.0	63.3	15.8	2.6	1.9	325	46,000
285.8	0.817	1.0	63.8	15.6	2.6	2.1	325	70,000
290.3	0.721	1.0	62.6	14.3	2.6	3.4	325	92,000
297.8	0.450	1.0	59.9	10.8	2.6	6.8	325	184,000
300.1	0.381	1.0	59.2	10.0	2.6	7.5	325	230,000
311.9	0.848	1.0	167.3	42.8	2.5	2.2	325	23,000
314.1	0.852	1.0	169.3	44.0	2.5	2.1	325	70,000
320.1	0.839	1.0	169.6	44.0	2.5	2.2	325	92,000
323.1	0.834	1.0	170.4	44.1	2.5	2.4	325	184,000
325.2	0.810	1.0	170.2	43.8	2.5	2.7	325	230,000
341.4	0.453	1.0	125.5	25.6	2.3	10.1	325	35,000
346.3	0.425	1.0	127.3	25.8	2.3	10.6	325	70,000
348.9	0.423	1.0	127.5	25.8	2.3	10.7	325	92,000
361.2	0.574	1.0	129.2	28.1	2.3	8.2	325	23,000
352.1	0.287	1.0	126.6	23.5	2.3	13.3	325	184,000
359.3	0.231	1.0	125.8	22.8	2.3	14.0	325	230,000
374.6	0.481	1.0	128.3	26.6	2.3	9.6	325	46,000
383.9	0.286	1.0	125.8	23.7	2.3	13.2	275	23,000
388.0	0.213	1.0	125.6	22.4	2.3	14.6	275	46,000
402.5	0.152	1.0	119.3	19.7	2.3	15.6	275	92,000
426.2	0.332	1.0	127.0	24.3	2.3	12.2	300	46,000
433.5	0.233	1.0	119.8	21.1	2.3	14.1	300	92,000
448.5	0.497	1.0	113.1	22.3	2.3	9.4	350	23,000
455.4	0.484	1.0	121.9	24.7	2.3	9.7	350	46,000

458.6	0.478	1.0	126.5	26.4	2.3	9.8	350	92,000
462.2	0.446	1.0	126.5	26.0	2.3	10.5	350	184,000
465.3	0.383	1.0	126.2	25.2	2.3	11.4	350	230,000
478.4	0.819	1.0	62.2	14.9	2.6	2.2	350	23,000
480.3	0.816	1.0	62.0	14.9	2.6	2.2	350	35,000
482.4	0.815	1.0	62.6	15.1	2.6	2.3	350	46,000
484.5	0.828	1.0	63.5	15.7	2.6	1.9	350	70,000
489.8	0.809	1.0	63.3	15.3	2.6	2.3	350	92,000
502.8	0.655	1.0	61.7	13.5	2.6	4.2	350	184,000
526.2	0.598	1.0	61.3	12.9	2.6	4.7	350	230,000
532.1	0.753	1.0	169.4	43.4	2.5	3.1	350	230,000
535.1	0.780	1.0	150.6	38.4	2.5	3.0	350	184,000
537.2	0.819	1.0	157.0	40.3	2.5	2.5	350	92,000
541.5	0.762	1.0	159.7	40.4	2.5	3.3	350	70,000
543.6	0.753	1.0	157.8	39.8	2.5	3.5	350	46,000
557.3	0.346	1.0	164.1	37.4	2.5	8.8	275	184,000
562.9	0.705	1.0	149.0	36.9	2.5	3.9	375	35,000
574.3	0.679	1.0	150.2	37.2	2.5	4.1	375	46,000
576.4	0.685	1.0	151.0	37.6	2.5	4.2	375	70,000
578.3	0.658	1.0	152.1	37.5	2.5	4.6	375	92,000
591.8	0.657	1.0	166.2	41.1	2.5	5.1	375	184,000
624.7	0.367	1.0	165.0	37.9	2.5	8.8	275	184,000
640.7	0.769	1.0	61.4	14.5	2.6	2.8	375	46,000
645.2	0.776	1.0	60.0	14.0	2.6	2.8	375	23,000
647.7	0.773	1.0	62.3	14.9	2.6	2.7	375	92,000
649.1	0.739	1.0	62.3	14.4	2.6	3.3	375	184,000

655.2	0.466	1.0	59.6	11.3	2.6	6.5	275	23,000
665.6	0.164	1.0	56.1	7.4	2.6	10.2	275	92,000
669.2	0.092	1.0	55.7	6.3	2.6	11.1	275	184,000
758.9	0.414	1.0	59.5	10.5	2.6	7.1	275	23,000

Experiment 7: Catalyst WY-2 under Feed 2 and 3

Time-on-stream (h)	X_{CO}	$C_{balance}$	F'_{H_2} (mol/min)	F'_{CO_2} (mol/min)	F'_{Ar} (mol/min)	F'_{CO} (mol/min)	Temperature (°C)	SV_{DRY} [ml/(hr.g)]
101.1	0.743	1.0	60.5	14.2	2.6	3.0	325	46,000
123.6	0.306	1.0	54.5	8.4	2.6	8.5	300	46,000
135.9	0.150	1.0	53.0	6.4	2.6	10.4	275	46,000
144.0	0.822	1.0	57.3	14.0	2.6	1.9	350	46,000
266.3	0.451	1.0	154.6	36.9	2.5	7.5	275	46,000
279.5	0.838	1.0	154.8	41.2	2.5	2.0	300	46,000
287.5	0.829	1.0	149.9	39.6	2.5	2.3	325	46,000
292.5	0.791	1.0	151.9	39.9	2.5	2.7	350	46,000
304.5	0.448	1.0	155.2	37.3	2.5	7.3	275	46,000

Experiment 8: HTS (G-3C) catalyst under Feed 2

Time-on-stream (h)	X_{CO}	$C_{balance}$	F'_{H_2} (mol/min)	F'_{CO_2} (mol/min)	F'_{Ar} (mol/min)	F'_{CO} (mol/min)	Temperature (°C)	SV_{DRY} [ml/(hr.g)]
21.7	0.476	0.9	55.1	9.1	2.6	6.5	375	11,500
24.3	0.425	1.0	56.5	9.6	2.6	7.0	375	17,000
28.1	0.368	1.0	56.8	9.3	2.6	7.6	375	23,000
31.1	0.293	1.0	56.9	8.7	2.6	8.6	375	35,000
33.2	0.232	1.0	56.5	8.0	2.6	9.3	375	46,000
36.3	0.125	1.0	55.7	6.8	2.6	10.6	375	92,000
44.5	0.348	1.0	57.4	9.1	2.6	8.1	375	23,000
55.4	0.523	0.9	57.0	10.4	2.6	5.9	400	17,000
57.2	0.521	1.0	57.5	10.7	2.6	6.0	400	23,000
59.4	0.482	1.0	58.1	10.6	2.6	6.4	400	35,000
61.3	0.434	1.0	57.8	10.1	2.6	7.0	400	46,000
63.4	0.349	1.0	57.3	9.2	2.6	8.0	400	70,000
66.1	0.292	1.0	57.1	8.6	2.6	8.7	400	92,000
73.8	0.592	0.9	54.6	10.5	2.6	5.1	425	23,000
76.5	0.582	0.9	54.6	10.6	2.6	5.1	425	35,000
90.6	0.555	1.0	57.4	11.2	2.6	5.5	425	46,000
96.5	0.492	1.0	57.1	10.6	2.6	6.3	425	70,000
99.1	0.448	1.0	57.1	10.2	2.6	6.8	425	92,000
103.2	0.612	0.9	49.3	9.4	2.6	4.7	425	23,000
113.4	0.581	0.9	50.9	9.6	2.6	5.1	450	35,000
119.9	0.541	0.9	53.1	9.8	2.6	5.7	450	46,000
123.9	0.490	0.9	55.0	9.9	2.6	6.3	450	70,000

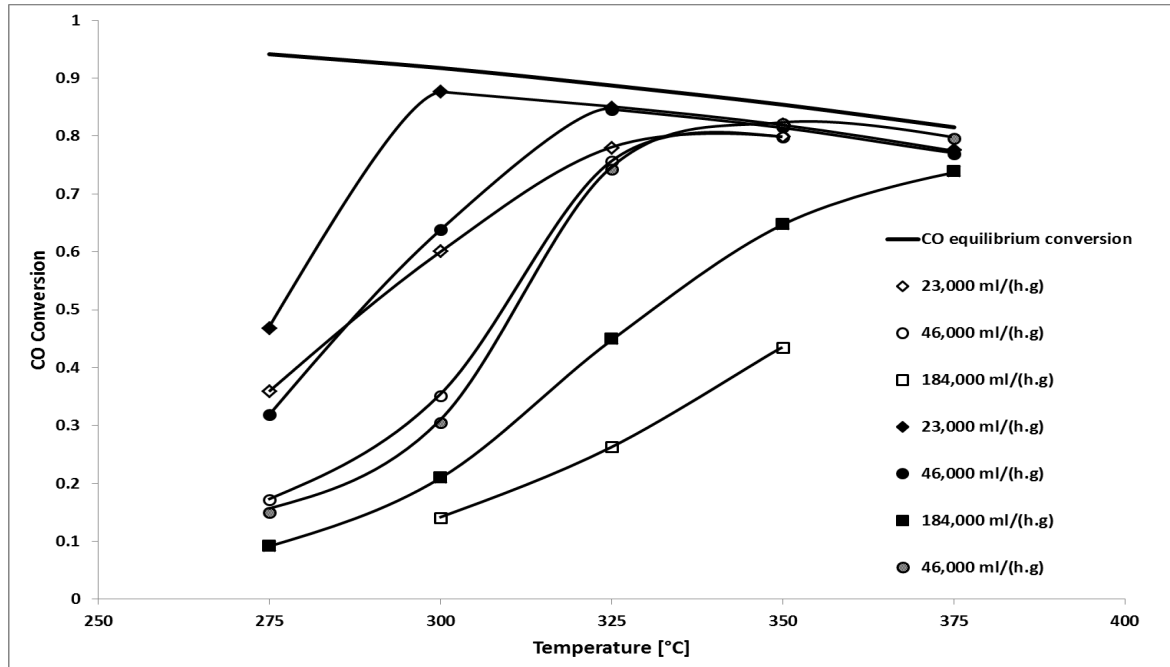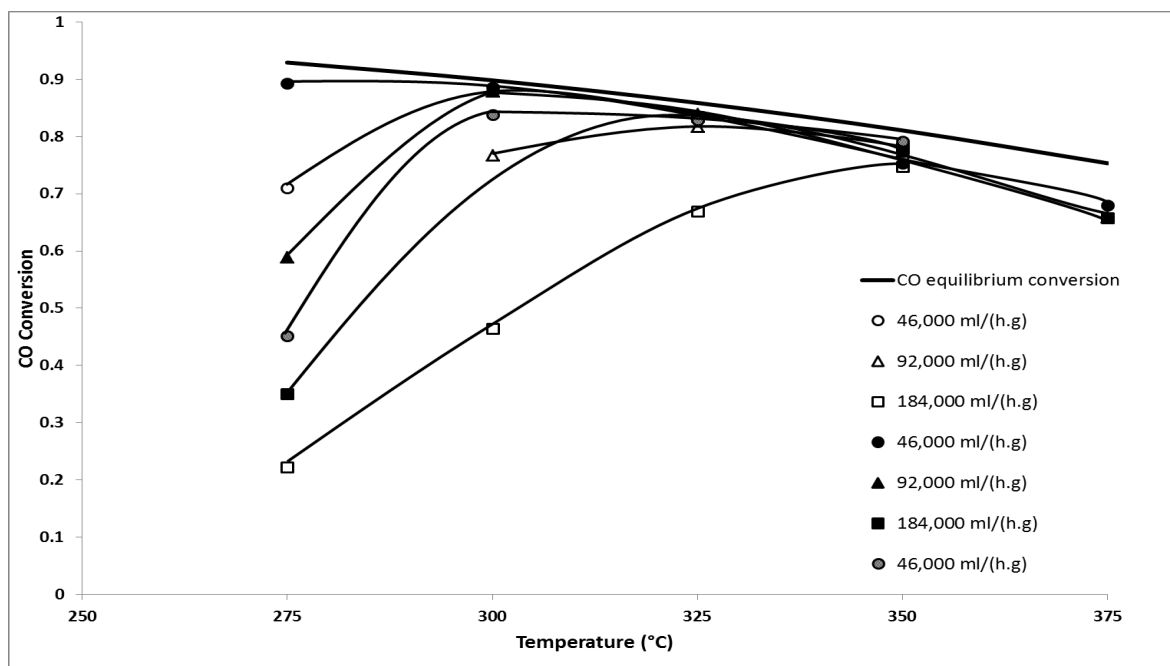|								
126.3	0.421	1.0	56.5	9.8	2.6	7.1	450	92,000
129.5	0.283	1.0	55.7	8.3	2.6	8.8	375	35,000

Appendix VI

Additional results

Figure VI-1: Experimental performance reproducibility and effect of temperature for catalyst WY-2 with Feed 2 (Table 4-6 in Section 4.4.1: Feed composition) at different *space velocities.* Experiments 5 (open symbols), 6 (dotted symbols) and 7 (grey dotted symbols)

Figure VI-2: Experimental performance reproducibility and effect of temperature for catalyst WY-2 with Feed 3 (Table 4-6 in Section 4.4.1: Feed composition) at different *space velocities.* Experiment 5 (open symbols), 6 (dotted symbols) and 7 (grey dotted symbols)